

Repair and Regeneration of Peripheral Nerve Fibrosis

Inaugural dissertation

to

be awarded the degree of Dr. sc. med.

presented at

the Faculty of Medicine, University of Basel

by

Nilabh Ghosh

From Asansol, India

Basel, 2021

Original document stored on the publication server of the University of Basel
edoc.unibas.ch



This work is licensed under a Creative Commons Attribution 4.0 International License.

Approved by the Faculty of Medicine

On application of

Prof. Dr. Dr. Raphael Guzman (Department of Neurosurgery, University Hospital
Basel)

Prof. Dr. Dr. Daniel Kalbermatten (Department of Surgery, University of Geneva)

Prof. Dr. Dr. Michael Kelly (Division of Neurosurgery, University of Saskatchewan)

Basel, ...29.11.2021.....

.....
Prof. Dr. Primo Leo Schär

Other supervisors

Dr. Srinivas Madduri - (University of Geneva).

Acknowledgement

My doctoral thesis and all the work would not have been possible without the intellectual and financial support, contribution and hard work of many colleagues, friends and family. I would like to express my gratitude to all those who helped me in this work and helped me learn a lot of things along the way.

First and foremost, I want to thank my **parents** for believing in me. I couldn't have made it so far without their motivation and support. My parents' hard work taught me to perform all of life's tasks, to the best of my ability, without complaint and I dedicate this thesis to them.

Raphael Guzman, my supervisor, Vice Chair, Department of Neurosurgery, University Hospital Basel. Thank you for making me realize my potential. Without your knowledge, dedication and support, this work would neither have been possible nor completed. You are an extraordinary mentor and an excellent researcher and clinician. I am so grateful to you for the fact that you took your time out from your busy schedule in the clinics to guide me whenever needed. Thank you so much!

Catherine Bregere, Alois Hopf, Pia Bustos, Bernd Schwendele, my colleagues at the BRIR laboratory. You all contributed to the friendly and inspiring atmosphere in the lab. I am grateful for your support on my experiments.

Mara Fornaro, Daniela Gabriel and Magalie Mathis, my colleagues at Novartis. Thank you so much for giving the amazing opportunity to work next to you. Your innovations inspired me to learn constantly and do things in a different and better way. Collectively, I would like to thank them for challenging my knowledge and guiding experiments as my work progressed in 2020 and 2021. Your unfailing support., encouragement and ideas will help me in the long run and I am fortunate to have worked with you all. Thanks a lot!

Alexander Schmidt, Robert Ivanek, Michael Abanto, Loic Sauter and Dominik Viscardi, my colleagues from the Core facilities, Department of Biomedicine for your invaluable cooperation and technical support. Things would have been difficult without you guys. Thank you so much for your professional help and understanding.

Sanj Singh (Temple Therapeutics), our industry partner. Thank you for the interesting work and discussions revolving around L-Alanyl-L-Glutamine.

Eurostar (Srinivas Madduri), Department of **Neurosurgery**, Department of **Plastic Surgery** and Department of **Biomedicine** for their financial and technical support. I

would like to thank all the surgeons involved with the surgeries for sample collection, clinical research and human experiments.

A big thank you to all my dear friends, **Deniz Kaymak**, **Jordan Loeliger**, **Alois Hopf**, **Lucas Degrugillier** and **Christoph Hafelfinger**. You guys made my transition to a new country much easier. Thank you for the immense support, advice and good memories.

Finally, I would like to express my gratitude to my thesis advisory committee, **Raphael Guzman**, **Daniel Kalbermatten**, **Michael Kelly**, **Mara Fornaro** and **Gregor Hutter** for allowing me to be a part of this work and for their constant guidance. Thank you for helping me to keep perspective on where my research fits best into the bigger picture and help me identify its clinical relevance. Your diligent support helped me strengthen my thesis.

Table of Contents

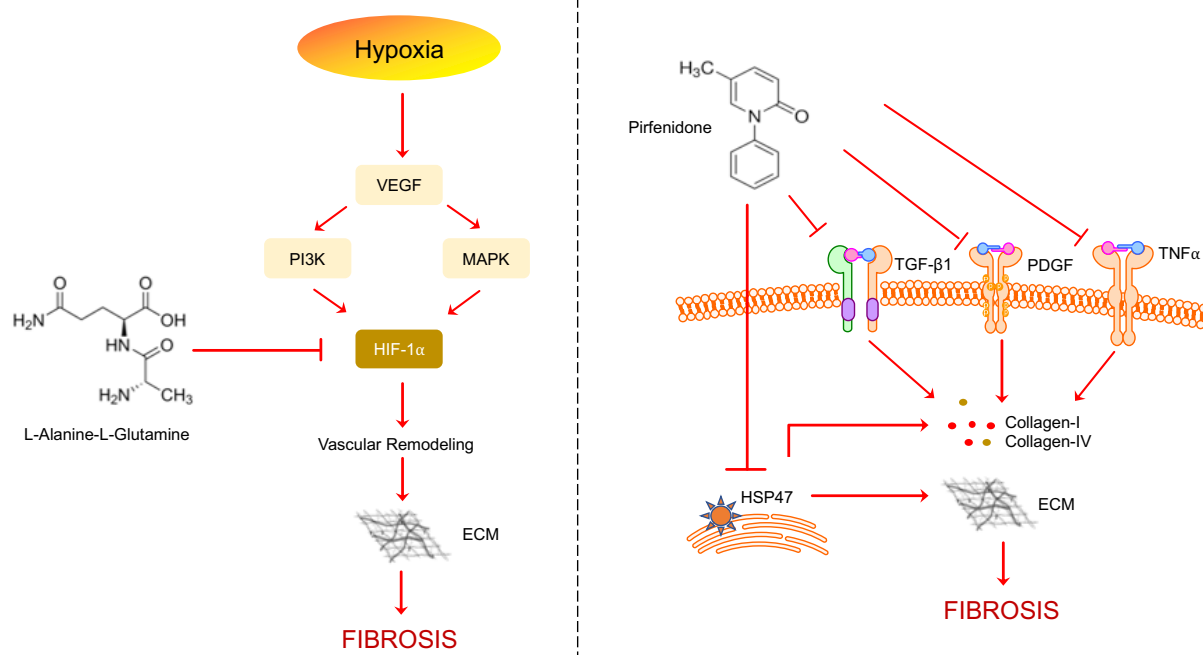
Acknowledgement.....	3
Abstract.....	7
List of Patent and Papers.....	9
Abbreviations.....	10
Introduction:	
The Peripheral Nervous System and Peripheral Nerves.....	12
Peripheral Nerve Injury.....	13
Peripheral Nerve Fibrosis.....	15
Hypoxia in Peripheral Nerve Fibrosis.....	19
TGF-β in Peripheral Nerve Fibrosis.....	21
L-Alanyl-L-Glutamine and Peripheral Nerve Fibrosis.....	25
Pirfenidone and Peripheral Nerve Fibrosis.....	26
Materials and Methods (Chapter: L-Alanyl-L-Glutamine)	29
Materials and Methods (Chapter: Pirfenidone)	36
Results (Chapter: L-Ala-L-Gln):	
L-Ala-L-Gln does not affect cell proliferation and viability of hypoxic primary fibroblasts.....	46
L-Ala-L-Gln down regulates expression of fibrotic proteins of primary fibroblasts exposed under Continuous Hypoxia.....	47
L-Ala-L-Gln down regulates expression of fibrotic proteins of primary fibroblasts exposed under Episodic Hypoxia.....	50
Identification of crucial proteins and pathway analysis in hypoxic fibroblasts treated with L-Ala-L-Gln.....	53
Results (Chapter: Pirfenidone):	
PFD inhibits viability and cell proliferation and induces cell death of primary rat fibroblasts, but not Schwann cells.....	56
PFD exposure significantly reduces cell viability and proliferation and promotes apoptosis of TGF-β1 activated primary rat fibroblasts.....	59
PFD exposure significantly reduces cell viability and proliferation and promotes apoptosis of hypoxic primary rat fibroblasts.....	60

PFD reverses differentiation of primary rat fibroblasts.....	62
PFD reduces expression of pro-fibrotic factors induced by TGF-β signaling.....	67
PFD reduces expression of pro-fibrotic factors induced by hypoxia signaling.....	73
Identification of crucial proteins and pathway analysis in TGF-β1 stimulated fibroblasts treated with PFD.....	75
PFD arrests pro-fibrotic processes and targets TGF-β mediated gene upregulation.....	84
Discussion (Chapter: L-Ala-L-Gln)	90
Discussion (Chapter: Pirfenidone)	95
Conclusions.....	99
Supplementary Data.....	102
Reference.....	107

Abstract

Twenty million Americans suffer from peripheral nerve injury (PNI) and is undoubtedly one of the major unmet medical needs. Approximately \$150 billion is spent annually in the United States for Nerve Injuries. Moreover, 50,000 cases of PNI repairs are performed annually in the United States with even less than 42% experiencing satisfactory sensory recovery. Despite extensive medical research, there aren't any approved small molecule antifibrotic treatment pertaining to nerve injuries. Peripheral nerve fibrosis (PNF) associated with chronic inflammation, perineural adhesions and scarring are often reported in patients with nerve injury. Surgical interventions including external neurolysis is the common available option. Unfortunately, post-surgical adhesions and fibrosis, often lead to aberrated wound healing and impairment of nerve functions. Though, various treatment strategies have been tried including use of grafts, biomaterials, no treatment modality seems to be promising as of now.

The aim of this study was to investigate the effects of L-Alanine-L-Glutamine (L-Ala-L-Gln) and Pirfenidone (PFD) on hypoxic and TGF- β 1 stimulated fibroblasts and their ability to induce anti-fibrotic phenotype. Rat perineurial derived fibroblasts were exposed to hypoxic conditions or externally activated by TGF- β 1 and expression of hypoxic and pro-fibrotic markers were assessed following treatment with L-Ala-L-Gln (0-100mM) or with PFD (0-0.25 mg/ml). PFD was found to act through targeted downregulation of the TGF- β pathway and significantly reduced pro-fibrotic and cell-adhesion inducing factors at the protein and RNA level. In rat perineurial derived fibroblasts, L-Ala-L-Gln and PFD modulated several pro-fibrotic factors and associated pathways to induce an anti-fibrotic phenotype. In conclusion, our results showed that L-Ala-L-Gln and PFD suppressed fibrotic phenotype and might prove to be effective anti-fibrotic agents for neural fibrosis. These promising results will lead to identification of a non-invasive biomarker for the assessment of neural fibrosis. These results can easily be translated into the clinical settings and we expect our discoveries to assist clinicians to identify a novel therapeutic strategy for neural fibrosis and support invasive surgical applications.



Graphical Abstract

List of Patent and Papers

This thesis is based on the following patent and papers:

Patent

Methods of Treating Fibrosis and Hypoxia-Associated Damage to Peripheral Nerves
U.S. Provisional Patent Application No. 63/185,456. Reference No:15982-28.

Inventors: Nilabh Ghosh, Raphael Guzman, Daniel Kalbermatten, and Srinivas Madduri

Publications

1. Ghosh N, Kalbermatten D, Madduri S, Guzman R. Fibrosis and Regulation of Nerve Regeneration in the Peripheral and Central Nervous Systems. *CNS Neurol Disord Drug Targets*. 2020;19(8):560-571. doi:10.2174/1871527319666200726222558
2. Ghosh N, Bregere C, Bustos P, Madduri S, Kalbermatten D, Guzman R*. L-Ala-L-Gln suppresses hypoxic phenotype and fibrogenic activity of rat perineurial fibroblasts. BMS-CNSNDDT-2021-91 (under final revisions).
3. Ghosh N, Bregere C, Bustos P, Ivanek R, Madduri S, Kalbermatten D, Guzman R*. Pirfenidone alleviates peripheral nerve fibrosis through TGF-beta/ SMAD 3/ PI3K pathways (In preparation).

Abbreviations

7AAD - 7-Aminoactinomycin D
AF - Alexa-Fluor
AKT - Protein kinase B (PKB)
ANOVA - Analysis of variance
BAM - Binary 75 alignment map
BNB - Blood nerve barrier
Cavin3 - caveolae associated protein 3
CDK1 - cyclin-dependent kinase 1
CFSE - carboxyfluorescein succinimidyl ester
CFSE - Carboxyfluorescein succinimidyl ester
CNS - Central Nervous System
COL1A1 - Collagen Type I Alpha 1 Chain
COL4A1 - Collagen Type IV Alpha 1 Chain
DAPI - 4',6-diamino-2-phenylindole, dihydrochloride
DMEM - Dulbecco's Modified Eagle Medium
DNA - Deoxyribonucleic acid
DPBS - Dulbecco's Phosphate Buffered Saline
ECM - Extracellular Matrix
EdU - 5-ethynyl-2'-deoxyuridine
EFNA3 - ephrin A3
ELISA - Enzyme-linked immunosorbent assay
ERK - Extracellular regulated protein kinase
FBN – Fibronectin
FBS - Foetal bovine serum
FDR - false discovery rate
GAPDH - Glyceraldehyde 3-phosphate dehydrogenase
GRB2 - growth factor receptor bound protein 2
HCD - high-collision-dissociation
HIF-1 α - Hypoxia-inducible factor 1-alpha
HIFs - Hypoxia inducible factors
HMOX1 - heme oxygenase 1
HSP47 – Heat shock protein 47
I-R - ischemic-reperfusion

ICC – Immunocytochemistry
IGF2 - Insulin-Like Growth Factor-2
IL1 β - interleukin 1 beta
IL2RG - interleukin 2 receptor subunit gamma
IRF7 - interferon regulatory factor 7
L-Ala-L-Gln - L-Alanine-L-Glutamine
LAP - Latency associated peptide
LIF - LIF interleukin 6 family cytokine
Lox - Lysyl oxidase
M6PR - Mannose-6-Phosphate Receptor
MAPK1 - mitogen activated protein kinase 1
MMPs - Matrix Metalloproteinases
mTOR - mammalian target of rapamycin
PFD - Pirfenidone
PI3k - Phosphatidylinositol 3-kinase
PLA2G12A - phospholipase A2, group XIA
PNF - Peripheral nerve fibrosis
PNI - Peripheral nerve injury
PNS - Peripheral Nervous System
PVR - Proliferative vitreoretinopathy
qPCR - quantitative real time-polymerase chain reaction
RAGs - regeneration-associated genes
RNAseq – RNA sequencing
SD - standard deviation
SEM - Standard error of the mean
STAT - signal transducer and activator of transcription
TGF- β - Transforming growth factor- β
TIMPs - Tissue Inhibitors of Metalloproteinases
TNF α - Tumor Necrosis Factor alpha
VEGFA - vascular endothelial factor A
WD - Wallerian degeneration
WT – Wild type
 α SMA - alpha smooth muscle actin

Introduction

The Peripheral Nervous System and Peripheral Nerves

The nervous system is divided into the central nervous system (CNS) and the peripheral nervous system (PNS). The CNS contains the brain and the spinal cord and the PNS refers to parts of the nervous system outside the brain and the spinal cord. The PNS consists of the nerves and ganglia outside the brain and the spinal cord. It is mainly divided into the somatic and the autonomic nervous system and connects the CNS to the limbs and organs (1, 2). The somatic neurons can be further divided into the motor and sensory neurons which are responsible for carrying efferent and afferent information from CNS to effector organs and vice versa. The autonomic nervous system comprises of the sympathetic and parasympathetic nerve fibers and are involved with visceral functions, including innervation of involuntary structures such as the heart, smooth muscles and glands within the body. Our work mainly focuses on somatosensory neurons. The axons (afferent nerve fibers) of sensory neurons connect with and respond to various receptor cells and activated by different stimuli such as heat. The somatosensory neurons are highly clinically significant as damage to peripheral nerves of the somatosensory origin often lead to debilitating conditions, permanent damage and reduced quality of life. Before we dwell into the details of peripheral nerve injury, let us first understand peripheral nerves.

Each individual peripheral nerve, or nerve trunk, such as the sciatic nerve, comprises of multiple somatic and autonomic axons, also known as nerve fibers. Each individual axon is surrounded by a thin layer of collagen fibers called the endoneurium. The endoneurium houses blood capillaries that ensures a constant supply of nutrients and oxygen to the nerves (3). In large nerves, fibers are bundled into fascicles and every individual fascicle is enveloped by a thin specialized fibrous tissue, perineurium. These nerve fibers are bound together by sheaths of three layers of connective tissue. The outermost layer covers the entire nerve and is known as epineurium (4). Individual nerve fibers vary in diameter and exist either as myelinated or unmyelinated nerve fibers. Schwann cells form the major components responsible for myelinating peripheral nerves. Schwann cells form the insulating laminin-rich myelin sheath, provides nutrients and are the primary glial cells of the PNS (5). This insulation further reduces membrane capacitance and increases impulse propagation and nerve conduction (6). In addition to myelination, the Schwann cells-axonal unit is also

enveloped by a basal lamina tube consisting of fibronectin, heparin sulphate, proteoglycan and type IV collagen. Schwann cells form the major cellular entities responsible for the production of these factors (7, 8) and are critical in response to PNS axon damage and axon regeneration. The endoneurium surrounds Schwann cells and fills the intrafascicular space between the axons with fibroblasts, macrophages and components of the extracellular matrix (ECM).

Fibroblasts are the most abundant type of cells found in the endoneurium. They are responsible for formation of fiber and ground substance. When observed on electron microscope, they appear spindle shaped and have long slender cytoplasmic processes (9). Lack of continuous basal lamina around fibroblasts distinguishes them from other cells including the Schwann cells and pericytes. The morphological characteristics and appearance of fibroblasts varies depending on the activation and functional activity. This thesis focusses on these perineurial fibroblasts and their role in regulating peripheral nerve fibrosis (PNF). Though the function of these fibroblasts has been debated and discussed for many years, it has been reported that these cells synthesize type I collagen (10) and are essential for Schwann cell basal lamina deposition and elongation (11). In addition to this, fibroblasts play an important role in Wallerian degeneration through the formation of cell-cell contacts with infiltrating macrophages frequently found around the perivascular endoneurium (12, 13).

Peripheral Nerve Injury

Peripheral nerves are well vascularized by blood vessels and extensive anastomotic connections are observed in the compartments. The endothelial cells of the endoneurial capillaries form tight junctions creating a blood nerve barrier (BNB) (14). The BNB maintains a homeostatic microenvironment and protects the endoneurial space (15). But the vascular network of blood vessels passing through the perineurium runs obliquely and this makes the nerve vulnerable to compression and injuries (16) and rupture of the BNB allows immune activation and infiltration of various factors including cytokines, chemokines and immune cells (17).

Injury to peripheral nerves have been under investigation for a long time. Common causes of peripheral nerve injury (PNI) include traumatic, non-traumatic injuries and iatrogenic injuries such as those during surgical or anesthetic procedures. Trauma resulting from motor vehicle accidents, lacerations, limb fractures and crush injuries

remains the common form of PNIs (18). Motor vehicle accidents remain the major cause of traumatic injuries, amongst others (19), with the radial and the peroneal nerves being the most frequently injured nerve in the upper and lower extremity respectively. Though the incidence of PNIs is relatively low, nearly 20 million individuals suffer from injuries to the peripheral nerves (20). Moreover, in a recently conducted epidemiological survey, PNIs were reported to significantly increase in the period between 2009 – 2018 in the US alone (21). PNI remains a major socio-economic burden because majority of the cases are reported in young males and patients suffer from reduced functional capacity and prolonged rehabilitation (22). Injury to peripheral nerves can have severe effects either on the axon or on the myelin sheath. PNI often leads to the disruption of contact between nerve cell body and the peripheral target organ, neuronal cell death and aberrant gene expression (23, 24). The nerve cell body of the surviving neurons undergoes mechanistic changes that promotes growth of neurons (25). Following the phenotypic changes in the neuronal cell body, injury mediated activation of various signal transduction events takes place. These include activation of transcription factors and genes leading to regeneration (26-28). In spite of this, the regenerative process in PNI is often incomplete due to the absence of growth promoting factors and deposition of ECM (29). Wallerian degeneration (WD) seems to be a critical factor in axonal regeneration following axotomy.

In 1850, Waller noted that cell nucleus is indispensable for survival of the axon and axons and the myelin sheath distal to the injury undergo degeneration (25). This is known as Wallerian Degeneration. WD involves a cascade of cellular and molecular events and have been thoroughly reviewed earlier (30). Briefly, traumatic injury causes severe tissue damage. Galectin-3/ MAC2⁺ hematogenous invading macrophages accumulate within 24 hours following injury at the lesion site. These macrophages are responsible for the digestion of myelin. Macrophages, a source of cytokine and growth factors play a crucial role in the regeneration process. Macrophages also induces proliferation of Schwann cells. Schwann cells are the most vital repair cells and they undergo a state of trans-differentiation following PNI. Schwann cells activate signaling pathways responsible for supporting axon survival and elongation. In addition, they also upregulate neurotrophic factors and remove myelin debris which forms a major barrier to axonal regrowth (31, 32). Repair promoting Schwann cells align themselves in an elongated bipolar morphology, called 'Bungner Bands', to form regenerative

tracks from the nerve target to the lesion site (31). These structures create the highly critical regenerative micro-environment to support axonal regrowth through the distal stump. However, full functional restoration is rarely achieved and myelin debris from the degenerating neurons often impairs axonal regeneration. Fibrosis and scarring at the repair site pose an eminent threat to axonal regeneration. Scarred tissue creates a mechanical barrier and limits the rate and number of axonal outgrowths (33, 34). In this study, we assessed the anti-fibrotic potential of two novel pharmaceutical compounds to promote repair following hypoxia and TGF- β 1 induced PNF in an *in vitro* insult/fibrotic model. Before we move into the details of these pharmaceutical compounds, let us first look into Peripheral Nerve Fibrosis.

Peripheral Nerve Fibrosis

Fibrosis in a tissue or organ occurs due to excessive deposition of ECM factors and fibrous connective tissue. It can occur under repair and regeneration processes (35). Uncontrolled wound healing and chronic inflammation leads to collagen accumulation, loss of tissue and organ failure. Different cellular populations have been associated with peripheral nerve fibrosis. These include cells of the epithelial and endothelium origin, fibrocytes, fibroblasts and macrophages. These cellular populations ultimately activate and stimulate fibroblasts and induce differentiation of fibroblasts into myofibroblasts (36). Myofibroblasts are the key cellular components of scarring/fibrosis and are responsible for aberrant ECM deposition, damage to tissue architecture and uncontrolled wound healing (37). Typically, damaged neurons are not replaced during tissue regeneration and scar-producing cells present a chronic microenvironment in peripheral nerve lesions. The fibrous tissue represents the central core and acute injuries which occur initially in lower intensities, accumulate gradually and become more severe giving rise to a chronic disease (38).

A cascade of physiological and morphological changes occurs in the nerve cell body following a traumatic crush or blast injury. The inflammatory response to WD is necessary for remyelination and involves activation and recruitment of macrophages and fibroblasts at the site of injury (30). However, extended proliferation of fibroblasts in the endoneurium under chronic inflammatory states results in scarring and fibrosis (39). The formation of the scarred tissue severely downregulates the myelinating fibers and denervation of Schwann cells (40). In addition, in a not so clear mechanism,

fibroblasts negatively impact the proliferative abilities of Schwann cells, indirectly affecting axonal regrowth and regeneration (41). As both fibroblasts and Schwann cells, in the PNS are major sources of ECM and collagen, the antagonistic roles of fibroblasts and Schwann cells under chronic inflammation regulate nerve repair and regeneration processes. Collagen deposition has been reported to negatively affect vascularization, and often creates an irreversible damage tissue architecture (42). Collagen deposition also significantly reduces nerve conduction, fibers and regeneration-promoting signaling mechanisms (39). The regeneration-inhibitory microenvironment was studied in 2003 and in 2004. In 2 separate studies (43, 44), the authors found the presence of class 3 semaphorins and proteoglycans at the injury site, hindering axonal regrowth. The Regeneration-Associated Genes (RAGs), also known to influence the regenerative capacity of peripheral nerves, is often found to be downregulated in injured peripheral nerves (45). The mechanism of action of RAGs in context of PNF is not clearly understood and would be of immense importance to learn the effect of ectopic expression of RAGs in PNF.

In the clinical perspective, the extent of injury to peripheral nerves in the different layers gave rise to a classification first established by Seddom in 1943 and later expanded by Sunderland in 1951 (46). This classification ([Table 1](#)) allows clinicians to adopt an orientation of the various therapeutic strategies following PNIs. Intra-neural scarring can be associated with Grade IV injury or Grade V lesion based on Sunderland's classification. Additionally, Elliot *et al* (47) provided a vital classification of peripheral neuropathies. Amongst pathological conditions affecting the nerve, both fibrosis around a nerve (traction neuropathy) and fibrosis inside/ outside the nerve (neuroma-in-continuity) is classified as scarring neuritis/ scar neuropathy. Pain at rest due to these conditions is a distinctive symptom affecting patients. Patients usually complain of four types of pain including spontaneous pain, pressure pain, movement pain and hypersensitivity to external stimuli (47). Of these, spontaneous pain is being reported in majority of the patients and is the most unpleasant of all. In addition to pain, edema, skin blood flow abnormalities and improper sudomotor activity might be present at the lesion site affected by pain and hence timely management of these symptoms is highly critical for functional recovery (48). We have briefly summarized the clinical consequences of PNF in Figure 1.

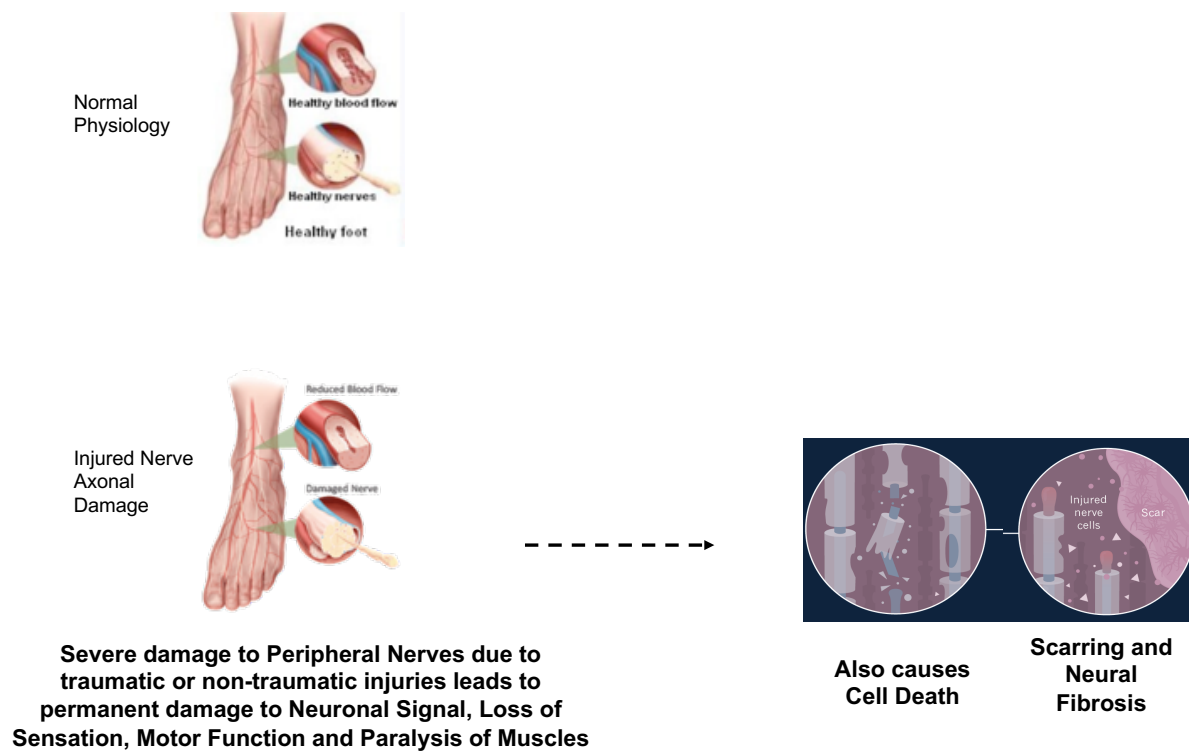


Figure 1: Understanding the consequences of Peripheral Nerve Fibrosis. (Adapted from <https://www.orlandopainandspine.com/conditions/peripheral-neuropathy/>).

An early diagnosis including examination of the pain type, at rest and/ or elicited by movement might be helpful in understanding the type of lesion. Clinical and diagnostic imaging with the help of ultrasound, might also provide relevant information on the extent of nerve injury, severity of scarring and effect of PNI on tissue architecture. In addition, ultrasound also enables direct visualization of the nerve injury and how the nerve interacts with the surrounding tissues. These diagnostic examinations and dynamic imaging technologies might provide important clinical information required for physicians prior to perform surgery (49). Eventually this vital diagnostic information could be exploited for enhanced repair and regeneration processes.

Research over the last few decades have helped us to identify major clinical strategies for peripheral nerve injury management. These include, but are not restricted to methods including microsurgical suture for small nerve injuries, nerve autologous grafting for bigger nerve gap injuries and nerve guidance conduits. Let us briefly look at these strategies and help us understand the advantages and their limitations in peripheral nerve regeneration after injury.

- Epineurial microsutures: This remains the gold standard surgical treatment for severe axonotmesis (50). Epineurial repair is conducted under the presence of a tension free coaptation in a well-vascularized bed. This is extremely important as the regenerating axons need to cross the site of coaptation. However, these procedures do develop tension in the suture line. This further leads to generation of ischemic insult at the lesion site. Ischemic insult further leads to scar formation, connective tissue proliferation and hindrance to axonal regeneration (50). Another major disadvantage of epineurial suturing is the significant loss of sensitivity in suture line and the limited availability of autologous donor tissue.
- Autologous Nerve Grafts: Bridging nerve gaps with autologous grafts, particularly interfascicular nerve grafting, is a reliable method to repair injured peripheral nerves with predictable outcomes. These autologous grafts are natural scaffolds containing Schwann cells and their basal lamina (51). PNI often results in damage and loss of Schwann cells and thus autografts often offer a reliable mechanism for axonal regeneration. Sensory cutaneous nerves, such as the sural nerve is used as the donor nerve. However, this method has severe limitations including loss of donor-site function, size mismatch, neuroma and scarring.
- Nerve Conduits: Artificial and non-artificial nerve grafts are valuable strategies in PNIs with excessive loss of nerve tissue and where direct end-to-end suturing is of little benefit. Different materials including collagen, poly(D L-lactide-ε-caprolactone) are currently in use (<https://www.fda.gov/medical-devices/device-advice-comprehensive-regulatory-assistance/medical-device-databases>). These artificial nerve grafts are of huge relevance in cases of multiple nerve lesions where limited availability of donor tissue restricts treatment with autografts (52). Low antigenicity and immunogenicity make these materials favorable for *in vivo* applications. Though these materials present an advantage, these approaches seem to have little or no beneficial outcomes for long gapped (>3 cm) peripheral nerve defects. These long-gapped defects, also considered as critical injuries often end up in the development of scarring and PNF and hence these materials might provide little help for better clinical outcome/ functional recovery. Also, the lack of axonal

outgrowth triggers and the lack of true guiding structures in current conduits, limit their benefit in critical injuries.

These methods, specifically suturing do offer clinical benefits and remains the gold standard therapeutic strategy following peripheral nerve injury. Unfortunately, expensive surgical interventions fail to address the importance of the interplay between key cellular components including growth factors, ECM, cell adhesion and regulation of signaling pathways. Despite extensive research on PNI and increase in hospital burden, therapeutic advancements have been limited. Fibrotic tissue normally develops within the first weeks after injury to the peripheral nerves and progresses continuously thereafter. Hence understanding the signaling regulation will be of immense help in order to develop pharmaceutical therapeutic strategies against neural fibrosis. Deciphering the signaling mechanisms will help us to identify the putative targets involved with the pathogenesis of PNF. We have previously identified the major signaling molecules and pathways critical for PNF. In this thesis, we will focus primarily on 2 major pathways – HIF-1 α and TGF- β 1 and their role in PNF. Our work also primarily focused on identifying pharmaceutical approaches to regulate these pathways and modulate PNF accordingly.

Hypoxia in Peripheral Nerve Fibrosis

Animal models especially rat PNI models have immensely helped us to understand the cellular and molecular mechanisms revolving around injury-induced peripheral neuropathies and PNF. Following degeneration of distressed axons at the lesion site, PNF can also induce ischemic stress in the involved fascicles (47), which further affects the repair process. Traumatic or iatrogenic nerve injuries results in increased endoneurial pressure and development of edema (53, 54). Increased endoneurial pressure can further lead to compression of vessels in the epineurial and trans-epineurial regions. Eventually, this rapid increase in endoneurial pressure can develop into ischemic insult and axonal degeneration (55). Though direct contribution of vascular dysfunction to neuropathic pain in humans, still remains an area for further investigation, similar changes have been reported in patients with nerve compression (56). In addition, damage to nerve blood vessels generates chronic neuropathic pain

in rodents (57) and similar findings have also been observed in patients with peripheral arterial disorders (58).

Hypoxia is a major pathophysiological condition that influences severity of PNIs. Chronic hypoxia and duration of hypoxia have been reported to induce peripheral polyneuropathy (59). Lim *et al.*, in 2015 reported the presence of endoneurial hypoxia in another animal model of PNI. The authors attributed persistent hypoxia with nerve fibrosis, increased metabolic requirements and microvascular dysfunction and found that treatment with hyperbaric oxygen alleviates neuropathic pain induced by traumatic injury in a mouse model of PNI (60). In hypoxic microenvironment, the Hypoxia Inducible Factors (HIFs) are involved in mediating adaptive reactions (61). HIFs are mainly composed of 2 subunits, the α and the β subunit. The α subunit, present in the cytoplasm, is oxygen regulated. Under hypoxic conditions the α subunit translocate to the nucleus and forms a heterodimer with the β subunit. The HIF heterodimer binds to the hypoxic responsive elements and further associates with other co-activators to regulate gene expression (62). Research over the last few years have shown that HIF-1 α signalling promotes fibrosis through the activation and production of excessive ECM (63). The 2019 Nobel Prize in Medicine was awarded to a trio of researchers including Gregg Semenza, for describing the myriads of how cells sense and respond to varying levels of oxygen. Excessive deposition of ECM factors such as collagen, fibronectin and proteoglycans are characteristic features of tissue fibrosis and HIF-1 α is involved in upregulation of ECM factors under hypoxic conditions (63, 64). Consequently, downregulation of HIF-1 α was found to reduce collagen secretion thereby improving clinical manifestations of fibrotic diseases (65). An elevated expression of HIF-1 α in fibrotic diseases further indicates its involvement in pathogenesis of fibrosis (66, 67) and deletion of *HIF-1 α* attenuates fibrotic phenotype (66, 67). Together, compelling evidence suggests HIF-1 α modulates the complexity of fibrosis of various organs and signalling of HIF-1 α is of important clinical relevance. Its role on the pathological outcome of fibroblasts and macrophages makes it a suitable target for pharmacological and genetic inhibition in PNI as well. There are some studies which aimed at identifying bioactive endogenous molecules targeting peripheral nerve recovery after injury. Unfortunately, these molecules have either reported to show unwanted adverse effects or lack of accurate therapeutic effect at the injury site. In some other cases, absence of proper delivery vehicles renders the therapeutic molecules inactive.

TGF- β in Peripheral Nerve Fibrosis

The Transforming Growth Factor- β (TGF- β) family, a group of pleiotropic cytokines consists of 3 isoforms - TGF- β 1, TGF- β 2 and TGF- β 3 in mammals. All the 3 isoforms are known to play vital roles in wound healing, inflammation, immune response, embryonic development and regulation of scarring and fibrotic mechanisms (68, 69). These 3 isoforms share nearly 80% homology and the precursor proteins of all the isoforms have three highly conserved regions - a N-terminal signal peptide, an intermediate latency associated peptide (LAP) and a C-terminal mature TGF- β peptide (70). Mature TGF- β , formed after the activation of latent TGF- β , binds to its receptors and activates other downstream targets. Various cellular processes such as reactive oxygen species, MMPs, and other enzymes can induce the activation of latent TGF- β into its mature form (69, 71). Activated TGF- β receptors regulate various signaling transduction pathways, including the Small mothers against decapentaplegic (Smad) pathway, crucial for various biological functions.

However, aberrated signaling of the TGF- β pathway may regulate growth, proliferation and migratory phenotypes of cells and the TGF- β pathway is often upregulated in various pathological conditions including cancer, autoimmune disorders and fibrosis. In tissue damage and fibrosis, TGF- β 1 is involved with excessive ECM deposition, increased fibroproliferation, differentiation of fibroblasts and increased collagen synthesis by regulating other downstream targets in collagen signaling (70, 72, 73). TGF- β 1 reportedly induces the activation of ECM components. This further leads to significant increase in the production of pro-fibrotic components including fibronectin and collagen. TGF- β 1 also regulates the balance of Tissue Inhibitors of Metalloproteinases (TIMPs) and Matrix Metalloproteinases (MMPs). This balance is highly critical for immune response and wound healing in response to tissue injury. MMPs are often found to play varied roles in fibrosis, with some MMPs are anti-fibrotic whereas others pro-fibrotic. As MMPs are important for clearance of fibrotic matrix by extracellular proteolysis, regulation of MMPs (74-76) by the TGF- β pathway holds the key in fibrogenic phenotype. We have summarized the signaling regulation of the TGF- β pathway in Figure 2.

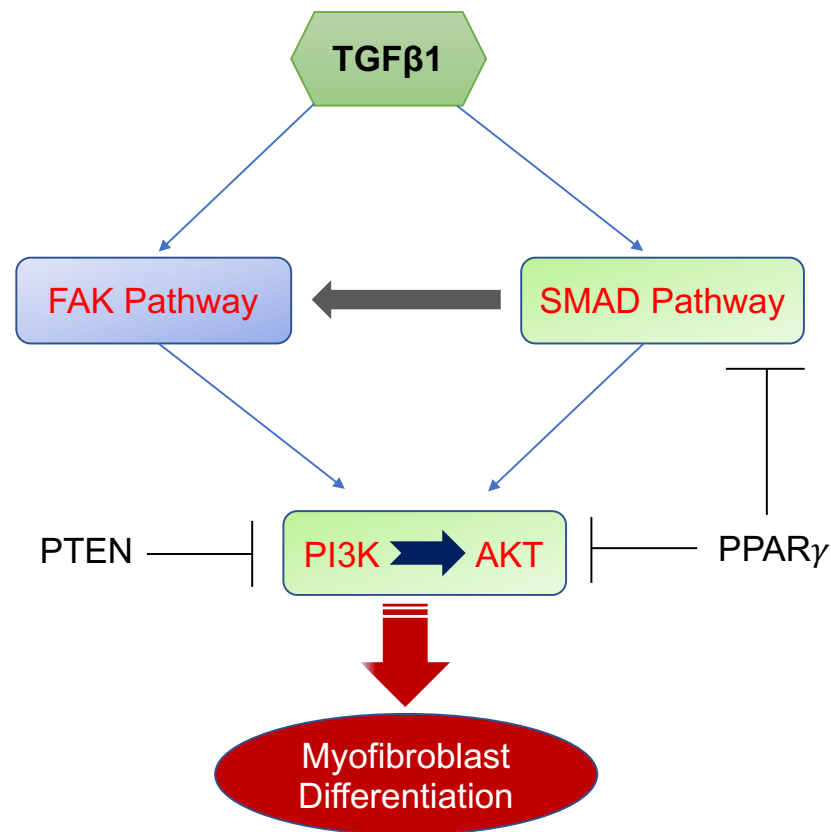


Figure 2: Illustration of the TGF- β signaling in Fibrosis (Adapted from: (77))

TGF- β 1 regulates the expression of α -SMA and collagen I in myofibroblasts through the activation of the FAK, PI3K/ Akt and SMAD and signaling pathways.

Evidence suggests an elevated expression of TGF- β 1 is observed in crushed and distal segments following peripheral nerve injury (78). Protein and mRNA levels of TGF- β 1 were found to be activated following sciatic nerve injury in rats. In addition, this induction was also reported to be critical for WD at the site of injury (79-81) (78-81). TGF- β mediated activation of Smad, AKT and extracellular regulated protein kinase (ERK) pathways were found to regulate nerve degeneration (82). Interestingly, activated levels of TGF- β 1 were found in the regions containing infiltrating macrophages (79), indicating a possible immune regulation in PNI. As immune regulation is crucial for chronic inflammation and immune response, it would be of high significance if we could identify if and how TGF- β modulates the inflammatory microenvironment following PNI.

Emerging evidence suggests upregulation of TGF- β induces scar formation and activated TGF- β forms the molecular bridge between vascular permeability and neural

fibrosis (81, 82). Consequently, administration of an antibody against TGF- β 1 successfully reduced fibroblast numbers, collagen production and attenuated the fibrous scar tissue in a crush injury rat model (83). In another study, Atkins *et al.*, showed reduction in scar formation significantly improves functional outcome (39). The authors observed that scarring increases with genetic ablation of interleukin expression (IL-4/ IL-10). In contrast to the interleukin expression, loss of Mannose-6-Phosphate Receptor (M6PR)/Insulin-Like Growth Factor-2 (IGF2), resulted in reduced scar formation. As M6PR is involved in activating TGF- β , the TGF- β -IL-4-IL-10 crosstalk might play an important role in regulating PNF. Interestingly, TGF- β stimulates the differentiation and migratory potential of Schwann cells through the regulation of Eph signaling in wound healing and repair (81). In addition, upregulated TGF- β negatively effects of other nerve regeneration related cytokines. Consequently, the loss of TGF- β and downregulation of TGF- β 1 signaling with delayed nerve regenerations, suggesting an essential nerve regeneration role of TGF- β signaling following PNI. As fibroblast proliferation and differentiation remains critical in fibrosis, regulation of fibroblast differentiation by TGF- β drives fibrotic phenotype. In 2004, Shephard *et al.* showed an inhibitory effect of IL-1 α on TGF- β 1 (82). As the balance between IL-1 α and TGF- β is critical for fibroblasts differentiation, this could offer a potential mechanism to exploit differentiation of fibroblasts. Numerous therapeutic strategies targeting the TGF- β pathway in fibrosis has been experimented. We have summarized these targets in Figure 3.

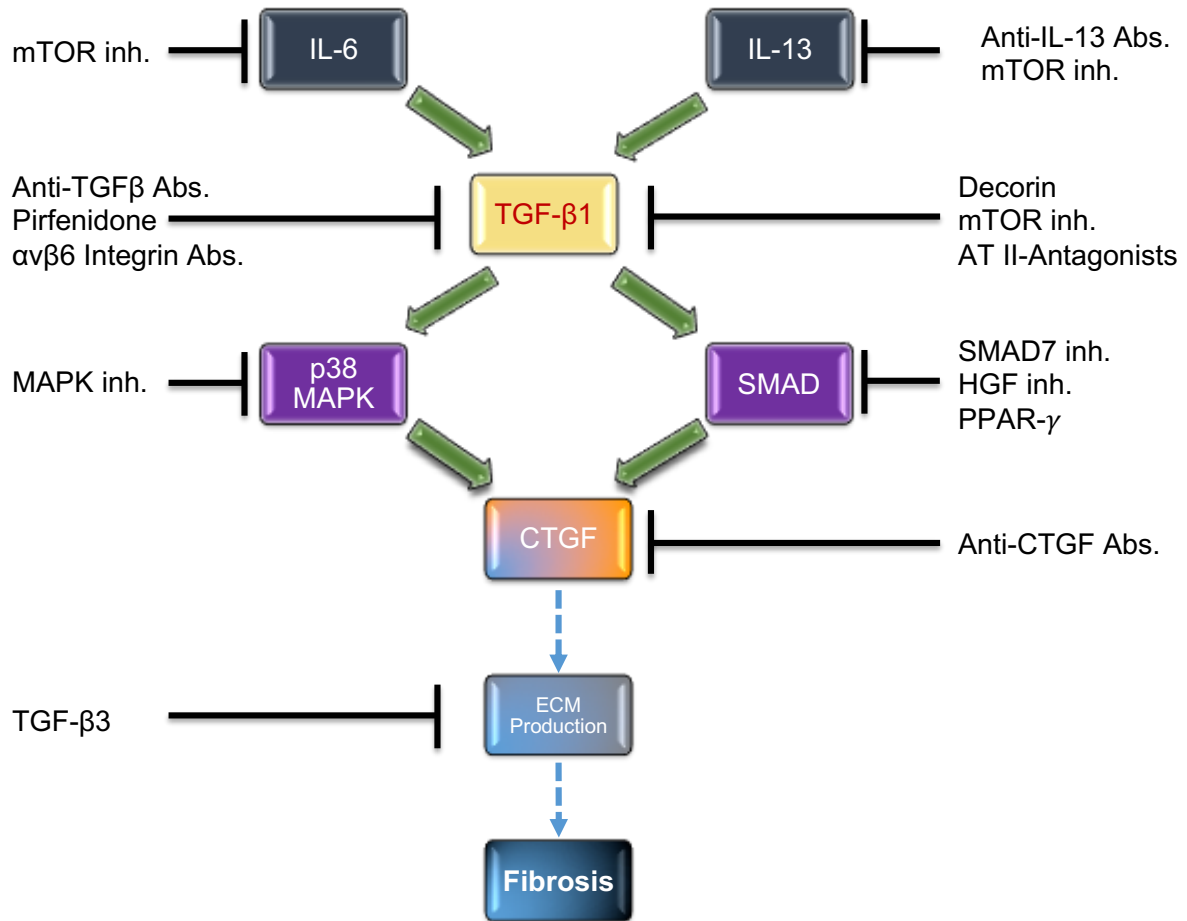


Figure 3: Therapeutic strategies to alter and improve tissue fibrosis

However, absence of targeted inhibition, absence of effective disease models and serious adverse events have posed serious questions regarding the implementation of these strategies. In addition to HIF and TGF- β 1, other growth factors and signaling pathways are also involved in regulating scarring and nerve regeneration after PNI and we have earlier presented the role of these pathways in PNI (83). Given the central role of HIF and TGF- β 1-SMAD signaling in scarring and fibrosis across tissues of various origin including peripheral nerves, inhibition of these pathways could offer potential therapeutic strategies against PNF. During this work, we identified two pharmaceutical compounds, L-Alanyl-L-Glutamine (L-Ala-L-Gln) and Pirfenidone (PFD) as critical regulators of hypoxic microenvironment and TGF- β 1-SMAD signaling in an *in vitro* PNF model respectively. In the next section we have provided an introduction of these pharmaceutical compounds and their role in fibrosis.

L-Alanyl-L-Glutamine and Peripheral Nerve Fibrosis

Glutamine is the most abundant nonessential free amino acid in the human body. Glutamine is largely produced by the skeletal muscle, is involved in carbon and nitrogen metabolism in the cell and hence remains an important source of fuel for immune cells. As critically ill patients suffer from trauma, the effectiveness of the immune system is decreased and this may happen due to the significant reduction in plasma glutamine concentrations (84). Similar stress responses result in an increased activity of glutamine synthetase resulting in an increased release of glutamine in the blood stream. Unfortunately, the rate of release exceeds the rate of synthesis and this causes significant reduction of intracellular glutamine during stress (85). These low concentrations of glutamine might limit the function of lymphocytes and macrophages (84) and hence, exogenous supply of glutamine could enhance the immune response under stress and improve outcome. Similar findings have been reported from animal studies as well.

Several studies have identified the beneficial effects of glutamine supplementation in animal models of infection and trauma (84, 86). Studies show that glutamine supplementation improved muscle protein synthesis, nitrogen balance and reduced protein degradation in an infection rat model (87) and therefore serves as a vital cell signaling molecule in the states of illness and injury. In another study, Stangl et al. showed preoperative use of glutamine might have a huge potential benefit in attenuating hepatic ischemic-reperfusion (I-R) injury and preventing postoperative functional disorder of the liver. The authors found severity of histologic damage was reduced in glutamine treated rats and spectroscopic analysis showed significant improvement of redox homeostasis of liver homogenate samples in these animals (86). As oxidative stress has a major contribution to I-R injury, an immunomodulatory and antioxidative role of glutamine comes to the forefront from these studies.

Alanyl-glutamine is a dipeptide consisting of the glutamine group bridged to an alanyl residue. As glutamine alone is highly unstable with limited solubility, alanyl-glutamine serves as a stable and soluble dipeptide suitable to oral administration (88). This stable form of glutamine is able to revert the stress microenvironment (89). Additionally, L-Ala-L-Gln prevents oxidant/ endotoxin induced cell death and ameliorated intestinal injury (90). Furthermore, previous studies have shown beneficial effects of the use of L-Ala-L-Gln in comparison to glutamine alone in multiple diseases

including hepatic I-R injury (86), endurance exercise (91) as well as reducing infectious complications and glucose intolerance, morbidity and mortality (92, 93). In another key finding the dipeptide was observed to regulate key factors involved with cell growth and survival mechanisms including regulation of mTOR, MAP. Kinase and other pro-inflammatory cytokines, IL-1 and IL-6 (94). Given the immune modulatory role of L-Ala-L-Gln in stress and infectious diseases, we also wondered if the dipeptide plays any role in fibrosis. Ferrantelli et al in 2016, showed that the dipeptide attenuates peritoneal fibroblasts and suppresses IL-17 expression induced by peritoneal dialysis (95). The study also highlighted an emerging anti-fibrotic role of L-Ala-L-Gln including prevention of peritoneal ECM deposition and downregulation of key fibrotic factors including TGF- β 1 and IL-6.

As hypoxic microenvironment acts synergistically along with immune regulation for fibrosis, we also hypothesized that Ala-Gln might play an important role to regulate cellular hypoxia thereby reducing ECM deposition. Prolonged hypoxia, induced by neural scarring and PNF at the lesion site has long been identified as a major factor that elicits oxidative stress, altering redox balance in humans. Considering these we hypothesized L-Ala-L-Gln might regulate the hypoxic microenvironment and hypoxic-mediated fibrotic response of fibroblasts and emerge as a potential pharmaceutical compound for hypoxic insult driven peripheral nerve fibrosis.

Pirfenidone and Peripheral Nerve Fibrosis

Mechanistically neural fibrosis falls into three main categories: cell damage, inflammation and eventually scarring and tissue fibrosis. As both, hypoxia and TGF- β pathway govern major signaling mechanisms in the development and progression of neural fibrosis, we hypothesized that PFD might have antifibrotic and anti-inflammatory effects on neural fibrosis as well. Pirfenidone (PFD) is a synthetic, pyridine (5 methyl-1-phenyl-2-(1H)-pyridone), commercially known as Esbriet is an orally bioavailable compound was initially developed as an antihelminthic and antipyretic agent (96). Highly soluble in alcohol and chloroform, is currently the only compound, beside nintedanib, approved by the FDA for the treatment of idiopathic pulmonary fibrosis (IPF) (97). Once administered, PFD is easily absorbed in the Gastrointestinal tract and reaches its maximum levels within 1 to 2 h in blood (96).

Though the exact mechanism of action is not fully understood, emerging evidence from *in vitro* and *in vivo* studies suggest PFD possess antifibrotic, anti-inflammatory and anti-oxidant properties (98). It is hypothesized that the anti-oxidant properties of PFD might govern its anti-inflammatory properties and these might account for the antifibrotic properties of PFD in tissue fibrosis (98).

PFD is found to induce its antifibrotic properties through the regulation of various cytokines and growth factors, however the most important aspect of its antifibrotic mechanism is associated with the inhibition of production and activity of TGF- β (98). The drug was found to elicit beneficial effects in the treatment of fibrotic diseases of various organs including lung, kidney, liver and also multiple sclerosis (96). In addition, several clinical trials are currently ongoing for patients suffering from neurofibromatosis, kidney disorders in diabetic patients and cardiomyopathy. Fibrosis in all these organs share pathological similarities including excessive deposition of collagen and other ECM components. The TGF- β pathway is a key regulator for collagen synthesis and maintaining ECM homeostasis and under certain conditions activation of TGF- β causes disruption of the balance between synthesis and degradation of ECM (72, 73). In animal models of fibrosis, PFD reduced TGF- β and collagen-I mRNA and further inhibited expression of heat shock protein 47, a key molecular chaperone in ECM remodeling (99). Similarly, PFD inhibited the activation and differentiation of fibroblasts to myofibroblasts, fibroblast mitogenesis and downregulation of connective tissue growth factor *in vitro* (98). Additionally, PFD induced a dose-dependent reduction in proliferation and migration was reported in TGF- β 1 activated dermal fibroblasts. The authors also found (100) inhibition in the development of essential myofibroblasts mechano-regulatory machinery such as F-actin containing stress fibers containing alpha smooth muscle actin (α SMA) and focal adhesion molecules, indicating a mechanistic role of PFD to regulate tissue fibrosis. As we highlighted the importance of hypoxia in regulation of tissue fibrosis and how hypoxia modulates disease progression, we also came across some recent findings where PFD was tested in hypoxia mediated fibrosis models. In a hypoxia rat model of severe pulmonary hypertension, the efficacy of PFD was tested. Interestingly, PFD reduced total pulmonary vascular resistance and remodeling. Consistent with earlier findings, PFD successfully inhibited proliferation and migratory potential of heightened pulmonary smooth muscle cells and reduced ECM deposition (101). These findings

implicate PFD as a potential therapeutic agent for treating hypoxia driven and hypoxia modulated fibrotic injury.

In an animal model of keloid formation, PFD reduced scarring acquired after burn injury in pediatric patients (96). In another recent study, the authors evaluated the potency of PFD in reducing proliferative vitreoretinopathy (PVR) in a rabbit model of penetrating ocular injury. PFD suppressed expression of pro-fibrotic factors including, collagen-I, α SMA and TGF- β and cytokines otherwise detected in untreated controls. To add to the benefit, PFD did not have any adverse effect and no abnormal clinical changes were detected in the eyes, suggesting a huge potential to treat fibrosis following traumatic injuries (102). Evidence also suggested PFD could be detected up to 48 h in the vitreous of rabbit eye following single intravitreal injection suggesting a long-term therapeutic effect. Taking these finding into consideration, Pirfenidone obviously shows effective antifibrotic and anti-inflammatory properties across various in vitro and in vivo models of fibrosis. PFD can reduce oxidative, inflammatory, pro-fibrotic markers and also has the potential to rescue tissue from hypoxic damage. As therapeutic inhibitors designed for specific markers often fail to elicit such responses against fibrotic disease progression, we decided to investigate the role of pirfenidone on neural fibrosis.

In the following chapters we will describe methods and findings of our experimental work in PNI using both L-Alanyl-L-Glutamine (Ghosh et al. 2021, under final revisions in CNSDDT) and PFD (Ghosh et al. 2021, and in preparation).

Materials and Methods (Chapter: *L-Alanyl-L-Glutamine*)

Animals

Animals used for sciatic nerve collection were surplus adult Sprague-Dawley rats bred and provided by the local animal facility, Department of Biomedicine, University Hospital Basel, University of Basel. Rats were euthanized in a CO₂ gas chamber by trained personnel under the animal facility husbandry license 1007H. All sample collection and experiments were conducted in accordance to the Swiss Federal Veterinary Office guidelines and were approved by the Cantonal Veterinary Office (Canton of Basel-Stadt, Switzerland).

Isolation and culture of primary rat fibroblasts

Adult Sprague-Dawley rats were *euthanized* by using a CO₂ gas chamber and sciatic nerves were dissected out immediately under aseptic conditions and placed in ice-cold Dulbecco's Phosphate Buffered Saline (DPBS) (Sigma-Aldrich). Each adult sciatic nerve was cleaned off excess tissue including muscle, fat and blood vessels while working under a Stereo dissecting microscope (Carl Zeiss Microscopy GmbH, Germany). Subsequently, the epineurium was stripped off using fine forceps. Nerve segments were then dissected into small sections (2-5mm) and 5-6 segments were transferred to 6-well plates containing culture medium consisting of Dulbecco's Modified Eagle Medium (DMEM) (Gibco) supplemented with 10% foetal bovine serum (FBS) (Biological Industries) and 1% penicillin/streptomycin (Gibco) for 12-14 days. The medium was replaced every 2-3 days. Primary fibroblasts sprouted from the nerve tissues (Figure 4A) and once cells approached 70% confluency, tissue segments were removed from the 6-well plates with forceps. Cells were washed twice with ice-cold PBS to remove tissue debris, trypsinized with 0.25% Trypsin (Gibco), followed by centrifugation at 1800 rpm for 5 minutes. Cells were counted using Trypan blue and plated in T25/ T75 culture flasks (Corning) for further experimentation. Prior to experimentation, all cells isolated were stained for α -SMA, HSP47, Vimentin and Phalloidin to confirm the phenotype of these cells (Figure 4B). All experiments with primary rat fibroblasts were performed from passages 1-5.

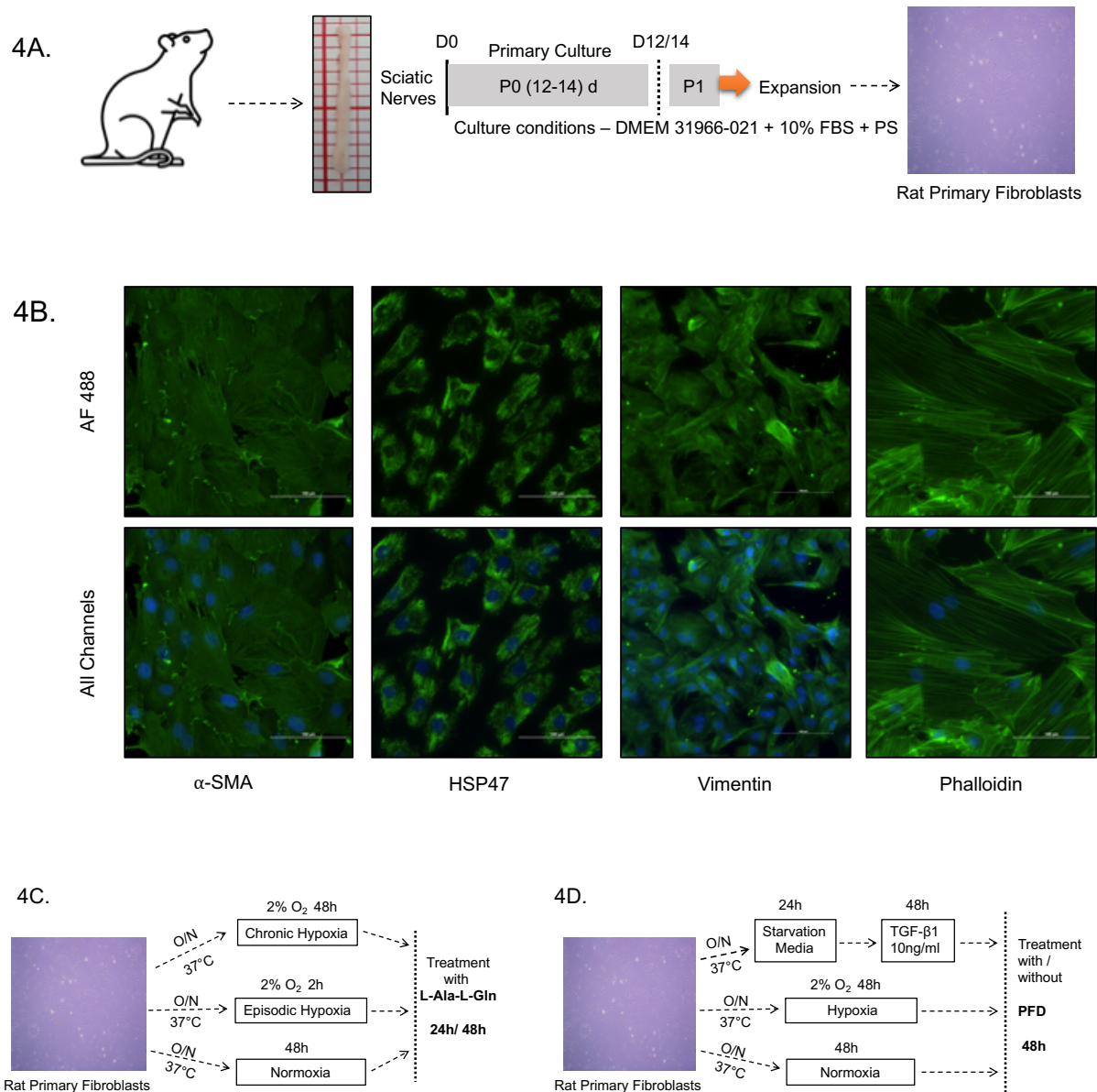


Figure 4: Isolation, maintenance of primary fibroblasts and experimental model

4A. Schematic of Primary Rat Fibroblasts isolation. Primary Rat fibroblasts were isolated from WT Sprague Dawley Rats. Sciatic nerves were resected and fibroblasts were isolated over a period of 12- 14 days in the presence of culture media. Following isolation, cells were washed with PBS and used for experiments.

4B. Morphology and phenotypic characteristics of isolated cells were identified and confirmed with ICC imaging for specific markers including α -SMA, HSP47, Vimentin and Phalloidin. Confirmation of fibroblasts were done for every isolation.

4C. Following phenotypic characterization, primary fibroblasts were used for experiments under 3 different experimental conditions. Cells were exposed under

chronic or episodic hypoxic conditions as described earlier and treated with or without L-Alanine-L-Glutamine. Cells under normoxic conditions were used as negative controls.

4D. Following phenotypic characterization, primary fibroblasts were used for experiments under 3 different experimental conditions. Cells were exposed under hypoxic conditions or activated with TGF- β 1 as described earlier and treated with or without Pirfenidone. Cells under normoxic conditions were used as negative controls.

Abbreviations: α -SMA – alpha-smooth muscle actin; HSP47 – Heat shock protein 47; ICC – Immunocytochemistry; PBS – phosphate buffered saline; WT – Wild type

Hypoxia and L-Ala-L-Gln treatment

To mimic the hypoxic micro-environment, primary rat fibroblasts were exposed to hypoxia. Cells were either exposed to continuous hypoxia, or to episodic hypoxia.

For continuous hypoxia, cells were incubated in a hypoxic chamber (2% O₂) for 48h and treated with or without L-Ala-L-Gln; normoxia was not restored (Figure 4C).

For episodic hypoxia, cells were incubated in a hypoxic chamber (2% O₂) for 2h, and then re-exposed to normoxia for 48h, at which time cells were treated with or without L-Ala-L-Gln (Figure 4C). 48 hours after exposure to continuous or episodic hypoxia, cells were collected and processed for subsequent experiments.

Proliferation assays

The proliferation of primary fibroblasts was determined by Alamar blue assay (Invitrogen). Briefly, cells were plated in a 96-well plate treated with or without L-Ala-L-Gln under the aforementioned hypoxic conditions for 48h. The interaction of Alamar blue with the cells was monitored for 4h by fluorescence readings at 540nm (excitation wavelength) and 585nm (emission wavelength).

Cell death assay

The effect of L-Ala-L-Gln on cell death of hypoxic fibroblasts was determined by Annexin V/ 7-AAD (BD Pharmingen) using flow cytometry. For the cell death assay, adherent fibroblasts were cultured under hypoxic conditions and treated with and without L-Ala-L-Gln at various concentrations. Cells were collected after 48h, washed, stained with Annexin V and 7-AAD, and analyzed by flow cytometry.

Western blotting

Protein samples were prepared by resuspending cells growing in 6-well plates in RIPA lysis and extraction buffer (Thermo) containing protease and phosphatase inhibitors (Roche). Protein concentration was quantified using the Bradford protein assay dye reagent (Bio-Rad). Samples were denatured by boiling at 95°C for 6 minutes in 4X LDS Sample buffer (Thermo), and 25µg total proteins were loaded and resolved in 4-15% Mini protean TGX gels (Bio-Rad). Proteins were then transferred to 0.2µm nitrocellulose membranes using Trans-Blot® Turbo™ Transfer System (Bio-Rad). Membranes were blocked with 5% Non-Fat dry milk and incubated overnight with primary antibodies.

The following primary antibodies were used: anti-collagen I (1:500; ab34710) and anti-collagen IV (1:500; ab6586), Abcam; anti-heat shock protein 47 (HSP-47) (1:400; sc-13150 and anti-fibronectin (1:500; sc-8422), Santa Cruz Biotechnology; anti-SMAD 2/3 (1:500; 85865S), anti-GAPDH (1:5000; 97166S) and anti-HIF-1α (1:750; 14179S), Cell Signaling Technology.

The nitrocellulose membranes were then incubated with the corresponding horseradish peroxidase-conjugated secondary antibodies (1:5000 for 1 hour), rinsed, and exposed to the Pierce™ ECL Plus Western Blotting Substrate (Thermo). The chemiluminescent signal was then detected on the ChemiDoc Imaging Systems (Bio-Rad).

Immunofluorescence

For immunofluorescence microscopy, cells were grown on 4-well chamber slides (IBIDI) under appropriate hypoxic conditions with or without L-Ala-L-Gln treatment. Cells were washed with ice-cold PBS followed by fixation with 4% paraformaldehyde. Fixed cells were permeabilized and incubated with blocking reagent (1% BSA in PBS) for 30 minutes, prior to overnight incubation with appropriate primary antibodies. After washing steps, slides were labelled and incubated with secondary antibodies. Nuclei were stained with 4'-6-diamino-2-phenylindole, dihydrochloride (DAPI, Sigma).

Fluorescence microscopy image analysis was performed using NIKON Ti2 inverted microscope equipped with Photometrics Prime 95B camera for fluorescence imaging. All images were digitally processed, all quantifications and further arrangements for the presentation were performed using NIS-Elements Advanced Research analysis

software. For quantification analysis, pictures from random fields in independent wells were taken at 10X and 40X magnification objectives and the total protein expression for each marker was determined in reference to the total number of cells based on DAPI quantification.

For immunofluorescence staining, the following primary antibodies were used: anti-collagen I (1:500; ab34710), anti-collagen IV (1:500; ab6586) and anti- α -SMA (1:500; ab124964), Abcam; anti-HSP-47 (1:250; sc-13150), anti-fibronectin (1:250; sc-8422), and anti-HIF-1 α (1:500; sc-13515), Santa Cruz Biotechnology; anti-SMAD 2/3 (1:500; 85865S), Cell Signaling Technology. After washes, fixed cells were incubated with the corresponding species-specific Alexa-Fluor (AF) conjugated secondary antibodies (1:500 for 1 hour), namely goat anti-mouse AF 488 (A11029), goat anti-mouse AF546 (A11030), goat anti-rabbit AF488 (A11034) and goat anti-rabbit AF546 (A11010) from Life Technologies. Nuclei were stained with DAPI (D9564) from Sigma at a concentration of 0.5 μ g/ml.

Sample preparation for Phosphoproteomics Analysis

Following fibroblast isolation from sciatic nerves of rats, (8E10 primary fibroblasts) were lysed in 80 μ l of 8M Urea, 0.1M ammonium bicarbonate, phosphatase inhibitors (Sigma P5726&P0044) by sonication (Bioruptor, 10 cycles, 30 seconds on/off, Diagenode, Belgium) and proteins were digested as described previously (103). Shortly, proteins were reduced with 5 mM TCEP for 60 min at 37 °C and alkylated with 10 mM chloroacetamide for 30 min at 37 °C. After diluting samples with 100 mM ammonium bicarbonate buffer to a final urea concentration of 1.6M, proteins were digested by incubation with sequencing-grade modified trypsin (1/50, w/w; Promega, Madison, Wisconsin) for 12 h at 37°C. After acidification using 5% TFA, peptides were desalted using C18 reverse-phase spin columns (Macrospin, Harvard Apparatus) according to the manufacturer's instructions, dried under vacuum and stored at -20°C until further use.

Peptide samples were enriched for phosphorylated peptides using Fe (III)-IMAC cartridges on an AssayMAP Bravo platform. Phospho-enriched peptides were resuspended in 0.1% aqueous formic acid and subjected to LC-MS/MS analysis using a Q-Exactive plus mass spectrometer fitted with an EASY-nLC 1000 (both Thermo Fisher Scientific) and a custom-made column heater set to 60°C. Peptides were resolved using a RP-HPLC column (75 μ m \times 30cm) packed in-house with C18 resin

(ReproSil-Pur C18–AQ, 1.9 μm resin; Dr. Maisch GmbH) at a flow rate of 0.2 $\mu\text{L}/\text{min}$. The following gradient was used for peptide separation: from 5% B to 8% B over 5 min to 20% B over 45 min to 25% B over 15 min to 30% B over 10 min to 35% B over 7 min to 42% B over 5 min to 50% B over 3 min to 95% B over 2 min followed by 18 min at 95% B. Buffer A was 0.1% formic acid in water and buffer B was 80% acetonitrile, 0.1% formic acid in water.

Mass spectrometry analysis was performed on Q-Exactive plus mass spectrometer equipped with a Nano electrospray ion source (both Thermo Fisher Scientific). Each MS1 scan was followed by high-collision-dissociation (HCD) of the 10 most abundant precursor ions with the dynamic exclusion for 20 seconds. The total cycle time was approximately 1 s. For MS1, 3×10^6 ions were accumulated in the Orbitrap cell over a maximum time of 100 ms and scanned at a resolution of 70,000 FWHM (at 200 m/z). MS2 scans were acquired at a target setting of 1×10^5 ions, accumulation time of 50 ms and a resolution of 17,500 FWHM (at 200 m/z). Singly charged ions and ions with unassigned charge states were excluded from triggering MS2 events. The normalized collision energy was set to 27%, the mass isolation window was set to 1.4 m/z and one Microscan was acquired for each spectrum.

The acquired raw files were imported into the Progenesis Q1 software (v2.0, Nonlinear Dynamics Limited), which was used to extract peptide precursor ion intensities across all samples applying the default parameters. The generated mgf-files were searched using MASCOT against a decoy database containing normal and reverse sequences of the predicted (Proteomes) UniProt entries of *Rattus norvegicus* (www.uniprot.org, release date 2020/03/10) and commonly observed contaminants (in total 60,690 sequences) generated using the SequenceReverser tool from the MaxQuant software (Version 1.0.13.13). The search criteria were set as follows: full tryptic specificity was required (cleavage after lysine or arginine residues, unless followed by proline); 3 missed cleavages were allowed; carbamidomethylation (C) was set as fixed modification; oxidation (M) and phosphorylation (STY) were applied as variable modifications; mass tolerance of 10 ppm (precursor) and 0.02 Da (fragments). The database search results were filtered using the ion score to set the false discovery rate (FDR) to 1% on the peptide and protein level, respectively, based on the number of reverse protein sequence hits in the datasets. Quantitative analysis results from

label-free quantification were processed using the SafeQuant R package v.2.3.2. , <https://github.com/eahrne/SafeQuant/>) to obtain peptide relative abundances. This analysis included global data normalization by equalizing the total peak/reporter areas across all LC-MS experiments data imputation using the k-nearest neighbours (knn) algorithm, summation of peak areas per and LC-MS/MS run, followed by calculation of peptide abundance ratios. Only isoform-specific peptide ion signals were considered for quantification. The summarized peptide expression values were used for statistical testing of between condition differentially abundant peptides. Here, empirical Bayes moderated t-Tests were applied, as implemented in the R/Bioconductor `limma` package (<http://bioconductor.org/packages/release/bioc/html/limma.html>) were used. The resulting per protein and condition comparison p-values were adjusted for multiple testing using the Benjamini-Hochberg method.

Statistical analysis

Statistical analysis was performed with Prism 7.0 software. Experimental data and graphical plots are expressed as the mean \pm standard deviation (SD) of a particular experiment out of at least 3 independent experiments including 3 biological replicates unless otherwise mentioned. Statistical significance of various conditions was characterized by the Student t-test or one-way ANOVA. For multiple comparisons, we used Sidak's multiple comparisons test and statistical significance was considered for P values <0.05 . Statistically significant values are shown with their degree significance - * ($p<0.05$), ** ($p<0.01$), ***($p<0.001$) and ****($p<0.0001$).

Materials and Methods (Chapter: *Pirfenidone*)

Animals

Animals used for sciatic nerve collection were surplus adult Sprague-Dawley rats provided by the local animal facility, Department of Biomedicine, University Hospital Basel, University of Basel. Rats were euthanized in a CO₂ gas chamber by trained personnel under the animal facility husbandry license 1007H.

Isolation and culture of primary rat fibroblasts

Adult Sprague-Dawley rats were *euthanized* by using a CO₂ gas chamber and sciatic nerves were dissected out immediately under aseptic conditions and placed in ice-cold Dulbecco's Phosphate Buffered Saline (DPBS) (Sigma-Aldrich). Each adult sciatic nerve was cleaned off excess tissue including muscle, fat and blood vessels while working under a Stereo dissecting microscope (Carl Zeiss Microscopy GmbH, Germany). Subsequently, the epineurium was stripped off using fine forceps. Nerve segments were then dissected into small sections (2-5mm) and 5-6 segments were transferred to 6-well plates containing culture medium consisting of Dulbecco's Modified Eagle Medium (DMEM) (Gibco) supplemented with 10% fetal bovine serum (FBS) (Biological Industries) and 1% penicillin/streptomycin (Gibco) for 12-14 days. The medium was replaced every 2-3 days. Primary fibroblasts sprouted from the nerve tissues (Figure 4A) and once cells approached 70% confluency, tissue segments were removed from the 6-well plates with forceps. Cells were washed twice with ice-cold PBS to remove tissue debris, trypsinized with 0.25% Trypsin (Gibco), followed by centrifugation at 1800 rpm for 5 minutes. Cells were counted using Trypan blue and plated in T25/ T75 culture flasks (Corning) for further experimentation. Prior to experimentation, all cells isolated were stained for α -SMA, HSP47, Vimentin and Phalloidin to confirm the phenotype of these cells (Figure 4B). All experiments with primary rat fibroblasts were performed from passages 1-5.

Cell Line

The Human foreskin fibroblast cell line (BJ (ATCC® CRL2522™)) was purchased from ATCC. CRL2522 cells were cultured according to the instructions from ATCC. Briefly, cells were maintained in ATCC-formulated Eagle's Minimum Essential Medium (ATCC 30-2003) supplemented with 10% fetal bovine serum (FBS) (Biological Industries) and 1% penicillin/streptomycin (Gibco). Cell cultures were maintained at 37°C in a

humidified atmosphere containing 5% CO₂. The medium was changed every 2 days until the culture reached 80% confluence. After reaching confluency, cells were washed twice with ice-cold PBS, trypsinized with 0.25% Trypsin (Gibco), followed by centrifugation at 1800 rpm for 5 minutes. Cells were counted using Trypan blue and plated in T25/ T75 culture flasks (Corning) for further experimentation.

The Rat Schwann cell line (FR (ATCC® CRL2943™)) was purchased from ATCC. CRL2943 cells were cultured according to the instructions from ATCC. Briefly, cells were maintained in ATCC-formulated Dulbecco's Modified Eagle's Medium (ATCC 30-2002) supplemented with 10% fetal bovine serum (FBS) (Biological Industries) and 1% penicillin/streptomycin (Gibco). Cell cultures were maintained at 37°C in a humidified atmosphere containing 5% CO₂. The medium was changed every 2 days until the culture reached 80% confluence. After reaching confluency, cells were washed twice with ice-cold PBS, trypsinized with 0.25% Trypsin (Gibco), followed by centrifugation at 1800 rpm for 5 minutes. Cells were counted using Trypan blue and plated in T25/ T75 culture flasks (Corning) for further experimentation.

Hypoxia and Pirfenidone treatment

In order to mimic the hypoxic micro-environment, primary rat fibroblasts and human fibroblast cell line were exposed to hypoxia. Cells were incubated in a hypoxic chamber (2% oxygen) for 48h and treated with or without PFD and no restoration to normoxia. Cells were collected and processed for experiments subsequently (Figure 4D). Solutions of PFD (Roche Pharmaceuticals, Basel, Switzerland) were prepared fresh for each experiment by dissolving the powder in molecular grade water (Merck Millipore) at 1.25 mg/ml, warmed to 37°C before diluting into culture media for treatment.

TGF-β1 activation and Pirfenidone treatment

Under chronic inflammation, fibroblasts get differentiated into myofibroblasts. Myofibroblasts are the key effector cells in tissue fibrosis and plays a major role in regulating ECM deposition and scarring. During fibrosis, fibroblasts get differentiated into myofibroblasts and the TGF-β1 signaling is key to this process. In order to mimic this differentiated state *in vitro*, we activated primary rat fibroblasts and/ or human cell line externally. Cell cultures were maintained as described earlier. To create cultures

of activated and differentiated fibroblasts, primary rat fibroblasts or human fibroblast cell line were serum starved in culture media containing 1% FBS (Biological Industries) for 24h and then treated with 1, 2.5, 5 and 10ng/ml TGF- β 1 (Human TGF- β 1; Catalog 100-21 Peprotech, New Jersey) for 48h. Following activation of fibroblasts with TGF- β 1, cells were treated with or without various concentrations of PFD for subsequent experiments (Figure 4D). Solutions of PFD were prepared as described earlier. 1, 2.5, 5 and 10ng/ml TGF- β 1 concentrations were initially used to identify and optimize the activation window (described in the **Results** section). Following optimization, we finalized 10ng/ml TGF- β 1 for further experiments.

Proliferation assays

Proliferation of primary rat fibroblasts were determined by Alamar blue assay (Invitrogen). Briefly, cells were plated in a 96-well plate treated with or without PFD under aforementioned hypoxic/ TGF- β 1 conditions for 48h. Followed by this we analyzed the interaction of Alamar blue with the cells for 4h by measuring fluorescence readings at 540nm and 585nm respectively.

To further confirm our observations, we detected proliferation using flow cytometry based EdU assay using EdU-Click 488 (baseclick) and the CellTiter-Glo assay, CTG reagent (Promega, G7572).

For the flow cytometry based EdU assay, primary rat fibroblasts were cultured under the presence of hypoxia/ TGF- β 1 conditions and treated with/ without PFD for 48h. Cells were incubated with 10 μ M EdU for 2 h. After trypsinization 0.5 X 10⁶ cells were stained using EdU-Flow cytometry 488 Kit (Base-Click, BCK-FC488-100) following manufacturer's instruction. Prior to FACS acquisition cells were fixed in 4% Paraformaldehyde in PBS, permeabilized in 1x saponin-based permeabilization buffer and incubated with click assay cocktail for 30 min. 50,000 cells/sample were analyzed by flow cytometry.

For the CellTiter-Glo assay, cells were plated in an opaque-walled 96-well plate treated with or without PFD under aforementioned hypoxic/ TGF- β 1 conditions for 48h. The CTG reagent was mixed in a 1:1 ratio with the supernatant from the treated/

control wells. The mix was placed in a shaker and incubated at room temperature for 10 min. Following incubation, luminescence measurement was performed.

Schwann cells were loaded prior to exposure to normoxic/ hypoxic conditions with the cell proliferation dye carboxyfluorescein succinimidyl ester (CFSE) (#C34554, Thermo) according to manufacturer's instructions. Subsequently, cells were washed, resuspended in indicated media and exposed to normoxic/ hypoxic conditions. Proliferation was assessed 5 days after hypoxic injury using flow cytometry. All flow data were acquired on a CytoFLEX flow cytometer (Beckman Coulter) and analyzed using Flowjo 10.3 (Tree Star) unless otherwise indicated.

Cell Death assays

10,000 cells were plated in a 96-well plate treated with or without PFD under aforementioned hypoxic/ TGF- β 1 conditions for 48h. Caspase-Glo® 3/7 Assay reagent (100 μ l) (Promega), prepared according to the Caspase-Glo® 3/7 Assay Technical Bulletin TB323, was added to each well; plates were briefly shaken and incubated at room temperature for 30 minutes. Caspase-Glo® 3/7 luminescent signal was read on the luminometer.

The effect of PFD on cell death of normal fibroblasts was determined by Annexin V/ 7-AAD (BD Pharmingen) using flow cytometry. For the cell death assay, adherent fibroblasts were cultured under culture conditions (mentioned above) and treated with and without PFD at various concentrations. Cells were collected after 48h, washed, stained with Annexin V and 7-AAD, and analyzed by flow cytometry.

Enzyme-Linked Immunosorbent Assay (ELISA)

Primary rat fibroblasts were seeded into 24-well plates (Corning). Following starvation, 0.1×10^6 cells were activated with TGF- β 1 or exposed under hypoxic conditions. Hypoxic fibroblasts/ TGF- β 1 activated fibroblasts were treated with/ without PFD for 48 h. Cell culture supernatants of all the samples were collected after centrifugation @1800 rpm for 5 min and stored for ELISA at -80°C. Subsequently, supernatants were analyzed and the concentrations of TGF- β 1 was measured using the TGF- β 1 Rat LAP ELISA kit (Invitrogen) according to the manufacturer's instructions.

Western blotting

Primary rat fibroblasts and human fibroblast cells were seeded at 1×10^6 cells/ well into 6-well cell culture treated plates (Corning). Following starvation and cells were either exposed to hypoxia or activated with TGF- β 1 and treated with/ without PFD for 48 h at desirable concentrations. Whole cell lysate was collected after PFD treatment for 48 h. RIPA buffer including protease and phosphatase inhibitors (Roche) was added to cultures on ice. Lysate was clarified by centrifugation @14000 rpm for 10 min at 4°C. Samples were either stored at -80°C or used immediately. Total protein concentration in each lysate was determined by protein assay dye reagent (Bio-Rad). Samples were mixed with 4X LDS Sample buffer (Thermo) and denatured by boiling at 95°C for 6 minutes. Following protein concentration estimations, equal protein samples containing 25 μ g total protein were loaded and resolved in 4-15% Mini protean TGX gels (Bio-Rad). Fractionated proteins were transferred to 0.2 μ m nitrocellulose membranes using Trans-Blot® Turbo™ Transfer System (Bio-Rad). Membranes were blocked with 5% Non-Fat dry milk and incubated overnight with primary antibodies. Horseradish peroxidase-conjugated secondary antibodies were used for immunoreactivity and detection of protein bands were done using Pierce™ ECL Plus Western Blotting Substrate (Thermo) and on the ChemiDoc Imaging Systems (Bio-Rad).

The primary antibodies and their respective concentrations used in the Western blotting is as follows. Anti-collagen-I (Collagen-I) (1:500; ab34710), anti-collagen-IV (Collagen-IV) (1:500; ab6586), anti-HIF-1 α (1:500; ab51608) and anti-alpha smooth muscle actin (α -SMA) (1:1000; ab124964) were purchased from Abcam. Anti-heat shock protein 47 (HSP-47) (1:500; sc-13150) and anti-fibronectin (1:400; sc-8422), were ordered from Santa Cruz Biotechnology. Other antibodies including anti-SMAD 2 (1:1000; 5339S), anti-pSMAD 2 (1:500; 3108S), anti-SMAD 3 (1:1000; 9513S), anti-pSMAD 3 (1:500; 9520S), anti-Cleaved Caspase 3 (1:1000; 9664L), anti-AKT (1:1000; 9272S), anti-pAKT (1:500; 2965S), anti-PI3Kinase (1:750; 4249S) and anti-GAPDH (1:5000; 97166S) were from Cell Signaling Technology.

Subsequently, the following secondary antibodies were used: HRP donkey anti-rabbit IgG (#AP182P, Merck Millipore) and HRP goat anti-mouse IgG (#31432, Thermo). Both secondary antibodies were used at a concentration of 1:5000.

Immunostaining

Differentiation of fibroblasts to myofibroblasts causes major changes to morphological features of these cells. Therefore, we wanted to image differentiated fibroblasts and compare the morphological changes with undifferentiated fibroblasts. In order to create cultures with visibly separable cells, primary rat fibroblasts were grown on 4-well chamber slides (IBIDI) under appropriate hypoxic/ TGF- β 1 conditions and treated with or without PFD at various desirable concentrations. Samples were collected after 48 h treatment and fixed with 4% paraformaldehyde. Fixed cells were permeabilized with 0.5% Triton X-100 and incubated with blocking reagent (1% BSA in PBS) for 30 minutes, prior to overnight incubation with appropriate primary antibodies. After wash steps, cultures were labelled and incubated with secondary antibodies and 4'-6-diamidino-2-phenylindole, dihydrochloride (DAPI, Sigma) were used to stain the nuclei.

The primary antibodies and their respective concentrations used in the immunofluorescence imaging is as follows. Anti-collagen-I (Collagen-I) (1:400; ab34710), anti-collagen-IV (Collagen-IV) (1:300; ab6586) and anti-alpha smooth muscle actin (α -SMA) (1:500; ab124964) were purchased from Abcam. Anti-heat shock protein 47 (HSP-47) (1:250; sc-13150) and anti-fibronectin (1:250; sc-8422), were ordered from Santa Cruz Biotechnology.

Subsequently, the following secondary antibodies were used at a concentration of 1:500. Goat anti-rabbit AF488 (A11034); Goat anti-mouse AF546 (A11030); Goat anti-rabbit AF546 (A11010) and Goat anti-mouse AF488 (A11029). All secondary antibodies were purchased from Life Technologies.

Fluorescence microscopy image analysis was performed using NIKON Ti2 inverted microscope equipped with Photometrics Prime 95B camera for fluorescence imaging. All images were digitally processed, all quantifications and further arrangement for presentation was done using NIS-Elements Advanced Research analysis software. For quantification analysis, pictures from random fields in independent wells were taken at 10X and 40X magnification objectives and the total protein expression for each marker was determined in reference to the total number of cells based on DAPI quantification. All experiments were conducted in biological triplicates. We used primary fibroblasts isolated from different rats for every replicate.

RNA Isolation

Primary rat fibroblasts were cultured as described earlier. 0.5×10^6 cells were used per treatment group. For every treatment at least 3 independent experiments including 3 biological replicates were performed unless otherwise mentioned. Each experiment was performed using primary rat fibroblasts isolated from different rats. RNA was isolated from cell lysate collected using TRIzol™ reagent (Ambion). Following homogenization in the TRIzol reagent, phase separation was conducted with chloroform (1/5 volume of TRIzol reagent). Phase separation was followed by RNA precipitation using isopropanol and RNA elution with 30 µl molecular grade water (Merck Millipore). RNA concentration was measured with a NanoDrop 2000 spectrophotometer (ThermoFisher Scientific) and stored at -80°C .

RNA Sequencing

Total RNA was extracted from 0.5×10^6 primary rat fibroblasts. We used 3 biological triplicates per condition. These triplicates included primary fibroblasts isolated from sciatic nerves from 3 different rats. RNA was extracted using TRIzol reagent and cleaned up with RNeasy Mini Kit (Qiagen) following manufacturer's instructions. Residual genomic DNA was removed from all the samples using DNase (Thermo). RNA concentration was measured with a NanoDrop 2000 spectrophotometer (Thermo) and stored at -80°C for further use. Purity and integrity of RNA from all samples were assessed on a Fragment BioAnalyzer System (Advanced Analytical Technologies). RNA concentration was recalculated using Quant-iT RiboGreen RNA Assay Kit (Thermo). Purification of poly(A)-containing mRNA, mRNA fragmentation and cDNA library preparation for RNA-Seq were performed using the TruSeq Stranded mRNA LT Sample Preparation kit (Illumina) according to the manufacturer's protocol. cDNA libraries were sequenced as single-end reads with 75 cycles on a NextSeq 500 sequencing system (Illumina) at the Genomics Facility, University of Basel, Switzerland.

For data analysis, sequencing reads were submitted to adapter and quality trimming by Trimmomatic to remove technical sequences like Illumina-specific sequencing adapters and low-quality bases. The TopHat2 spliced alignment software and its underlying mapping engine Bowtie2 were used to align the reads to the human reference genome, thereby creating binary 75 alignment map (BAM) files. BAM files were sorted and indexed using SAMtools. and then visualized in the UCSC Genome Browser. Counting of reads that map to each genomic feature was done with the

'Summarize Overlaps' function from the GenomicAlignments package in R. Genes differentially expressed between TNV and TEM cells were identified with the R package DESeq2.

Quantitative Real-Time PCR

The RNA sequencing results for major pro-fibrotic and ECM deposition factors were validated by quantitative real time-polymerase chain reaction (qPCR). RNA samples from isolated primary fibroblasts as described above that were not included in the RNA sequencing analysis (500 pg per sample, $n = 3$ animals for normal untreated, $n = 3$ for HI per time point, respectively). RNA (1 μ g) was reverse-transcribed with the QuantiTect Reverse Transcription Kit (Qiagen), and qPCR was performed in triplicates using Fast SYBR Green MasterMix (Roche) on a LightCycler 480 (Roche). Primers for α -SMA, TGF- β 1, Collagen Type I Alpha 1 Chain (COL1A1), Collagen Type IV Alpha 1 Chain (COL4A1) and Fibronectin (FBN) were designed using Primer-BLAST (<https://www.ncbi.nlm.nih.gov/tools/primer-blast/>). The entire list of primers can be accessed ([Table 2](#)). All samples were analysed concurrently in one experiment. Runs were normalized to the housekeeping gene GAPFH by measuring Δ CT. The $2^{-\Delta\Delta$ CT method was used for the calculation of the desired target gene fold change (FC) of the TGF- β 1 activated fibroblasts vs. PFD treated fibroblasts group.

Proteomics

Following primary fibroblast isolation from sciatic nerves of rats, (1×10^6 cells/condition) were lysed in 80 μ l of 8M Urea, 0.1M ammonium bicarbonate, phosphatase inhibitors (Sigma P5726&P0044) by sonication (Bioruptor, 10 cycles, 30 seconds on/off, Diagenode, Belgium) and proteins were digested as described previously (103). Shortly, proteins were reduced with 5 mM TCEP for 60 min at 37 °C and alkylated with 10 mM chloroacetamide for 30 min at 37 °C. After diluting samples with 100 mM ammonium bicarbonate buffer to a final urea concentration of 1.6M, proteins were digested by incubation with sequencing-grade modified trypsin (1/50, w/w; Promega, Madison, Wisconsin) for 12 h at 37°C. After acidification using 5% TFA, peptides were desalted using C18 reverse-phase spin columns (Macrospin, Harvard Apparatus) according to the manufacturer's instructions, dried under vacuum and stored at -20°C until further use.

Sample aliquots comprising 10 µg of peptides were labeled with isobaric tandem mass tags (TMT 16-plex, Thermo Fisher Scientific). Peptides were resuspended in 20 µl labeling buffer (2 M urea, 0.2 M HEPES, pH 8.3) by sonication and 2.5 µl of each TMT reagent were added to the individual peptide samples followed by a 1 h incubation at 25°C shaking at 500 rpm. To control for ratio distortion during quantification, a peptide calibration mixture consisting of six digested standard proteins mixed in different amounts was added to each sample before TMT labeling (for details, please refer to 107). To quench the labelling reaction, 0.75 µl aqueous 1.5 M hydroxylamine solution was added and samples were incubated for another 15 min at 25°C shaking at 500 rpm followed by pooling of all samples. The pH of the sample pool was increased to 11.9 by adding 1 M phosphate buffer (pH 12) and incubated for 20 min at 25°C shaking at 500 rpm to remove TMT labels linked to peptide hydroxyl groups. Subsequently, the reaction was stopped by adding 2 M hydrochloric acid until a pH <2 was reached. Finally, peptide samples were further acidified using 5% TFA, desalted using Sep-Pak Vac 1cc (50 mg) C18 cartridges (Waters) according to the manufacturer's instructions and dried under vacuum.

TMT-labeled peptides were fractionated by high-pH reversed phase separation using a XBridge Peptide BEH C18 column (3,5 µm, 130 Å, 1 mm x 150 mm, Waters) on an Agilent 1260 Infinity HPLC system. Peptides were loaded on column in buffer A (20 mM ammonium formate in water, pH 10) and eluted using a two-step linear gradient from 2% to 10% in 5 minutes and then to 50% buffer B (20 mM ammonium formate in 90% acetonitrile, pH 10) over 55 minutes at a flow rate of 42 µl/min. Elution of peptides was monitored with a UV detector (215 nm, 254 nm) and a total of 36 fractions were collected, pooled into 12 fractions using a post-concatenation strategy as previously described (104) and dried under vacuum.

Dried peptides were resuspended in 0.1% aqueous formic acid and subjected to LC-MS/MS analysis as described above with a few modifications and using a Q-Exactive HF instrument. In brief, the gradient used for TMT-labeled peptide separation started from 5% B to 15% B over 10 min to 30% B over 60 min to 45 % B over 20 min to 95% B over 2 min followed by 18 min at 95% B. Buffer A was 0.1% formic acid in water and buffer B was 80% acetonitrile, 0.1% formic acid in water. For MS1 analysis, a higher resolution of 120,000 FWHM (at 200 m/z) was used. For MS2 analysis, a smaller mass isolation window of 1.1 m/z, a higher normalized collision energy of 35%, a higher

resolution of 30,000 FWHM (at 200 m/z), fill time of 100 ms and a first mass setting of 110 m/z were applied.

The acquired raw-files were analysed using the SpectroMine software (Biognosis AG, Schlieren, Switzerland). Spectra were searched against the same rat protein database used above for phosphoproteomics analysis. Standard Pulsar search settings for TMT (“TMTpro_Quantification”) were used and resulting identifications and corresponding quantitative values were exported on the PSM level using the “Export Report” function. Acquired reporter ion intensities in the experiments were employed for automated quantification and statistical analysis using our in-house developed SafeQuant R script (v2.3) (103) as described above.

Statistical Analysis

Collected data was analyzed for statistical significance and conclusive evidence by plotting the data using GraphPad Prism (GraphPad Software, Inc., San Diego). For image analysis, mean cell intensity measurements were calculated using the NIS elements software. For image analysis, we took 6-12 independent images per treatment group. All experiments were conducted using biological triplicates. Statistical significance of various conditions was characterized by the Student t-Test or one-way ANOVA. For multiple comparisons, we used Sidak’s multiple comparisons test and statistical significance was considered for P values <0.05. Statistically significant values are shown with their degree significance - * (p<0.05), ** (p<0.01), ***(p<0.001) and ****(p<0.0001).

Results (Chapter: *L-Ala-L-Gln*)

***L-Ala-L-Gln* does not affect cell proliferation and viability of hypoxic primary fibroblasts**

Hypoxia being a primary microenvironment in fibrotic tissues, we performed all our *in vitro* analysis using primary rat perineurium derived fibroblasts exposed to hypoxic conditions. To investigate whether *L-Ala-L-Gln* treatment affects the viability of primary rat fibroblasts, we examined viability over 48h using the Alamar Blue assay. Our *in vitro* analysis showed that, *L-Ala-L-Gln* does not affect the viability and cell proliferation of hypoxic primary rat fibroblasts. None of the concentrations including 1mM, 10mM and 100mM induced any significant changes on cell viability and proliferation. Compared with the untreated controls, primary rat fibroblasts exposed under continuous (48h) and episodic (2h) hypoxia exhibited no change in cell proliferation when treated with *L-Ala-L-Gln* under various concentrations Figure 5 (A-D).

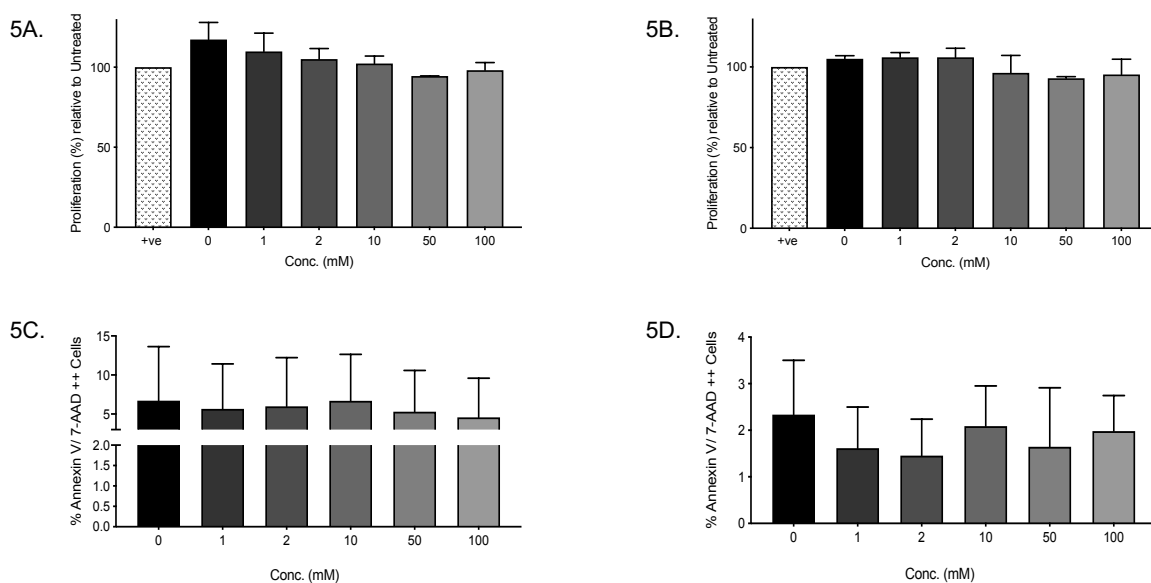


Figure 5: *L-Ala-L-Gln* does not affect cell proliferation and cell death of hypoxic primary rat fibroblasts

Primary Rat fibroblasts were treated with *L-Ala-L-Gln* under different hypoxic conditions and treated with various concentrations of *L-Ala-L-Gln* for 48h. Cell proliferation was estimated with Alamar Blue (Thermo) assay as described in the

methods section. Cell death was characterized by the Annexin V 7AAD Apoptosis assay as described in the methods section. Cells under normoxic conditions were used as positive control and proliferation of hypoxic cells was calculated relative to the normoxic controls. **A, C.** Cells were under Continuous Hypoxia (2% O₂ for 48h). **B, D.** Cells were under Episodic hypoxia (2% O₂ for 48h).

Abbreviations: 7AAD - 7-Aminoactinomycin D; L-Ala-L-Gln - L-Alanyl-L-glutamine

L-Ala-L-Gln down regulates expression of fibrotic proteins of primary fibroblasts exposed under Continuous Hypoxia

Hypoxia increases expression of pro-fibrotic and adhesion biomarkers in fibrotic diseases. To determine whether L-Ala-L-Gln induces any change on hypoxic microenvironment, we tested the expression of HIF-1- α , under the treatment of various concentration of L-Ala-L-Gln. Western blotting of whole cell lysates of hypoxic primary fibroblasts showed that L-Ala-L-Gln significantly down regulates markers involved with induction of hypoxic microenvironment, HIF-1 α and SMAD 2/3 (Figure 6A). HIF-1 α was significantly down regulated upon treatment with L-Ala-L-Gln at concentration of 1mM, 10mM and 100mM. We did not observe a dose-dependent downregulation of HIF-1- α . Interestingly, SMAD 2/3 was also significantly downregulated in hypoxic primary fibroblasts by 100 mM L-Ala-L-Gln only (Figure 6A).

Additionally, we further investigated the effect of L-Ala-L-Gln on other pro-fibrotic factors. We observed that continuous hypoxia for 48h induces the expression of pro-fibrotic markers including Collagen-IV, Collagen-I, and Fibronectin as compared to normoxic untreated controls. Treatment with L-Ala-L-Gln at 1mM, 10mM and 100mM significantly reduced the expression of these fibrotic proteins in a dose-dependent manner (Figure 6B). As HYP47 is another key pro-fibrotic factor responsible for collagen biosynthesis, we tested our hypothesis on HSP47 and found that L-Ala-L-Gln reduces expression of HSP47 but we did not observe a significant downregulation (Figure 6B).

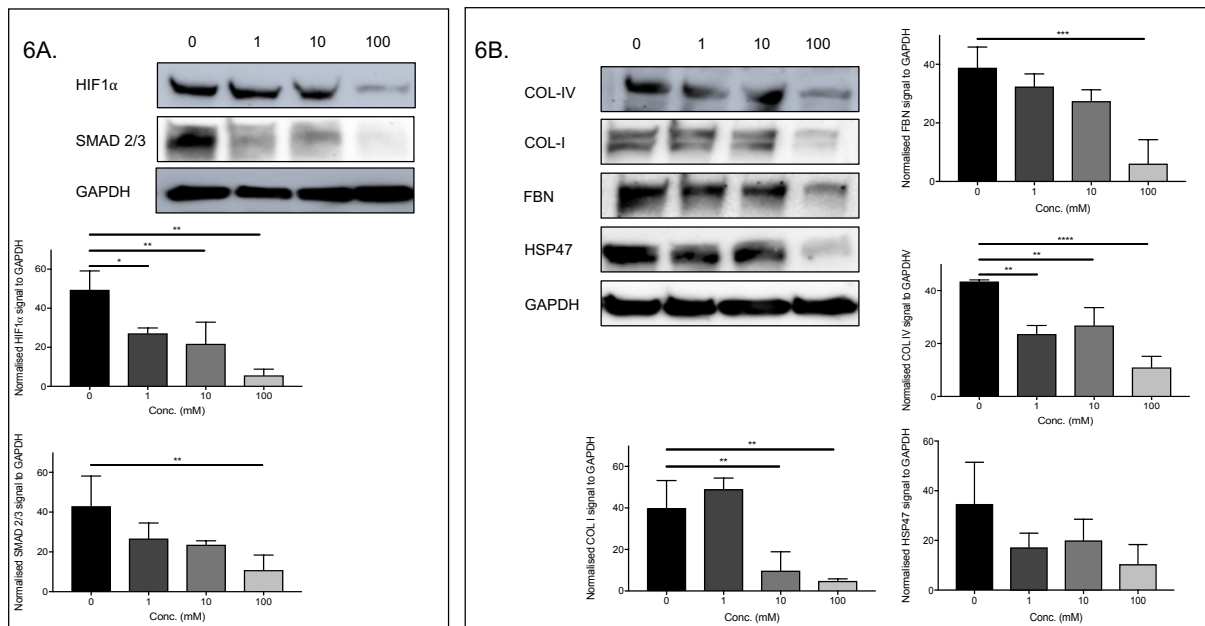


Figure 6: L-Ala-L-Gln reduces expression of HIF-1A and pro-fibrotic factors involved with PNF.

Primary Rat fibroblasts were treated with L-Ala-L-Gln under Continuous Hypoxia (2% oxygen for 48h) for 48h. **A.** Representative Western blot visualization of proteins involved in HIF-1A signaling in Primary Rat fibroblasts exposed under Continuous Hypoxia (2% oxygen) for 48h with 1mM, 10mM and 100mM L-Ala-L-Gln or not treatment (0mM). Below: Quantification of HIF-1A and SMAD 2/3 protein abundance by densitometry, normalized against GAPDH (n=2 independent experiments). **B.** Representative Western blot visualization of proteins involved with fibrosis disease progression. Primary Rat fibroblasts exposed under Continuous Hypoxia (2% oxygen) for 48h with 1mM, 10mM and 100mM L-Ala-L-Gln or not treatment (0mM). Below: Quantification of COL-I, COL-IV, FBN and HSP47 protein abundance by densitometry, normalized against GAPDH (n=2 independent experiments).

Abbreviations: COL-I – Collagen I; COL-IV – Collagen IV; FBN – Fibronectin; GAPDH - Glyceraldehyde 3-phosphate dehydrogenase; HIF-1A- Hypoxia-inducible factor 1-alpha; HSP47 – Heat shock protein 47; L-Ala-L-Gln - L-Alanyl-L-glutamine; PNF – Peripheral nerve fibrosis; SMAD 2/3 - Mothers against decapentaplegic homolog 2/3

To further confirm our findings, we performed immunofluorescence analysis of hypoxic primary fibroblast treated with or without L-Ala-L-Gln under various concentrations.

Our *in vitro* immunofluorescence analysis revealed that treatment with L-Ala-L-Gln resulted in a significant reduction of factors responsible for cellular response to hypoxia including HIF-1 α and SMAD 2/3 (Figure 7A, 7B and 7C; Supplementary Figure 1A). HIF-1 α and SMAD 2/3 were stained in the nuclei and both were downregulated upon treatment with L-Ala-L-Gln. In order to investigate our earlier hypothesis, we performed cytoplasmic staining of pro-fibrotic factors including Fibronectin, Collagen-IV, Collagen-I and HSP47. We found these targets were accumulating in hypoxic primary fibroblasts (Figure 7A, 7B, 7D and 7E; Supplementary Figure 1B) and correspondingly were significantly downregulated in L-Ala-L-Gln treated fibroblasts. Our statistical analysis revealed a dose-dependent downregulation of HIF-1- α , SMAD 2/3, Collagen-IV, and HSP47 in L-Ala-L-Gln treated fibroblasts (Figure 7A, 7C, 7D and 7E), but was significantly reduced in a non-dose dependent manner for Fibronectin and Collagen-I (Figure 7A and 7B). Further experiments to understand this regulation should be conducted to understand this behaviour of L-Ala-L-Gln in reducing factors involved with collagen biosynthesis.

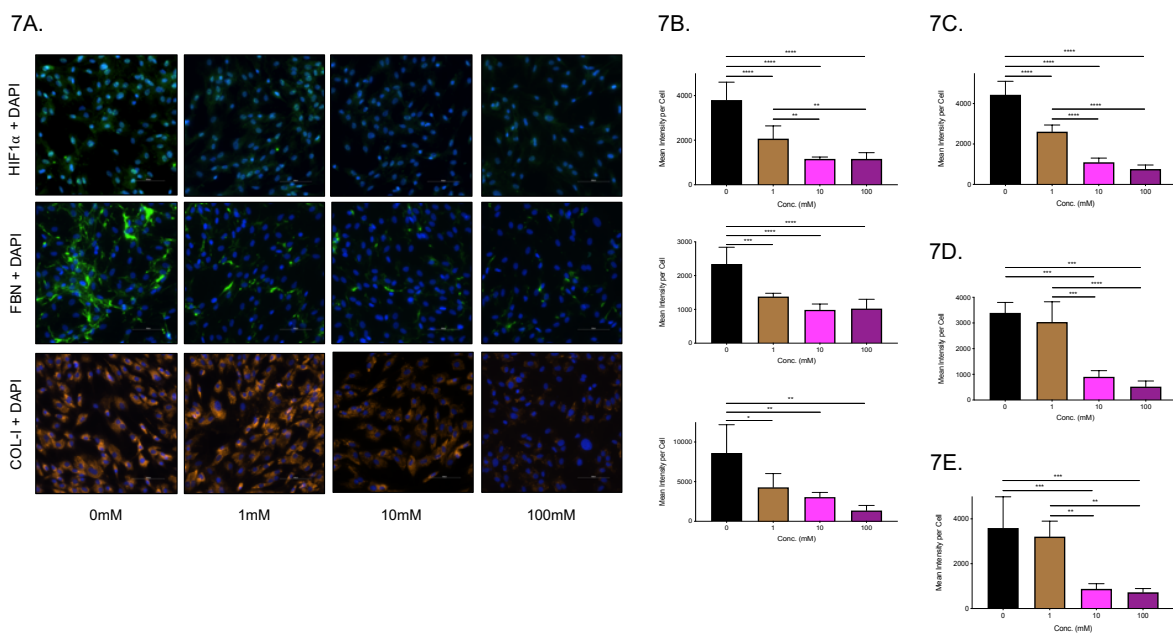


Figure 7: L-Ala-L-Gln reduces expression of pro-fibrotic markers in an *in-vitro* chronic hypoxic PNF model.

Hypoxic Primary Rat fibroblasts treated with different concentrations of L-Ala-L-Gln for 48h. Expression of HIF-1 α , FBN and COL-I was characterized by immunofluorescence imaging. **A**. Representative immunofluorescence images of HIF-1 α , FBN and COL-I staining. Nuclei were stained with DAPI. Original magnification, X40. Scale bar, 100

μm . **B.** Quantification data of HIF-1 α , FBN, COL-I, SMAD2/3, HSP47 and COL-IV expression using one-way ANOVA. Quantification data of **C.** SMAD2/3, **D.** HSP47 and **E.** COL-IV expression using one-way ANOVA. Results are shown as mean \pm SEM. * $p < 0.05$, ** $p < 0.01$, *** $p < 0.001$. Data are representative of 2 independent experiments. Please refer to **Supplementary Figure 1** for the immunofluorescence images of SMAD2/3, HSP47 and COL-IV staining. Results are shown as mean \pm SEM. * $p < 0.05$, ** $p < 0.01$, *** $p < 0.001$. Data are representative of 2 independent experiments.

Abbreviations: ANOVA - Analysis of variance; COL-I – Collagen I; COL-IV – Collagen IV; DAPI - 4',6-diamidino-2-phenylindole; FBN – Fibronectin; HIF-1A- Hypoxia-inducible factor 1-alpha; HSP47 – Heat shock protein 47; L-Ala-L-Gln - L-Alanyl-L-glutamine; PNF – Peripheral nerve fibrosis; SMAD 2/3 - Mothers against decapentaplegic homolog 2/3; SEM - Standard error of the mean

L-Ala-L-Gln down regulates expression of fibrotic proteins of primary fibroblasts exposed under Episodic Hypoxia

Overexpression of HIF-1 α in fibrotic tissues can generate chronic or acute hypoxic microenvironments. Owing to this, we tested the effects of L-Ala-L-Gln on pro-fibrotic factors in episodic hypoxic primary rat fibroblasts. We investigated the effect of L-Ala-L-Gln in hypoxic primary fibroblasts exposed to episodic hypoxia for 2h followed by treatment with or without L-Ala-L-Gln for 48h. (Figure 8) and (Figure 9).

We performed intracellular staining of specific targets responsible for fibrogenic potential as well as proteins regulated in HIF-1 α signalling. Our immunofluorescence analysis showed that L-Ala-L-Gln effectively reduces expression of pro-fibrotic proteins including Fibronectin, Collagen-I, Collagen-IV and HSP47 (Figure 8A, 8B, 8D and 8E; Supplementary Figure 2B). Significant downregulation of downstream targets of HIF-1 α signalling pathway namely HIF-1 α and SMAD 2/3 (Figure 8A, 8B, 8C; Supplementary 2A) in L-Ala-L-Gln were observed as well. Following immunocytochemistry, mean intensity per cell were calculated for these proteins in L-Ala-L-Gln treated samples and compared to untreated hypoxic samples. L-Ala-L-Gln significantly reduced expression of adhesion and fibrotic proteins in a dose-dependent

fashion. All above factors were significantly upregulated in hypoxic samples (Figure 8 B-E). We observed a dose-dependent downregulation of intra-expression of all the proteins except Collagen-I. Collagen I was found to be significantly reduced at 1mM L-Ala-L-Gln, but remained constant thereafter (Figure 8A, 8B; Supplementary 2B). To further confirm our findings, we performed Western blotting on whole cell lysates of episodic hypoxic primary fibroblasts. In contrast to immunocytochemistry, our Western analysis did not reveal any dose-dependent regulation of our desired targets. HIF-1 α signalling factors and pro-fibrosis mechanistic targets were significantly upregulated in hypoxic samples in comparison to L-Ala-L-Gln treated samples. We did not observe any significant downregulation across the various concentrations of L-Ala-L-Gln (Figure 9) Interestingly, we found significant downregulation of COL-IV in 1mM L-Ala-L-Gln treated hypoxic fibroblasts, which is slightly different from our immunofluorescence analysis (Figure 9 vs Figure 8E). Further experiments should be conducted to identify regulation of collagen biosynthesis to understand these subtle differences.

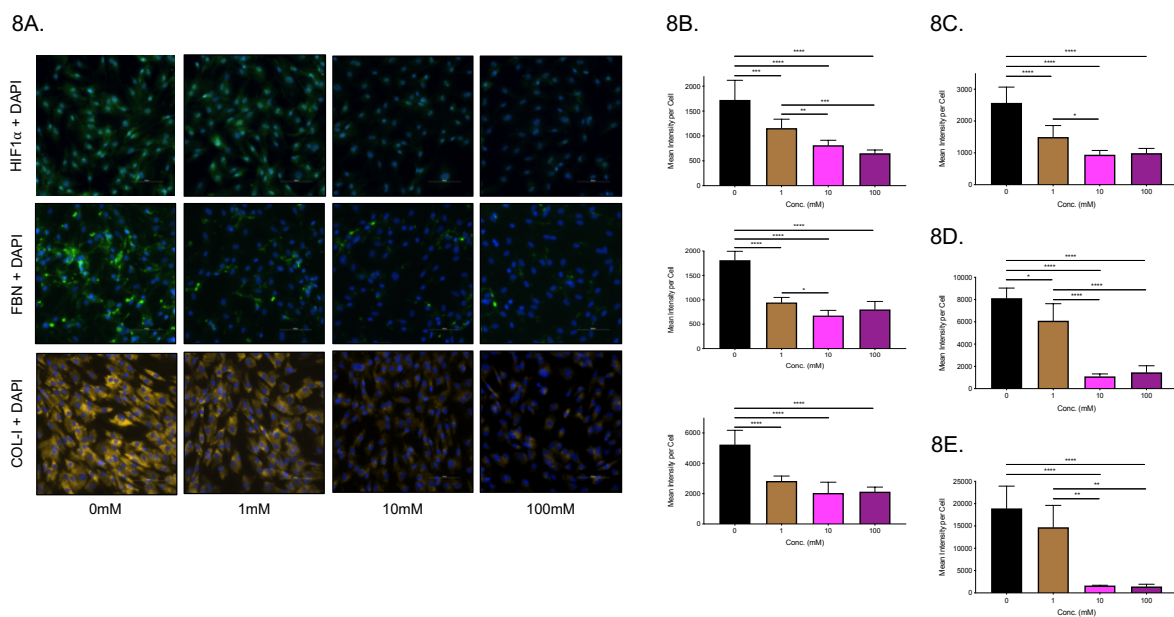


Figure 8: L-Ala-L-Gln reduces expression of pro-fibrotic markers in an *in-vitro* acute hypoxic PNF model.

Episodic hypoxic (2% O₂ for 2h) Primary Rat fibroblasts were treated with different concentrations of L-Ala-L-Gln for 48h. Expression of HIF-1 α , FBN, COL-I, SMAD2/3, HSP47 and COL-IV was characterized by immunofluorescence imaging. **A.**

Representative immunofluorescence images of HIF-1 α , FBN and COL-I staining. Nuclei were stained with DAPI. Original magnification, X40. Scale bar, 100 μ m. **B.** Quantification data of HIF-1 α , FBN and COL-I expression using one-way ANOVA. Quantification data of **C.** SMAD2/3, **D.** HSP47 and **E.** COL-IV expression using one-way ANOVA. Results are shown as mean \pm SEM. * p < 0.05, ** p < 0.01, *** p < 0.001. Data are representative of 2 independent experiments. Please refer to **Supplementary Figure 2** for the immunofluorescence images of SMAD2/3, HSP47 and COL-IV staining. Results are shown as mean \pm SEM. * p < 0.05, ** p < 0.01, *** p < 0.001. Data are representative of 2 independent experiments.

Abbreviations: ANOVA - Analysis of variance; COL-I – Collagen I; COL-IV – Collagen IV; DAPI - 4',6-diamidino-2-phenylindole; FBN – Fibronectin; HIF-1A- Hypoxia-inducible factor 1-alpha; HSP47 – Heat shock protein 47; L-Ala-L-Gln - L-Alanyl-L-glutamine; PNF – Peripheral nerve fibrosis; SMAD 2/3 - Mothers against decapentaplegic homolog 2/3; SEM - Standard error of the mean

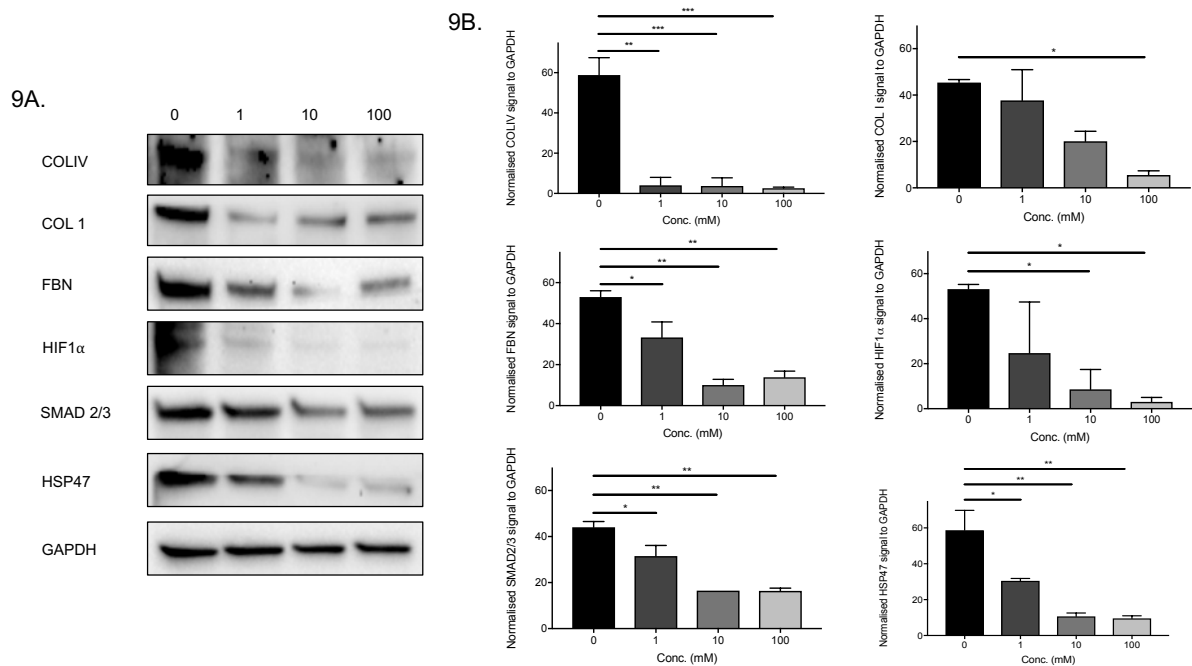


Figure 9: L-Ala-L-Gln reduces expression of FBN and other pro-fibrotic factors involved with PNF.

Primary Rat fibroblasts were treated with L-Ala-L-Gln for 48h under Episodic Hypoxia (2% oxygen for 2h). **A.** Representative Western blot visualization of proteins involved in HIF-1 α and fibrogenic signaling in Primary Rat fibroblasts exposed under Episodic Hypoxia (2% oxygen for 2h) followed by treatment with 1mM, 10mM and 100mM L-

Ala-L-Gln or not treatment (0mM) for 48h. **B.** Quantification of HIF-1 α and SMAD 2/3, COL-I, COL-IV, FBN and HSP47 protein abundance by densitometry, normalized against GAPDH (n=3 independent experiments). Results are shown as mean \pm SEM. *p < 0.05, ** p < 0.01, *** p < 0.001.

Abbreviations: COL-I – Collagen I; COL-IV – Collagen IV; FBN – Fibronectin; GAPDH - Glyceraldehyde 3-phosphate dehydrogenase; HIF-1A- Hypoxia-inducible factor 1-alpha; HSP47 – Heat shock protein 47; L-Ala-L-Gln - L-Alanyl-L-glutamine; PNF – Peripheral nerve fibrosis; SMAD 2/3 - Mothers against decapentaplegic homolog 2/3; SEM - Standard error of the mean

Identification of crucial proteins and pathway analysis in hypoxic fibroblasts treated with L-Ala-L-Gln

This study is the first attempt to compile the phospho-proteome profile of L-Ala-L-Gln treated hypoxic primary rat fibroblasts. We tried to identify the phosphor-proteome of perineurial derived primary rat fibroblasts treated under chronic hypoxic conditions treated with the different concentrations of L-Ala-L-Gln. Total of 5110 proteins were profiled in all 4 conditions (0mM, 1mM, 10mM and 100mM). While 1322 proteins were found to be significantly regulated across the treatment group (1mM, 10mM and 100mM) when compared with 0mM hypoxic samples. Out of these 1322 proteins, 607 proteins were significantly downregulated and 715 were significantly upregulated across the L-Ala-L-Gln samples. We used biological triplicates of each condition and we performed a pooled analysis of all biological triplicates between the treated group and the untreated 0mM condition. Positive values of log₂ ratios indicate upregulation of associated protein in L-Ala-L-Gln treated group while negative values indicate downregulation. Further analysis for identification of critical factors and associated pathways were performed using DAVID statistical software and KEGG pathway analysis as described earlier. We initially focused on downregulated targets as we were interested to identify proteins and associated pathways regulated by in L-Ala-L-Gln to reduce fibrogenic phenotype.

Pathway analysis showed that proteins significantly downregulated in the treated groups were associated with mTOR ([Table 3](#)), PI3k ([Table 4](#)), cell adhesion ([Table 5](#)) and Focal adhesion ([Table 6](#)). Our evaluation indicates that L-Ala-L-Gln effectively

downregulates crucial factors involved with cell adhesion and fibrosis progression but we were also able to identify a dose-dependent effect of L-Ala-L-Gln in the expression of these factors (Figure 10 A-C). We also found several targets associated with the HIF-1- α , ECM-interaction, ERBb, FOXO and TGF- β signalling pathways (Data not shown). Importantly, we noted that crucial pro-fibrotic factors including *Fndc1*, *Fndc3b*, *Col1a1* and *Akt1s1* and *Pxn* were significantly downregulated (Figure 11) in L-Ala-L-Gln treated samples, compared to untreated chronic hypoxic samples, in agreement to our initial *in-vitro* findings through Western blotting and immunofluorescence imaging.

We further went on to analyse the proteins found to be significantly upregulated in the L-Ala-L-Gln treated primary fibroblasts. Our pathway analysis indicates that these proteins are associated with upregulation of GnRH signalling (Table 7), Glutaminergic and axon guidance signalling (Data not shown). Our findings of upregulated factors have been summarized in the Volcano plots (Figure 10 A-C).

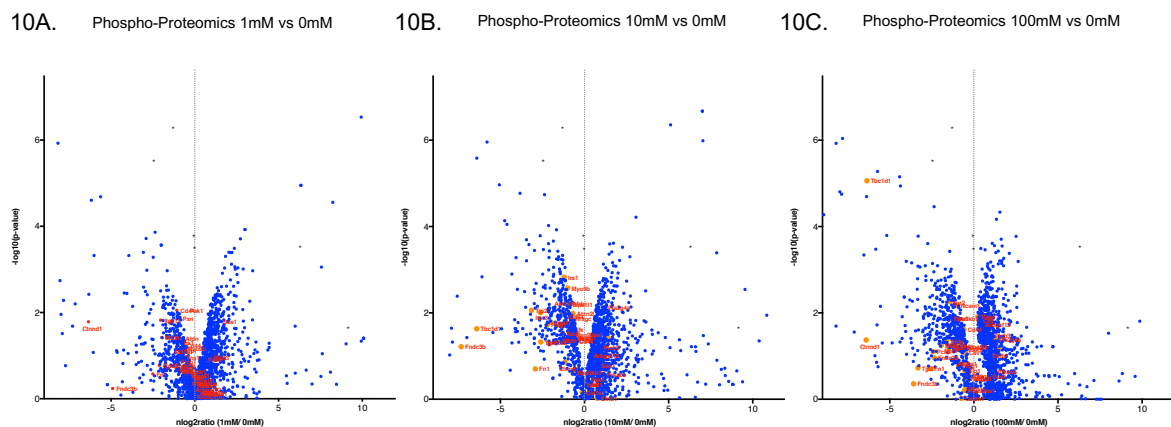


Figure 10. L-Ala-L-Gln reduces expression of pro-fibrotic and adhesion biomarkers of hypoxic primary rat fibroblasts.

A, **B** and **C**. Volcano plots of phospho-proteomics analysis comparing 1mM, 10mM and 10mM L-Ala-L-Gln treated primary rat fibroblasts exposed under chronic hypoxic conditions for 48h with untreated hypoxic fibroblasts (0mM condition). Proteins related to pro-fibrosis, cell-adhesion, PI3k, mTOR and Glutaminergic signaling pathways have been depicted in red, if detected. Hits with $p < 0.05$ are marked in blue. Volcano plots are representative of ($n=3$ independent experiments for each sample).

Abbreviations: L-Ala-L-Gln - L-Alanyl-L-glutamine; mTOR - mammalian target of rapamycin; PI3k - Phosphatidylinositol 3-kinase

11.

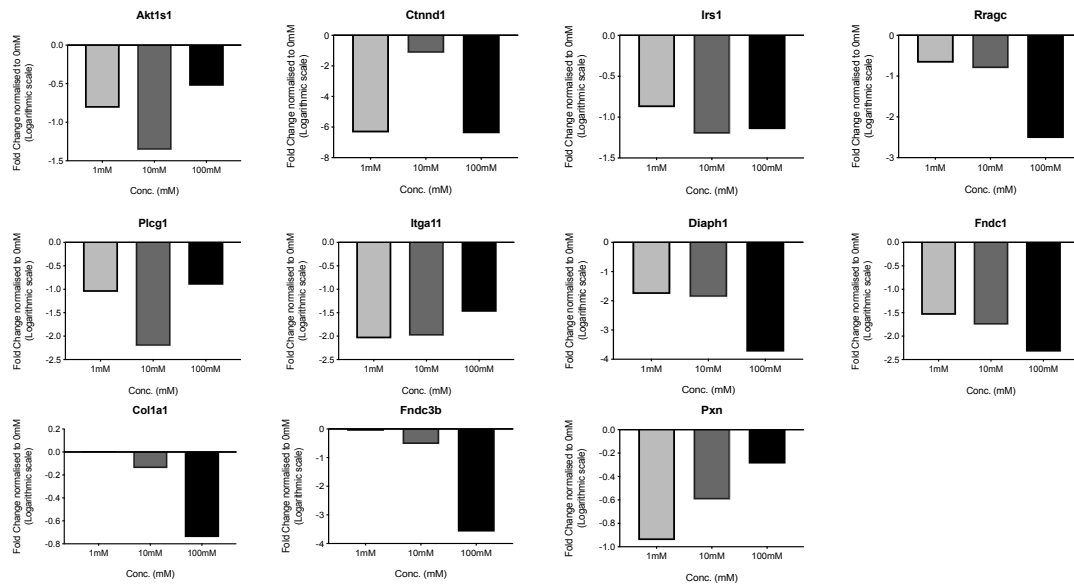


Figure 11. L-Ala-L-Gln modulates signaling pathways through the regulation of specific of pro-fibrotic and adhesion biomarkers of hypoxic primary rat fibroblasts.

Graphs are representative of expression of key targets specific to various fibrogenic pathways including mTOR, PI3k, Focal adhesion and ECM-interaction. Data includes phospho-proteomics analysis comparing 1mM, 10mM and 10mM L-Ala-L-Gln treated primary rat fibroblasts exposed under chronic hypoxic conditions for 48h normalized to untreated hypoxic fibroblasts (0mM condition). Data are representative of (n=3 independent experiments for each sample).

Abbreviations: ECM – Extracellular matrix; L-Ala-L-Gln - L-Alanyl-L-glutamine; mTOR - mammalian target of rapamycin; PI3k - Phosphatidylinositol 3-kinase

Results (Chapter: *Pirfenidone*)

PFD inhibits viability and cell proliferation and induces cell death of primary rat fibroblasts, but not Schwann cells

We investigated the effects of PFD on the viability, proliferation and cell death characteristics of primary rat fibroblasts. We used the Alamar blue assay to determine viability and flow cytometry based EdU assay to quantify proliferation. When compared with untreated negative control (0mg/ml, without pirfenidone in the culture medium), pirfenidone-treated samples showed reduced viability and proliferation (Figure 12A, 12B). We used various concentrations (0.1, 0.2, 0.3, 0.4, 0.5 and 0.75 mg/ml) of PFD to determine the response of primary rat fibroblasts to PFD. Viability of primary rat fibroblasts were reduced by around 20% in (0.1 – 0.5 mg/ml) concentrations of PFD and was significantly reduced in 0.75 mg/ml. On the other hand, PFD was found to reduce the proliferative capacity of primary rat fibroblasts in a dose-dependent manner. Proliferation of primary rat fibroblasts were significantly reduced at (0.4, 0.5 and 0,75 mg/ml) concentrations of PFD ($p < 0.05$) when compared to that of untreated negative control samples. The reduction of proliferation and viability was more profound in the 0.75 mg/ml PFD treatment and hence, we decided to use concentrations below 0.75 mg/ml for subsequent experiments.

We also evaluated the impact of PFD on cell death of primary rat fibroblasts. As shown in (Figure 12C), we identified a significant increase in the proportion of primary fibroblasts undergoing apoptosis. To identify the apoptotic effects of PFD, we used various concentrations (0.1, 0.2 and 0.3 mg/ml) of PFD to determine the if there lies a dose-dependent response to cell death. In comparison to untreated controls (data not shown), PFD induced a significant increase in early and late apoptotic population of primary rat fibroblasts. Highest cell death was seen at 0.3 mg/ml and nearly 4.2% of the primary fibroblasts stained double positive for Annexin V/ 7-AAD. The apoptotic effects following 48 h of PFD treatment was dose-dependent and the cell death inducible properties of PFD falls in line with its anti-proliferative effects.

Having identified the anti-proliferative effects of PFD on primary rat fibroblasts, we wondered if PFD also affects Schwann cells. As Schwann cells are critical for wound healing and nerve repair and regeneration mechanisms, it is of primary concern if PFD shows similar effects on Schwann cells. To test out hypothesis, we conducted viability,

proliferation and cell cycle analysis on normoxic and hypoxic Schwann cells. We found, 0.4 mg/ml and above concentrations of PFD reduce viability of normoxic and hypoxic Schwann cells to some extent, but there was no significant reduction in viability (Figure 13A, 13B, Supplementary Figure 3). We next conducted flow cytometry-based proliferation analysis and we found even extremely high concentration of PFD does not have any anti-proliferative effect on Schwann cells in normoxic or hypoxic conditions (Figure 13C). We further analyzed cell division to understand if Schwann cells undergo G2/M arrest using CFSE assay. Interestingly, we found Schwann cells divide irrespective of presence of PFD (Figure 13D). Having identified the anti-proliferative effect of PFD on primary rat fibroblasts alone, we further hypothesized if the same is true for TGF- β 1 stimulated fibroblasts.

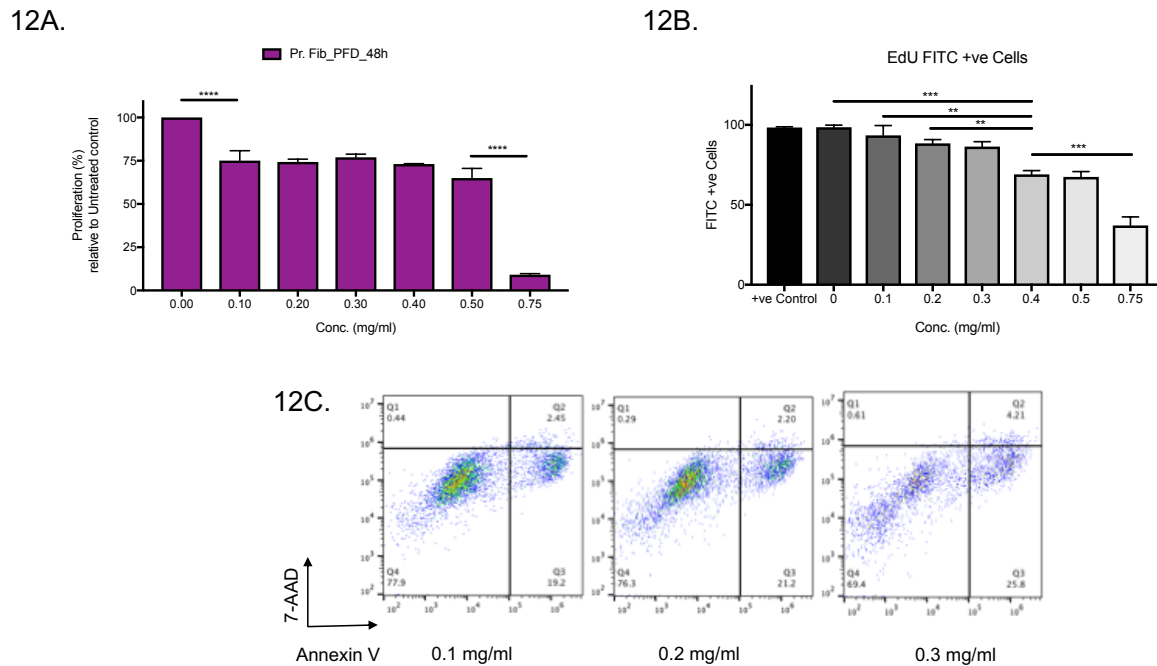


Figure 12: Effect of PFD on cell viability, cell proliferation and cell death of primary rat fibroblasts.

Primary Rat fibroblasts were cultured with PFD under normoxic conditions. **12A.** Cell viability was estimated with Alamar Blue (Thermo) assay as described in the methods section. **12B.** Cell proliferation was estimated with EdU (baseclick) assay as described in the methods section. **12C.** Cell death was characterized by the Annexin V/ 7-AAD Apoptosis assay using flow cytometry as described in the methods section. Untreated

normoxic fibroblasts were as positive control and proliferation of treated cells was calculated relative to the normoxic controls.

Abbreviations: 7AAD - 7-Aminoactinomycin D; EdU - 5-ethynyl-2'-deoxyuridine; PFD - Pirfenidone

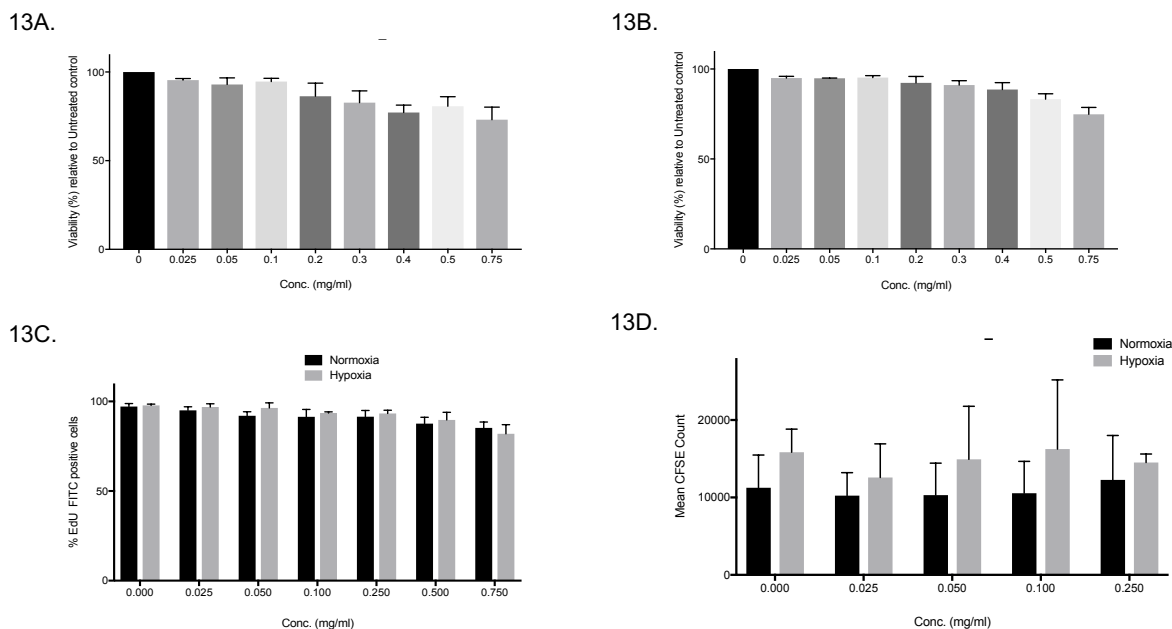


Figure 13: Effect of PFD on cell viability, cell proliferation and cell division of Schwann cells.

Schwann cells were cultured with PFD under normoxic conditions. **13A.** Cell viability of normoxic Schwann cells was estimated with Alamar Blue (Thermo) assay as described in the methods section. **13B.** Cell viability of hypoxic (2% O₂ for 48h) Schwann cells was estimated with Alamar Blue (Thermo) assay as described in the methods section. **13C.** Cell proliferation was estimated with EdU (baseclick) assay as described in the methods section. **13D.** Cell cycle and cell division was characterized by the CFSE assay using flow cytometry as described in the methods section. Untreated fibroblasts were as positive control and proliferation of treated cells was calculated relative to the normoxic/ hypoxic controls.

Abbreviations: CFSE - Carboxyfluorescein succinimidyl ester; EdU - 5-ethynyl-2'-deoxyuridine; PFD - Pirfenidone

PFD exposure significantly reduces cell viability and proliferation and promotes apoptosis of TGF- β 1 activated primary rat fibroblasts

TGF- β 1 is the key regulator of tissue fibrosis and TGF- β 1 activated fibroblasts are known to be apoptosis-resistant (105). Therefore, following our understanding of the effects of PFD on primary rat fibroblasts, we were particularly interested to observe its effects on TGF- β 1 activated fibroblasts. We investigated the effects of PFD on the viability, proliferation and cell death characteristics of TGF- β 1 activated primary rat fibroblasts. While TGF- β 1 activated fibroblasts remained viable and proliferation of TGF- β 1 activated fibroblasts were comparable to normal untreated primary rat fibroblasts, PFD treated TGF- β 1 activated fibroblasts showed reduced proliferative capacity. PFD at (0.4 and 0.5 mg/ml) significantly ($p < 0.001$) inhibited viability and TGF- β 1 activated fibroblasts were found to be less proliferative at 0.25 mg/ml in comparison to +ve controls (TGF- β 1 activated fibroblasts) as well as in comparison to other doses of PFD (Figure 14A). We did not observe any reduction in proliferation of TGF- β 1 activated fibroblasts at concentrations lower than (0.4 and 0.5 mg/ml).

Similarly, proliferation of TGF- β 1 activated fibroblasts, remained stable for all other concentrations and we observed 10% decrease in the proliferative capacity of TGF- β 1 activated fibroblasts at 0.25 mg/ml treatment with PFD (Figure 14B).

Following our viability and proliferation analysis, we also looked at cell death of TGF- β 1 activated fibroblasts upon PFD treatment. We found PFD induces cell death at concentrations of 0.25 and 0.5 mg/ml (complete this sentence after analysis). PFD treatment induced a significant upregulation in the relative luminescence count and PFD effectively induced cell death. In order to characterize the mode of apoptosis, we used the Caspase 3/ 7 Glo assay. PFD was found to induce apoptosis of TGF- β 1 activated fibroblasts through the activation of Caspase 3/ 7 pathway (Figure 14C). We also performed a Western blotting analysis to further confirm our analysis (Figure 14D). Our Western analysis indicates that PFD induces activation of cleaved caspase 3 mediated apoptosis at concentrations (0.05, 0.1 and 0.25 mg/ml). We did not observe a dose-dependent activation of cleaved caspase 3 in our Western analysis. PFD at (0.05, 0.1 and 0.25 mg/ml) significantly upregulated the expression of cleaved caspase 3 in comparison of normal untreated and TGF- β 1 activated fibroblasts.

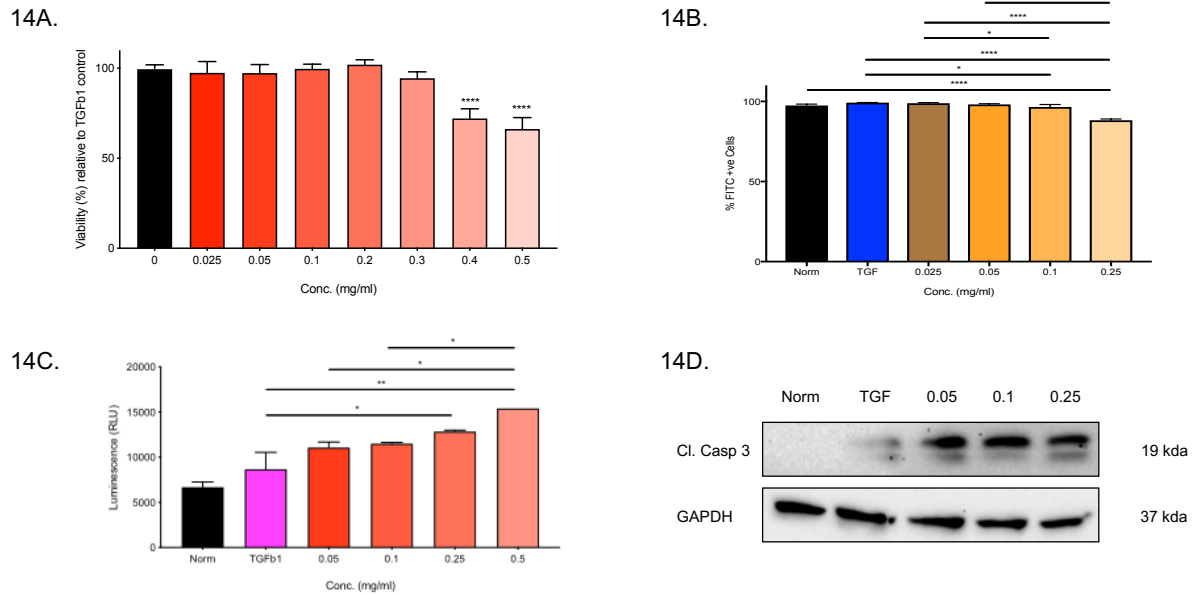


Figure 14: Effect of PFD on cell viability, cell proliferation and cell death of TGF-β1 activated primary rat fibroblasts.

Primary Rat fibroblasts were cultured with PFD under normoxic conditions. **14A.** Cell viability was estimated with Alamar Blue (Thermo) assay as described in the methods section. **14B.** Cell proliferation was estimated with EdU (baseclick) assay as described in the methods section. **14C.** Cell death was characterized by the Caspase-Glo 3/7 assay as described in the methods section. Relative caspase 3/7 activity after 48 h treatment with PFD. Data represents the mean \pm SD ($n = 3$), analyzed using one-way ANOVA. Untreated normoxic fibroblasts were used as negative controls. **14D.** Representative Western blot visualization of Cleaved Caspase 3 of TGF-β1 activated primary rat fibroblasts treated with or without PFD at (0.05, 0.1 and 0.25 mg/ml).

Abbreviations: ANOVA - Analysis of variance; EdU - 5-ethynyl-2'-deoxyuridine; PFD - Pirfenidone

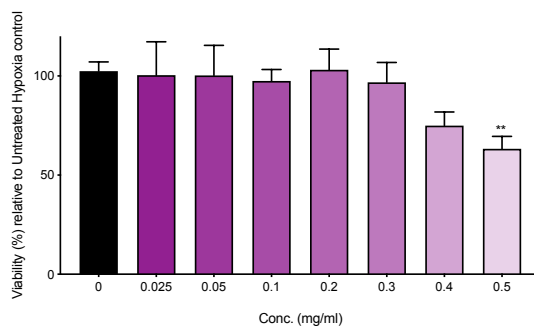
PFD exposure significantly reduces cell viability and proliferation and promotes apoptosis of hypoxic primary rat fibroblasts

As hypoxia and the hypoxic microenvironment is known to regulate disease progression and pro-fibrotic factors, we decided to identify the effects of PFD on the aspects of cell viability, proliferation and cell death of hypoxic primary rat fibroblasts. We tested various concentrations of PFD on hypoxic primary fibroblasts. We did not

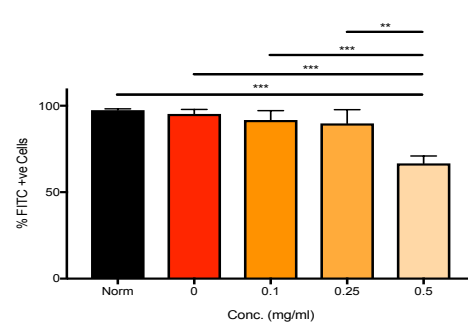
observe any dose dependent inhibition of PFD on hypoxic primary fibroblasts. Viability of hypoxic primary fibroblasts remained stable (>95% in comparison to untreated hypoxic controls) at concentrations of (0 – 0.3 mg/ml) of PFD. We also observed reduction in viability of hypoxic primary fibroblasts at 0.4 mg/ml. 0.5 mg/ml PFD induced significant reduction in viability of hypoxic primary fibroblasts (Figure 15A). Our viability analysis of hypoxic primary fibroblasts falls in line with cell proliferation of hypoxic primary fibroblasts when treated with PFD for 48 h. PFD at concentrations of (0.1 and 0.25 mg/ml) did not induce any anti-proliferative effect on hypoxic primary fibroblasts. Only 0.5 mg/ml PFD treatment showed significant reduction in proliferation of hypoxic primary fibroblasts (Figure 15B).

We continued our PFD exposure studies on cell death analysis of hypoxic primary fibroblasts as well. We found PFD induce Caspase 3/7 mediated cell death. In line with our cell death analysis in TGF- β 1 activated primary rat fibroblasts, we found PFD induces cell death at concentrations of 0.25 and 0.5 mg/ml. One-way ANOVA further revealed that this change is significant in comparison to hypoxic untreated primary fibroblasts. Furthermore, we also observed a significant increase in caspase 3/7 luminescence at 0.5 mg/ml PFD in comparison to 0.25 mg/ml, indication a partial dose response in cell death (Figure 15C).

15A.



15B.



15C.

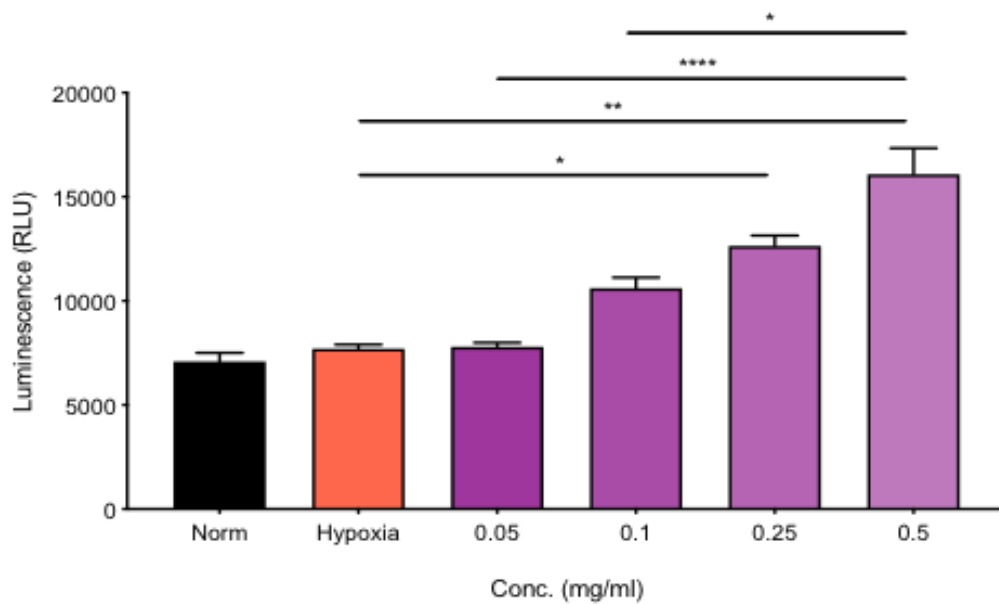


Figure 15: Effect of PFD on cell viability, cell proliferation and cell death of hypoxic primary rat fibroblasts.

Primary Rat fibroblasts were cultured with PFD under normoxic and hypoxic (2% O₂ for 48h) conditions. **15A**. Cell viability was estimated with Alamar Blue (Thermo) assay as described in the methods section. **15B**. Cell proliferation was estimated with EdU (baseclick) assay as described in the methods section. **15C**. Cell death was characterized by the Caspase-Glo 3/7 assay as described in the methods section. Relative caspase 3/7 activity after 48 h treatment with PFD. Data represents the mean \pm SD (n = 3), analyzed using one-way ANOVA. Untreated normoxic fibroblasts were used as negative controls. Untreated hypoxic fibroblasts were used as positive controls.

Abbreviations: ANOVA - Analysis of variance; EdU - 5-ethynyl-2'-deoxyuridine; PFD - Pirfenidone

PFD reverses differentiation of primary rat fibroblasts

Prior to characterizing the anti-fibrotic effects of PFD on TGF- β 1 activated primary fibroblasts, we investigated if PFD is able to reduce/ reverse differentiation of TGF- β 1 activated fibroblasts. To test this, we first determined TGF- β 1 activation on primary rat

fibroblasts. In order to identify the differentiation potential of TGF- β 1, we tested various concentrations on activation and differentiation of primary fibroblasts, by characterizing the expression of α -SMA in TGF- β 1 fibroblasts. Primary rat fibroblasts and human fibroblasts were serum starved and exposed to 1, 2.5, 5 and 10 ng/ml concentrations of TGF- β 1 for 48 h, as described in the methods section earlier. We observed a dose-dependent effect of TGF- β 1 on the expression of α -SMA (Figure 16A-D). We also observed that primary rat fibroblasts and human fibroblasts were activated in a similar manner upon treatment TGF- β 1. α -SMA expression was significantly increased at 10ng/ml TGF- β 1 in primary rat fibroblasts (Figure 16A, 16B) and human fibroblasts (Figure 16C, 16D). Upregulation of α -SMA expression in TGF- β 1 activated fibroblasts confirmed the generation of differentiated myofibroblast cultures and this helped us to proceed to understand the effects of PFD on differentiated fibroblast population.

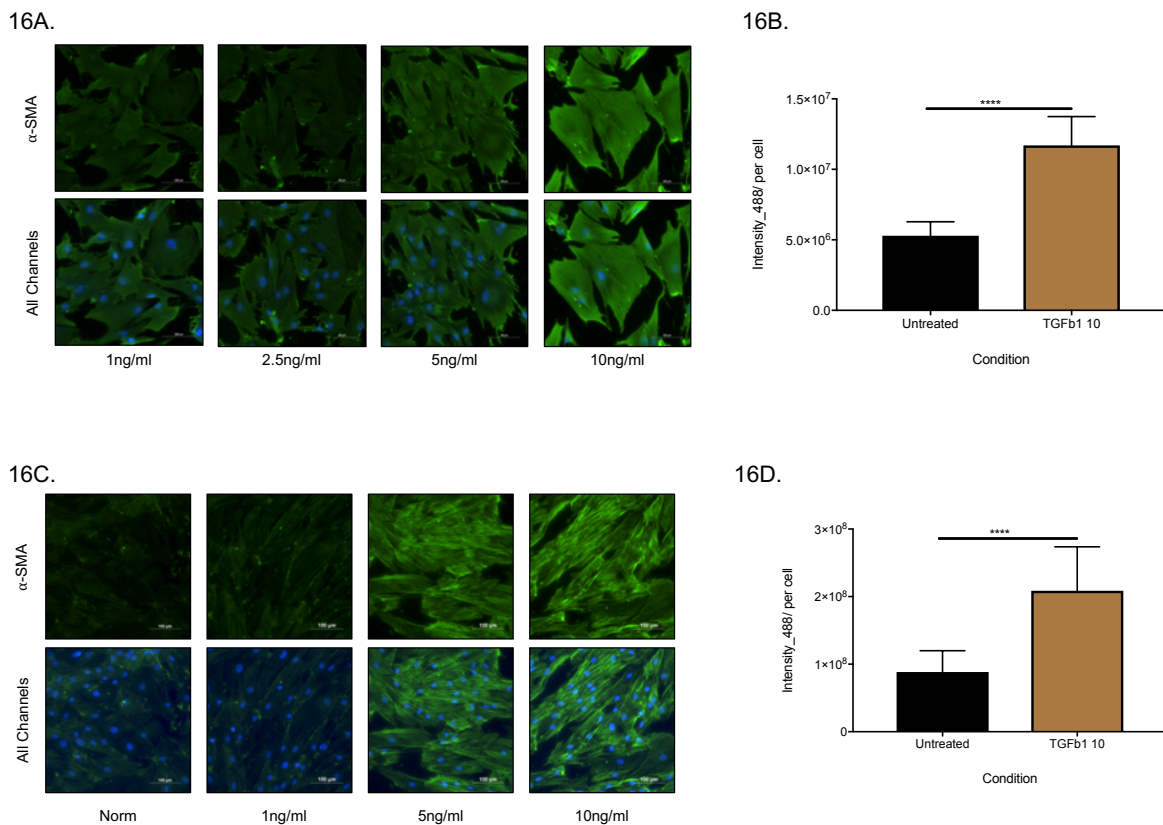


Figure 16: Effect of TGF- β 1 to transdifferentiate fibroblasts into myofibroblasts. **(A)** Primary Rat Fibroblasts were cultured in serum-free conditions in the absence or presence of increasing concentrations of TGF- β 1 (1, 2.5, 5 and 10 ng/mL) for 48 h.

Then, the cells were fixed with 4% PFA, permeabilized, and immunoassayed for α -SMA (green) and counterstained for DNA (blue), as shown on representative images. Scale bar = 100 μ m. **(B)** The intensity of AF488 per nuclei count (per cell) indicates the intensity of α -SMA-positive stress fibers in fibroblast populations was determined using fluorescence microscopy, each in three independent experiments. **(C)** Human Fibroblast cells were cultured in serum-free conditions in the absence or presence of increasing concentrations of TGF- β 1 (2.5, 5 and 10 ng/mL) for 48 h. Then, the cells were fixed with 4% PFA, permeabilized, and immunostained for α -SMA (green) and counterstained for DNA (blue), as shown on representative images. Scale bar = 100 μ m. **(D)** The intensity of AF488 per nuclei count (per cell) indicates the intensity of α -SMA-positive stress fibers in fibroblast populations was determined using fluorescence microscopy, each in three independent experiments. Untreated normal fibroblasts were used as negative controls.

Abbreviations: α -SMA – alpha Smooth Muscle Actin; AF488 - Alexa Fluor 488; DNA - Deoxyribonucleic acid; PFA – Paraformaldehyde; PFD – Pirfenidone; TGF- β 1 - Transforming Growth Factor Beta 1

As PFD is known to negatively regulate TGF- β signaling, we investigated if PFD reduces activation of TGF- β 1. This will be key for further experiments as TGF- β 1 is a potent modulator of fibroblast proliferation and differentiation (Figures 17 A-C), inhibition of TGF- β 1 might prove to be the key to regulate fibroblast differentiation. To test our hypothesis, we determined the effect of PFD on TGF- β 1 on primary rat fibroblasts, TGF- β 1 activated primary rat fibroblasts and hypoxic primary rat fibroblasts. We used ELISA to investigate our hypothesis. We found PFD effectively blocks TGF- β 1 in primary rat fibroblasts (Figure 17A) and TGF- β 1 activated primary fibroblasts in a dose-dependent manner (Figure 17B). PFD was extremely effective in blocking activation of primary rat fibroblasts by TGF- β 1 and significantly reduced TGF- β 1 levels at concentrations as low as 0.1 mg/ml in TGF- β 1 activated primary fibroblasts and hypoxic primary fibroblasts. In TGF- β 1 activated primary fibroblasts, 0.5 mg/ml PFD reduced TGF- β 1 levels comparable to that of normal untreated fibroblasts (figure 17B). Interestingly, we did not observe a dose-dependent reduction

of TGF- β 1 levels in hypoxic primary rat fibroblasts, and concentrations (0.1, 0.25 and 0.5 mg/ml) showed equal potency in reducing TGF- β 1 levels (figure 17C).

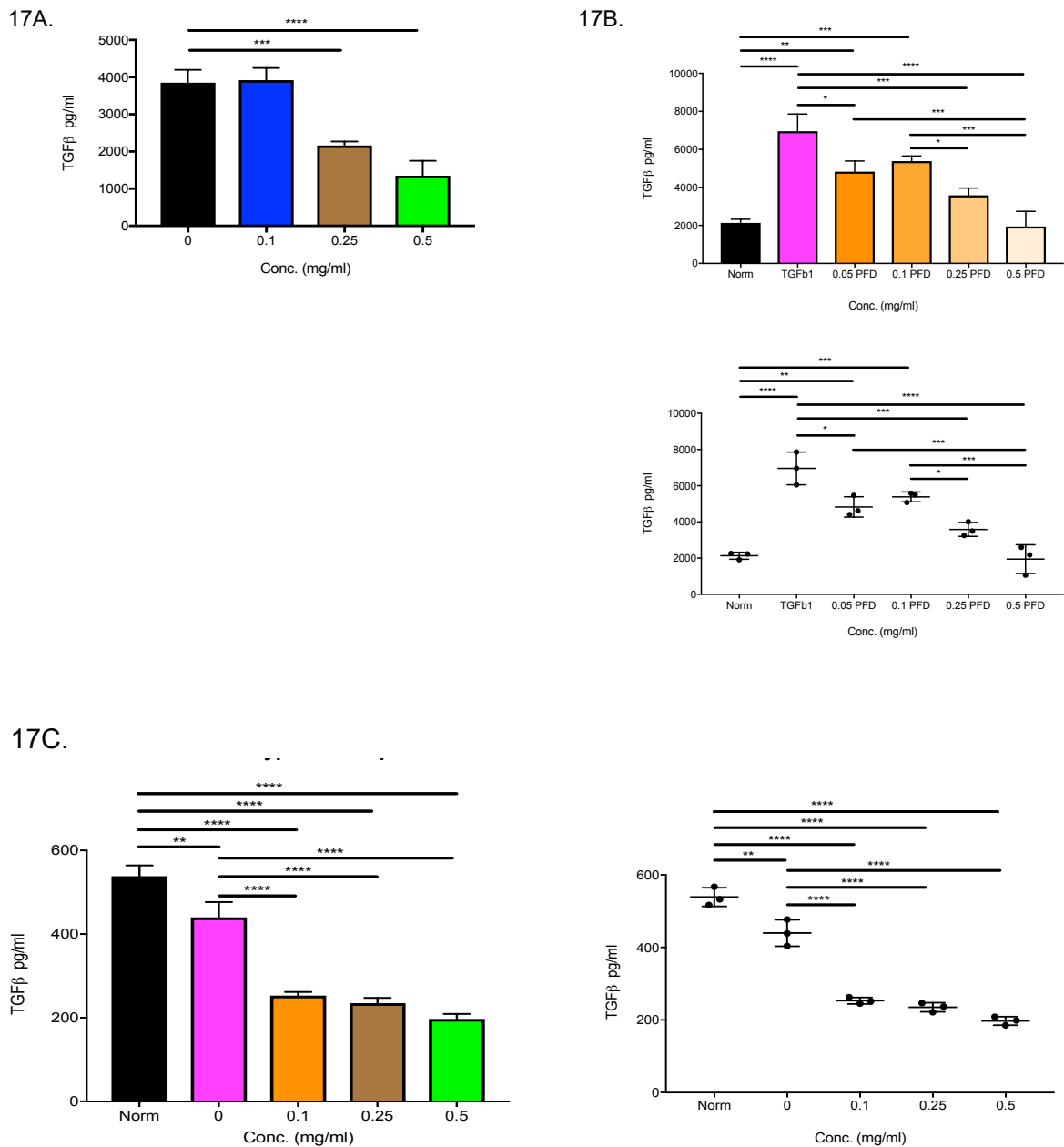


Figure 17: Effect of PFD on TGF- β 1 levels of primary rat fibroblasts.

Main markers of myofibroblast differentiation: TGF- β 1 levels were assessed using *ELISA* tests, and the results are presented as the mean value of absorbance (450 nm) reflecting the protein content. Data represent the mean \pm SEM carried out on fibroblasts each in triplicate. (A) Normal untreated primary rat fibroblasts treated with

or without PFD **(B)** Primary Rat Fibroblasts activated with TGF- β 1, treated with or without PFD **(C)** Hypoxic Primary Fibroblasts treated with or without PFD.

Abbreviations: ELISA - Enzyme-linked immunosorbent assay; PFD – Pirfenidone; TGF- β 1 - Transforming Growth Factor Beta 1

Our ELISA analysis significantly helped us to understand how PFD functions in differentiated fibroblast population. Following characterizing the effects of PFD on TGF- β 1 levels, we decided to look into the ability of PFD to reduce differentiation of TGF- β 1 activated primary fibroblasts. We again tested various concentrations of PFD (0.01, 0.025 and 0.05 mg/ml) on the α -SMA expression of TGF- β 1 activated primary fibroblasts. As PFD was found to induce inhibition of cell proliferation at 0.1 mg/ml (Figure 18B), we decided to use lower concentrations so as to avoid loss of cells. Our immunocytochemistry and quantitative image analysis results showed that α -SMA expression was significantly upregulated in TGF- β 1 activated primary fibroblasts and PFD effectively reduced α -SMA expression in a dose-dependent fashion (Figure 18A, 18B). These results were further confirmed with examination of total α -SMA protein levels present in whole cell lysates (Figure 19A). Interestingly, we also observed PFD to alter the cellular morphology as measured by the area covered per cell (data not shown), further indicating that PFD in neural fibrosis could reverse differentiation potential induced by TGF- β 1 activated and differentiated fibroblasts.

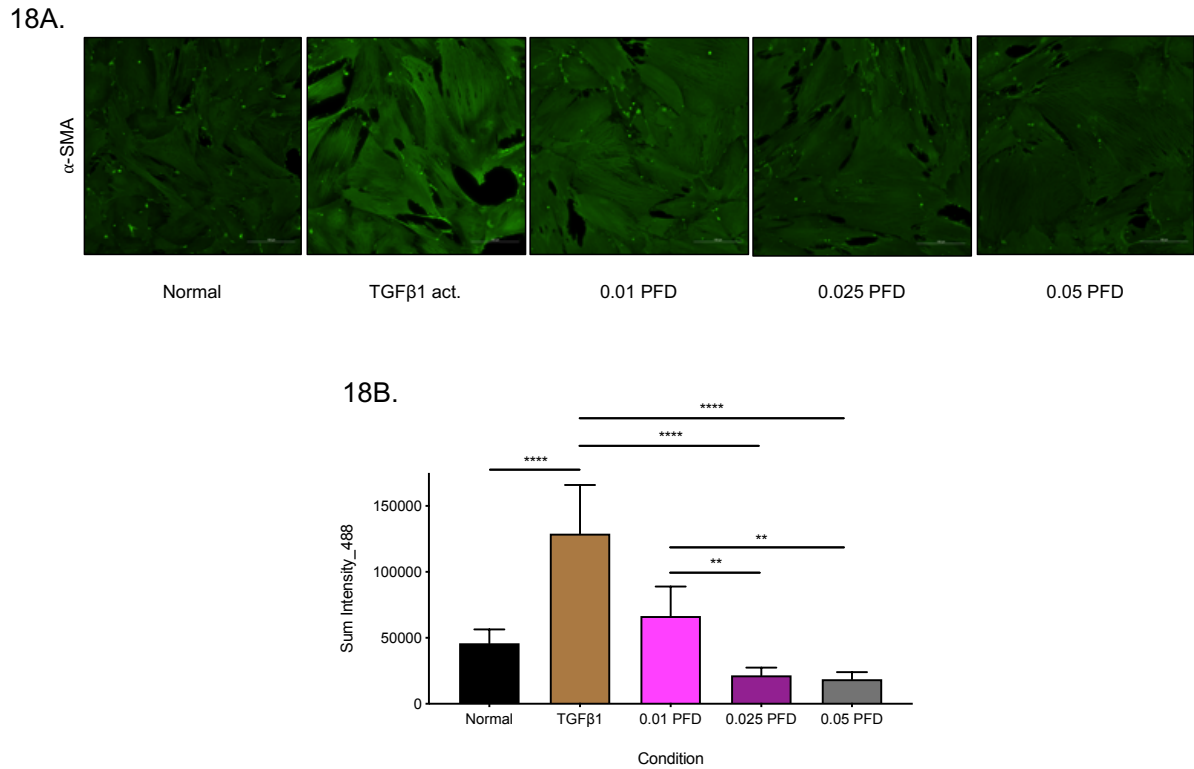


Figure. 18: PFD reduces expression of protein levels of fibroblast differentiation marker.

Primary Rat fibroblasts were treated with PFD under TGF- β 1 activated conditions for 48h. Expression of α -SMA was characterized by immunofluorescence imaging. **A.** Protein expression levels of α -SMA was characterized by ICC after treatment with different concentrations of PFD. Imaging of cells was done as mentioned earlier the methods section. Statistical analysis of cytosolic α -SMA as observed after the treatment of activated cells. Description of the statistical analysis was mentioned earlier the methods section.

Abbreviations: α -SMA – alpha Smooth Muscle Actin; PFD – Pirfenidone; TGF- β 1 - Transforming Growth Factor Beta 1

PFD reduces expression of pro-fibrotic factors induced by TGF- β signaling

In order to further assess the effects of PFD on pro-fibrotic phenotype as observed in TGF- β 1 activated fibroblasts, protein expression was analyzed with Western blotting and immunocytochemistry. We selected targets based on TGF- β signaling and all

other key markers of pro-fibrotic myofibroblast phenotype as was previously shown by (Ghosh et al. under final revisions: **L-Ala-L-Gln suppresses hypoxic phenotype and fibrogenic activity of rat perineurial fibroblasts**). We investigated whether the pro-fibrotic factors induced by TGF- β 1 would be regulated by PFD. Later we tried to quantify this effect to understand the degree of regulation by PFD. Protein expression quantified by Western blotting showed profound effects from PFD treatment. Expression of collagen-I, collagen-IV, HSP47 and α -SMA, showed a near complete reversal of the TGF- β 1 stimulated primary rat fibroblasts (Figure 19A). PFD treatment showed a dose-dependent reduction in the expression of collagen-IV. PFD as low as 0.05 mg/ml was highly potent and was found to significantly reduce the expression of collagen-I HSP47 and α -SMA (Figure 19A, 19B).

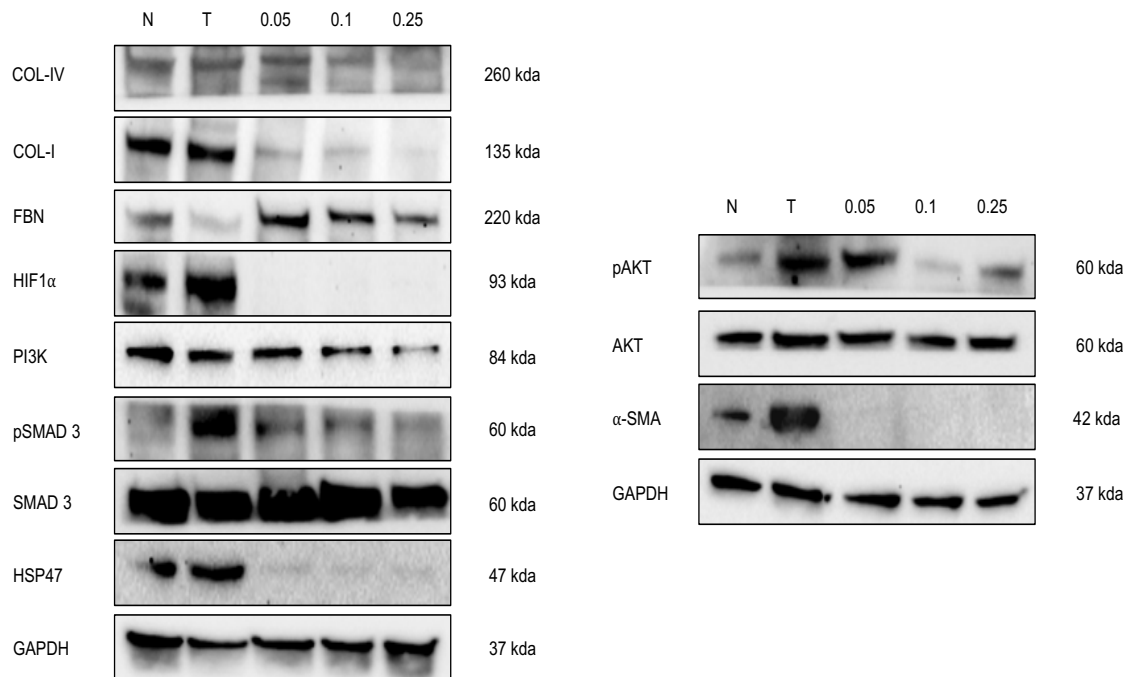
In order to further confirm our analysis, we performed immunofluorescence-based image quantification on TGF- β 1 stimulated primary rat fibroblasts, treated with PFD. In line with our Western analysis, PFD reduced the expression of pro-fibrotic factors including α -SMA (Figure 18A, 18B), collagen-I, collagen-IV and HSP47 and exhibited a dose-dependent inhibition (Figure 19C, 19D, 19E). Our immunofluorescence-based image quantification also showed that PFD completely abolished the expression of α -SMA, thereby indicating that PFD promotes reversal of differentiation of myofibroblast phenotype. We also wanted to investigate if this holds true for human fibroblasts as well. Following our immunocytochemistry analysis on TGF- β 1 stimulated primary rat fibroblasts, we repeated the same experiments on human fibroblasts. We found a similar dose-dependent downregulation of pro-fibrotic factors upon treatment with PFD in TGF- β 1 stimulated human fibroblasts (Supplementary Figure 4).

Increased TGF- β signaling is known to function through the activation of downstream targets namely SMAD2/3. As all the key components found in TGF- β signaling are involved with ECM deposition, we were also interested to understand the effects of PFD on downstream TGF- β signaling. Our Western blot analysis revealed that PFD inhibits activation of SMAD 3 (indicated by expression of pSMAD 3), but not SMAD2. Interestingly, we also found PFD negatively regulates HIF-1 α / SMAD 3 axis as well as the PI3K/AKT axis. PFD significantly downregulated phosphorylation mediated activation AKT and downregulated expression of PI3K levels in a dose-dependent fashion. Similarly, TGF- β signaling upregulated HIF-1 α in primary rat fibroblasts and

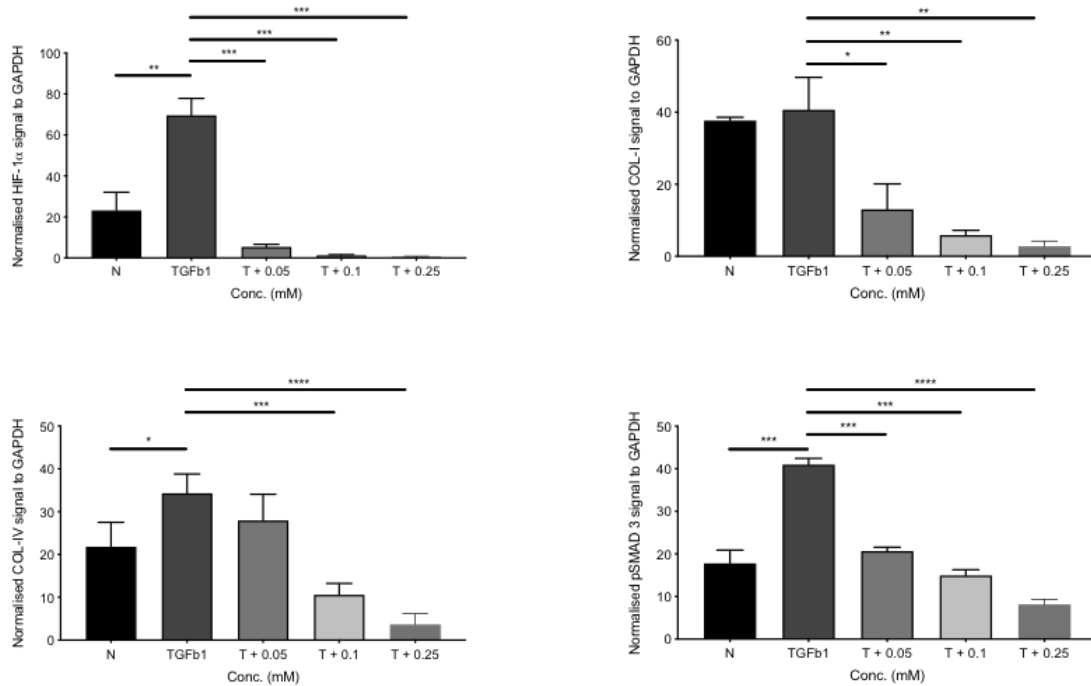
PFD completely abolished TGF- β mediated HIF-1 α expression in TGF- β 1 activated primary rat fibroblasts (Figure 19A, 19B).

Interestingly, though PFD was found to downregulate key TGF- β activated pro-fibrotic targets, fibronectin was found to be upregulated in PFD treated TGF- β 1 activated primary rat fibroblasts. Conversely, fibronectin was significantly downregulated in differentiated fibroblasts, opposite to expression of other ECM targets.

19A.



19B.



19B.

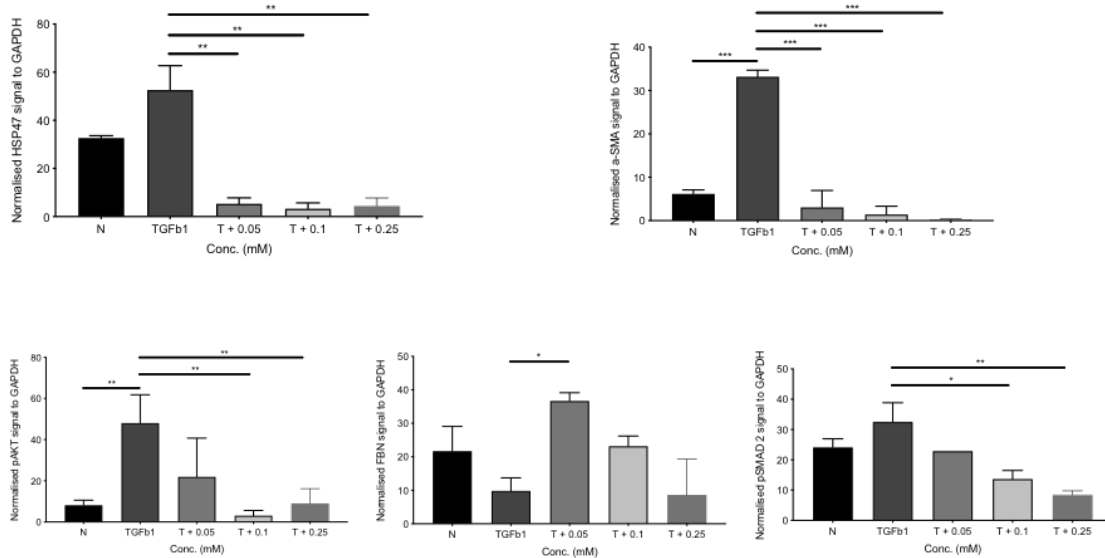
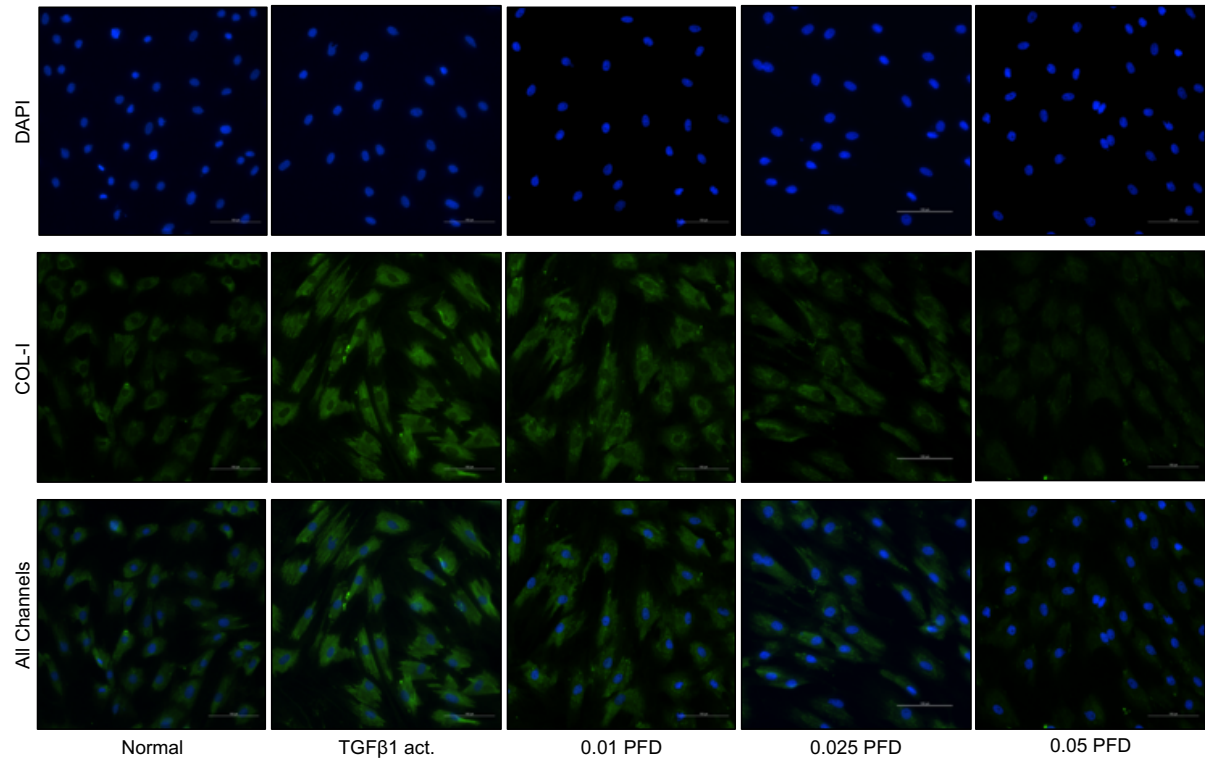


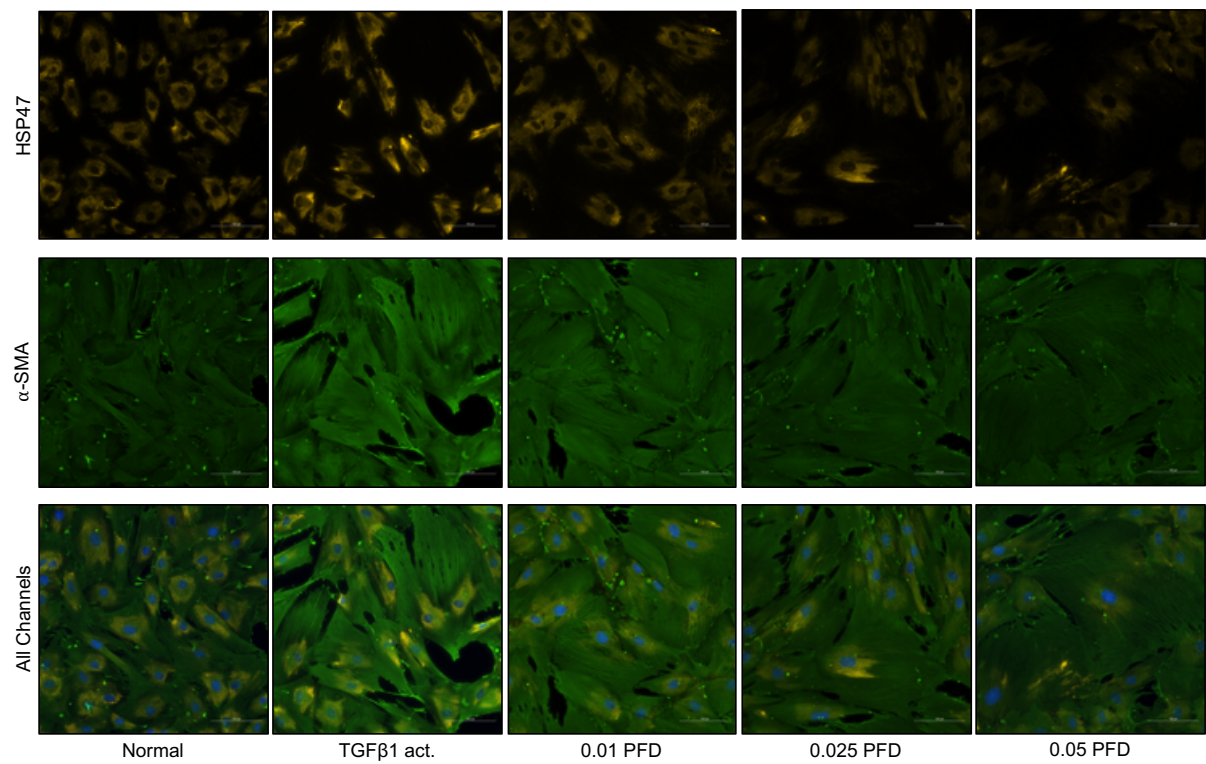
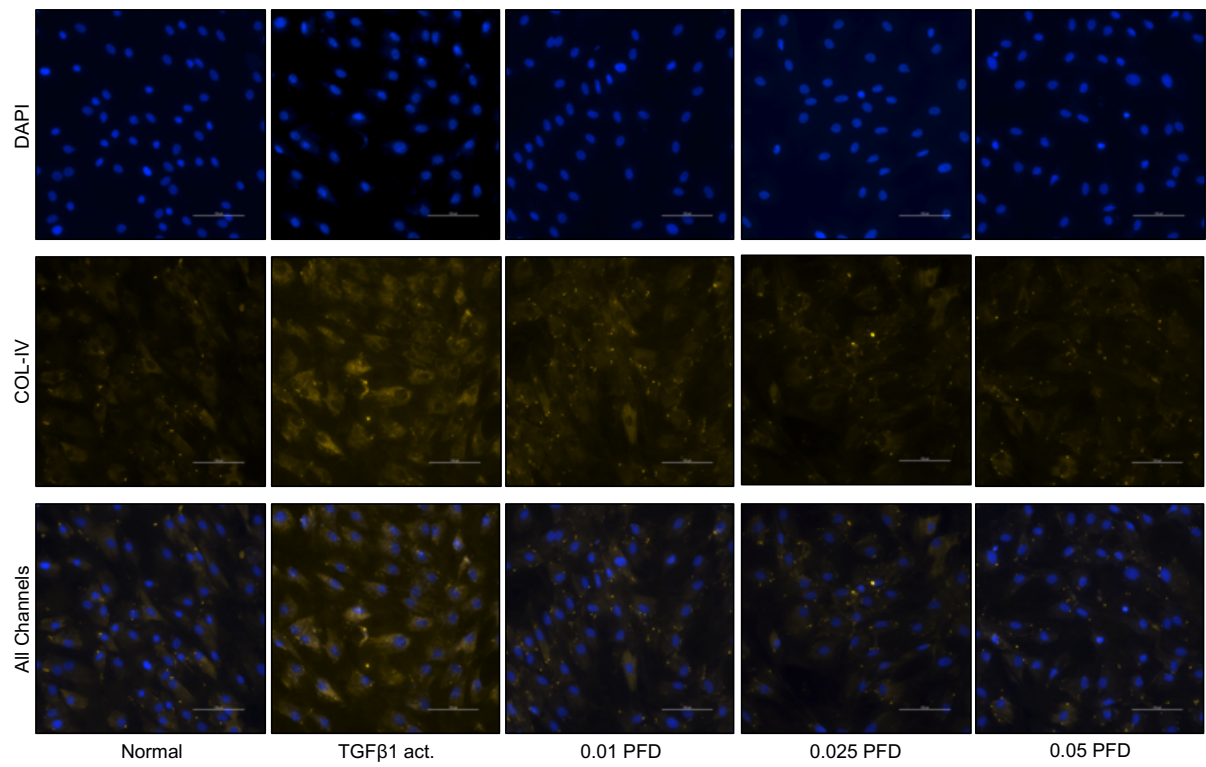
Figure 19: PFD reduces expression of Collagen-I and other pro-fibrotic factors involved with PNF.

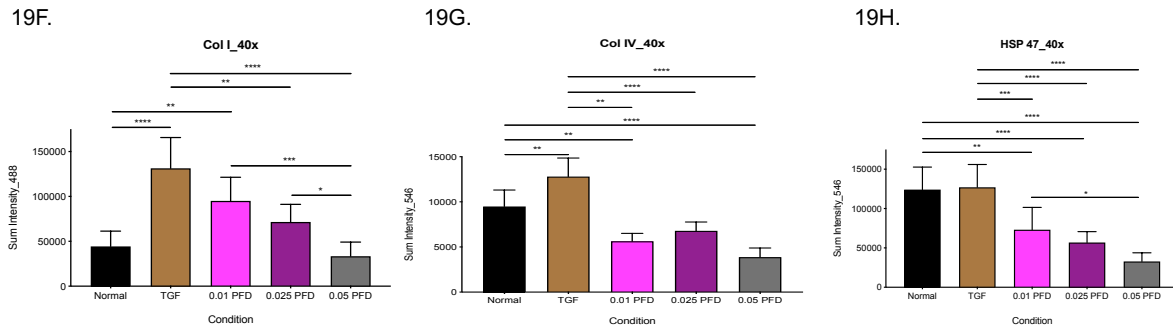
Primary Rat fibroblasts were activated with TGF- β 1 prior to treatment with PFD for 48h **A**. Representative Western blot visualization of proteins involved in TGF- β and other fibrogenic signaling in Primary Rat fibroblasts exposed under 10 ng/ml TGF- β , followed by treatment with 0.05 mg/ml, 0.1 mg/ml and 0.25 mg/ml PFD or no treatment (TGF- β and N) for 48h. **B**. Quantification of COL-IV, COL-I, FBN HIF-1 α and PI3K, pSMAD 3, pAKT, α -SMA, and HSP47 protein abundance by densitometry, normalized

against GAPDH (n=3 independent experiments). Results are shown as mean \pm SEM.

* $p < 0.05$, ** $p < 0.01$, *** $p < 0.001$.







Primary Rat fibroblasts activated externally with TGF- β 1 10 ng/ml were treated with PFD for 48h. Expression of pro-fibrotic factors was characterized by immunofluorescence imaging. **C.** COL-I **D.** COL-IV. **E.** HSP47 Protein expression levels of COL-I, COL-IV and HSP47 was characterized by ICC after treatment with different concentrations of PFD. Imaging of cells was done as mentioned earlier the methods section. **F, G and H** Statistical analysis of and cytosolic COL- I, COL-IV and HSP47 as observed after the treatment of activated cells. Description of the statistical analysis was mentioned earlier the methods section.

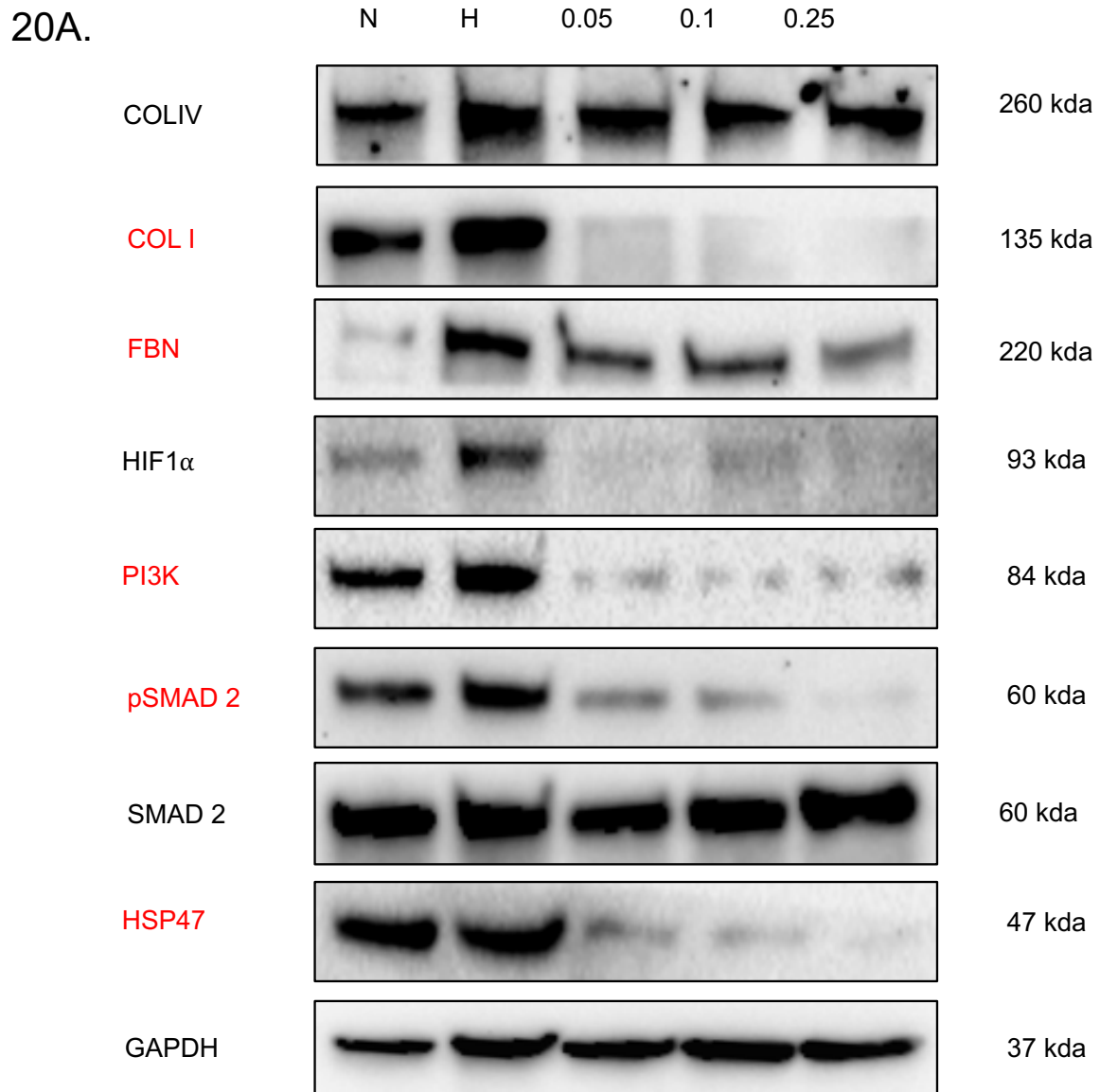
Abbreviations: α -SMA – alpha Smooth Muscle Actin; COL-I – Collagen I; COL-IV – Collagen IV; FBN – Fibronectin; GAPDH - Glyceraldehyde 3-phosphate dehydrogenase; HIF-1A- Hypoxia-inducible factor 1-alpha; HSP47 – Heat shock protein 47; PFD – Pirfenidone; PNF – Peripheral nerve fibrosis; SMAD 3 - Mothers against decapentaplegic homolog 2/3; SEM - Standard error of the mean

PFD reduces expression of pro-fibrotic factors induced by hypoxia signaling

While PFD showed potent anti-fibrotic effects through the downregulation of the TGF- β signaling by blocking TGF- β 1 and other downstream targets, we were further interested to understand if this hold true for hypoxic injury as well. As the hypoxic microenvironment is key to disease progression, understanding the molecular mechanisms of PFD in hypoxic insult is essential. Our Western analysis of primary rat fibroblasts exposed under hypoxic conditions for 48 h, treated with or without PFD showed how PFD regulates hypoxic primary rat fibroblasts. PFD successfully abolished expression of key pro-fibrotic factors activated in hypoxic primary rat

fibroblasts. Downregulation of collagen-I, HSP47 and fibronectin was observed already at 0.05 mg/ml PFD. In addition, PFD at 0.05 mg/ml also significantly inhibited PI3Kinase, exhibiting a HIF-1 α /PI3K axis mediated anti-fibrotic effect in hypoxic primary rat fibroblasts (figure 20A, 20B). Downregulation of these ECM deposition and remodeling targets occur in a non-dose-dependent manner. PFD at 0.05 mg/ml showed potent anti-fibrotic effect in regulating key pro-fibrotic targets in hypoxic primary rat fibroblasts.

Furthermore, PFD significantly inhibited phosphorylation mediated activation of SMAD 2, in a dose-dependent manner, but not SMAD 3 (Figure 20A, 20B). Interestingly, we also did not see any negative regulation of AKT in hypoxic primary rat fibroblasts treated with PFD (data not shown).



20B.

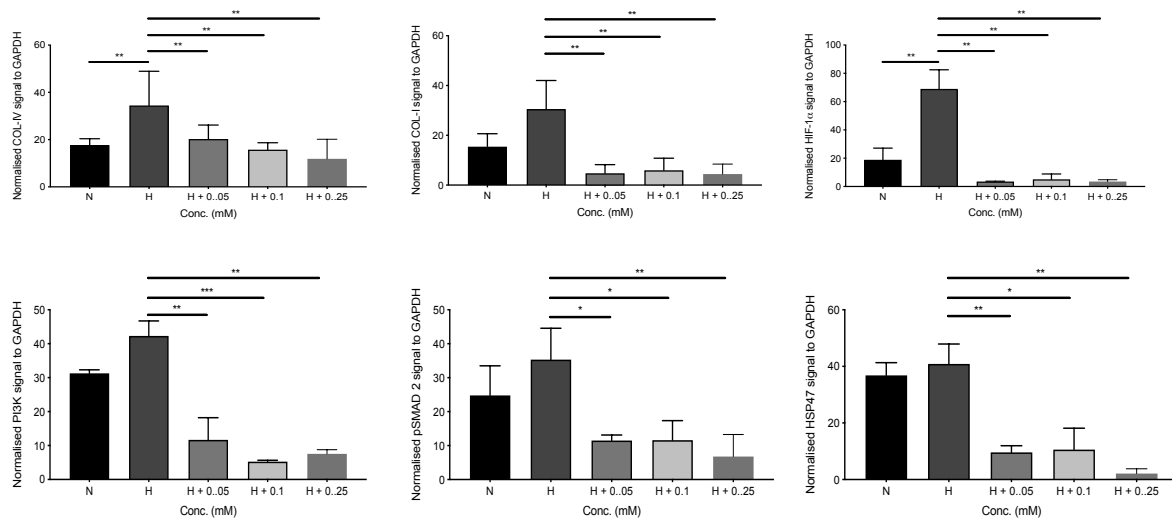


Figure 20: PFD reduces expression of Collagen-I and other pro-fibrotic factors involved with PNF in hypoxic fibroblasts.

Primary Rat fibroblasts were exposed under hypoxic conditions (2% O₂ for 48) prior to treatment with PFD for 48h **A**. Representative Western blot visualization of proteins involved in HIF-1 α and other fibrogenic signaling in Primary Rat fibroblasts exposed under hypoxic conditions (2% O₂ for 48), followed by treatment with 0.05 mg/ml, 0.1 mg/ml and 0.25 mg/ml PFD or no treatment (H and N) for 48h. **B**. Quantification of COL-IV, COL-I, FBN HIF-1 α and PI3K, pSMAD 2, pAKT, α -SMA. and HSP47 protein abundance by densitometry, normalized against GAPDH (n=3 independent experiments). Results are shown as mean \pm SEM. * p < 0.05, ** p < 0.01, *** p < 0.001.

Abbreviations: α -SMA – alpha Smooth Muscle Actin; COL-I – Collagen I; COL-IV – Collagen IV; FBN – Fibronectin; GAPDH - Glyceraldehyde 3-phosphate dehydrogenase; HIF-1A- Hypoxia-inducible factor 1-alpha; HSP47 – Heat shock protein 47; PFD – Pirfenidone; PNF – Peripheral nerve fibrosis; SMAD 2 - Mothers against decapentaplegic homolog 2; SEM - Standard error of the mean

Identification of crucial proteins and pathway analysis in TGF- β 1 stimulated fibroblasts treated with PFD

In an attempt to confirm the mechanisms and pathway analysis of PFD regulation, in a more quantitative manner, we conducted a full proteomic analysis of TGF- β 1

stimulated fibroblasts. We began by undertaking an unsupervised Principal Component Analysis (PCA) of our dataset, which reduces a high-dimensional expression profile of single variables or components, retaining most of the variation (Figure 21A). As the primary rat fibroblasts were isolated from sciatic nerves of different individual animal, we performed a PCA analysis where individual treatment of every replicate (sorted by negative controls, positive controls, PFD treated samples), to ascertain if differences in the proteomic profiles correlate with this parameter. A clear separation was observed between controls (normal vs TGF- β 1 stimulated primary fibroblasts) and PFD treated primary rat fibroblasts. We observed a homogeneous segregation amongst all the PFD treated samples (0.05, 0.1 and 0.25 mg/ml) and an extremely low intragroup variability, including absence of outliers. Our PCA analysis accounted for \sim 20% variability, which is extremely low (Figure 21A). Overall, nearly 5000 proteins were significantly regulated across the treatment groups in comparison to positive controls ([Table 8](#)).

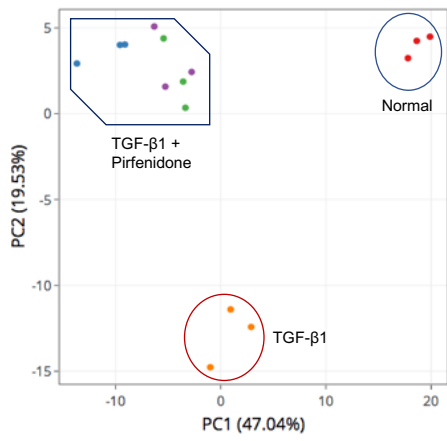
Data used in functional and pathway analysis were selected at the cut off values of adjusted p value ($p < 0.01$). Hallmark signatures showed that Genesets involved with the Epithelial-Mesenchymal Transition, Myogenesis and TGF- β signaling were the most upregulated Genesets in TGF- β 1 stimulated primary rat fibroblasts. Whereas, hallmark signature analysis further showed that Genesets involved with the cell cycle regulation particularly G2/M checkpoint and E2F targets were significantly upregulated normal untreated primary rat fibroblasts. Similarly, PFD treated samples (0.05, 0.1 and 0.25 mg/ml) showed a similar response when compared to positive controls, TGF- β 1 stimulated primary rat fibroblasts ([Table 9](#), [Table 10](#)). We have compiled the list of downregulated ([Table 9](#)) and upregulated ([Table 10](#)) pathways. A large number of Genesets were significantly disturbed below stringent q-value thresholds. In addition, the statistical analysis of differential expression of TGF- β 1 stimulated primary rat fibroblasts, when compared to normal untreated or to PFD treated samples are far greater than what can be expected just by chance and further confirms the effect of PFD.

Following our hallmark signature analysis, we next performed a differential expression analysis using a gene list ([Table 11](#)). As there are no currently available gene list for neural fibrosis, this list was designed after through research into pro-fibrotic factors across fibrosis in various organs (106) and list of targets used for TaqMan Array rat fibrosis analysis (<https://www.thermofisher.com/order/genome->

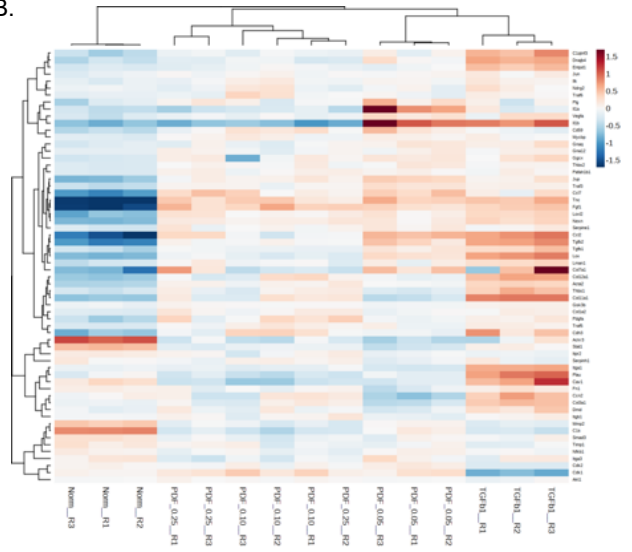
database/?pearUXVerSuffix=pearUX2&elcanoForm=true#!/ge/arrays/ge_all/?keyword=Fibrosis). We conducted a heatmap analysis using this list (Figure 21B). Our heatmap analysis clearly indicates PFD effectively downregulates pro-fibrotic targets. TGF- β 1 stimulated primary rat fibroblasts significantly upregulated fibroblast differentiation and ECM deposition targets (3-6fold difference) in comparison to untreated normal primary rat fibroblasts. PFD reversed the expression of these targets in primary fibroblasts stimulated with TGF- β 1 (Figure 21B).

Our differential expression analysis, gene ontology and hallmark signature analysis, further modulation of key pro-fibrotic signalling mechanisms. The TGF- β , PI3K/ AKT, SMAD and HIF-1 α signalling pathways were found to be enriched among the proteomic profiles of TGF- β 1 stimulated and differentiated primary fibroblast population. Additionally, PFD treatment after TGF- β 1 activation reduced expression of key targets involved with these pathways. Expression levels of these targets in PFD treated samples were comparable to normal untreated controls (Figure 21C-E). Following this analysis, we conducted a dose-dependent analysis of PFD using volcano plots (Figure 21F-I). Amongst the most downregulated targets, including Tenascin, Fibroblast Growth Factors, Collagen, Acta 2 and various other molecules responsible for fibroblast differentiation, cell-adhesion and ECM deposition were identified in normal untreated fibroblasts when compared to TGF- β 1 stimulated fibroblasts (Figure 21F). Dose-dependent PFD treatment inhibited expression of these targets as well (Figure 21G-I). Apart from regulating targets involved with the TGF- β , PI3K/ AKT, SMAD and HIF-1 α signalling pathways, PFD was also found to downregulate integrin signalling.

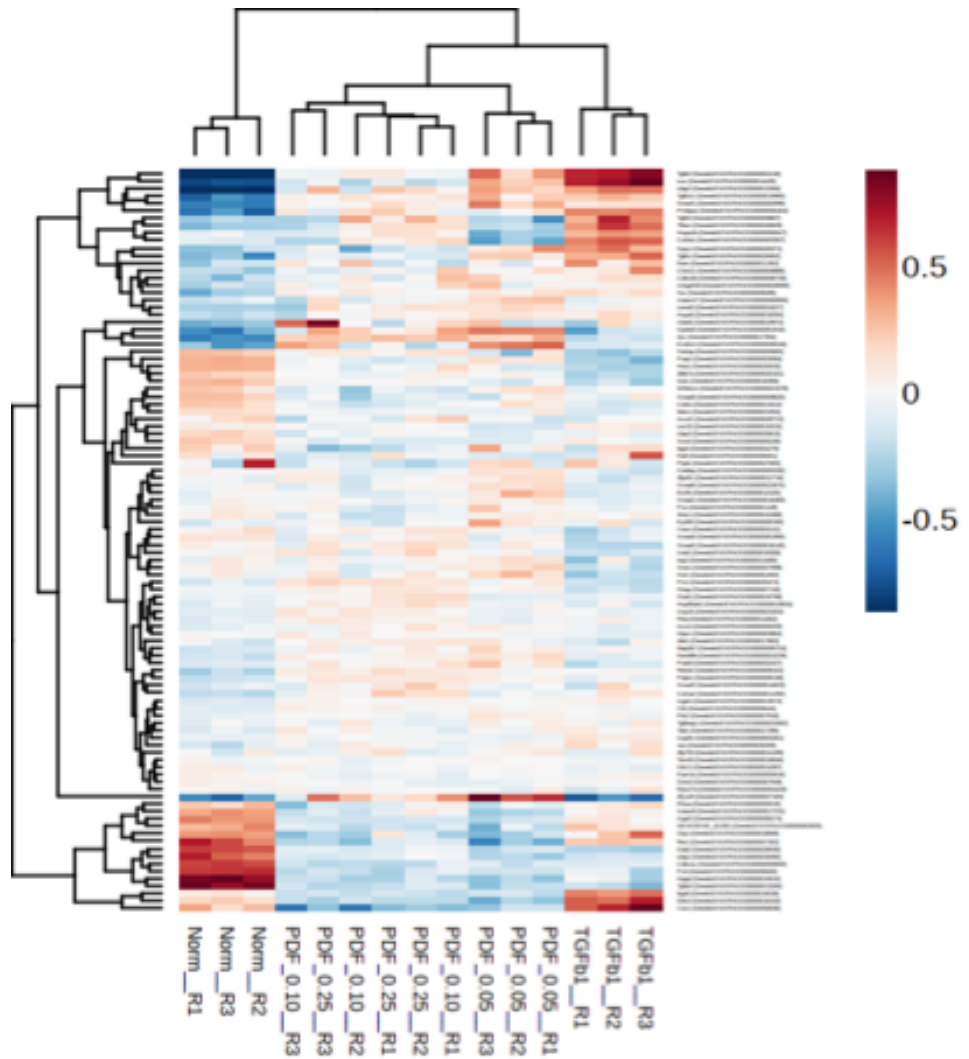
21A.



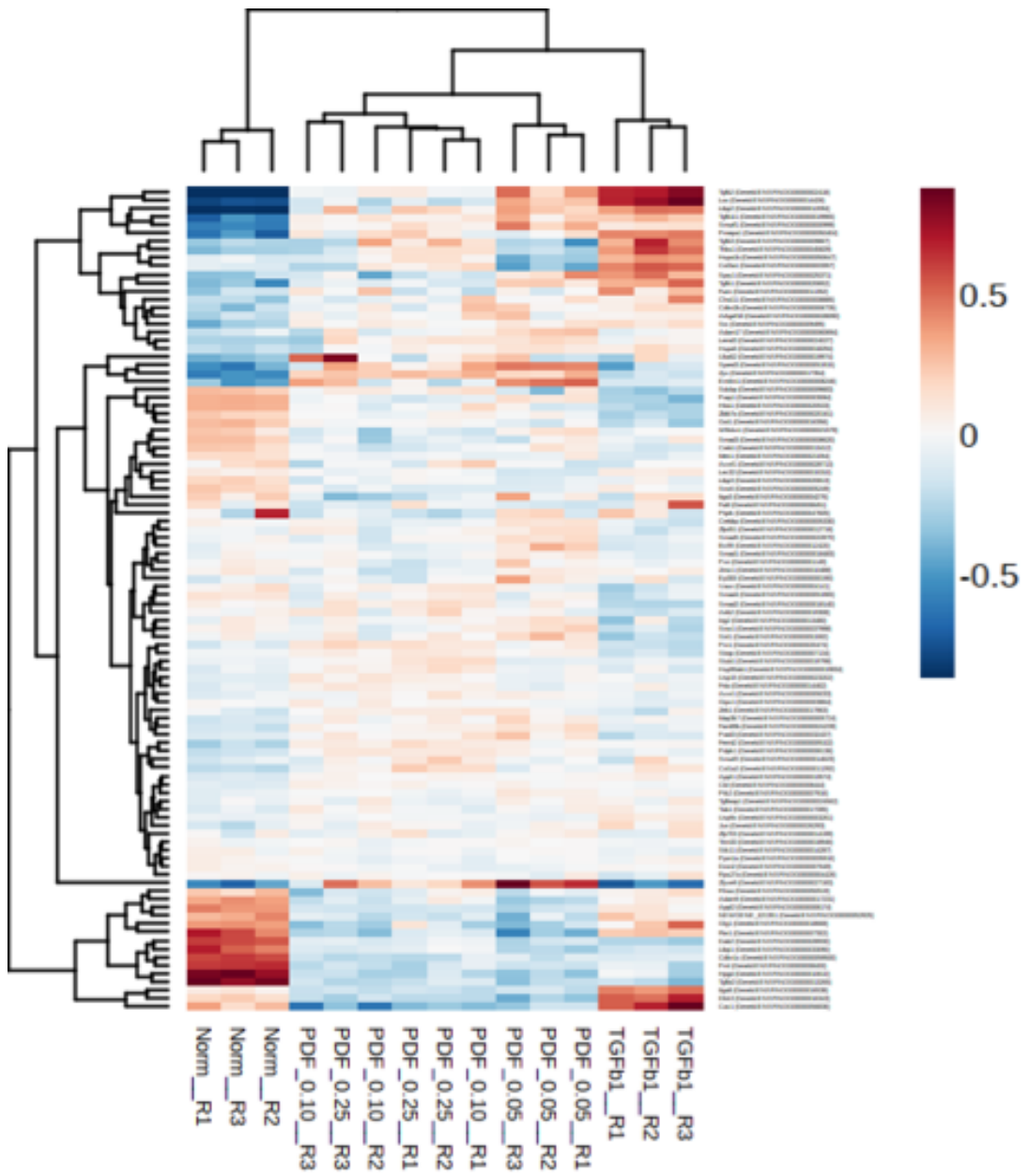
21B.



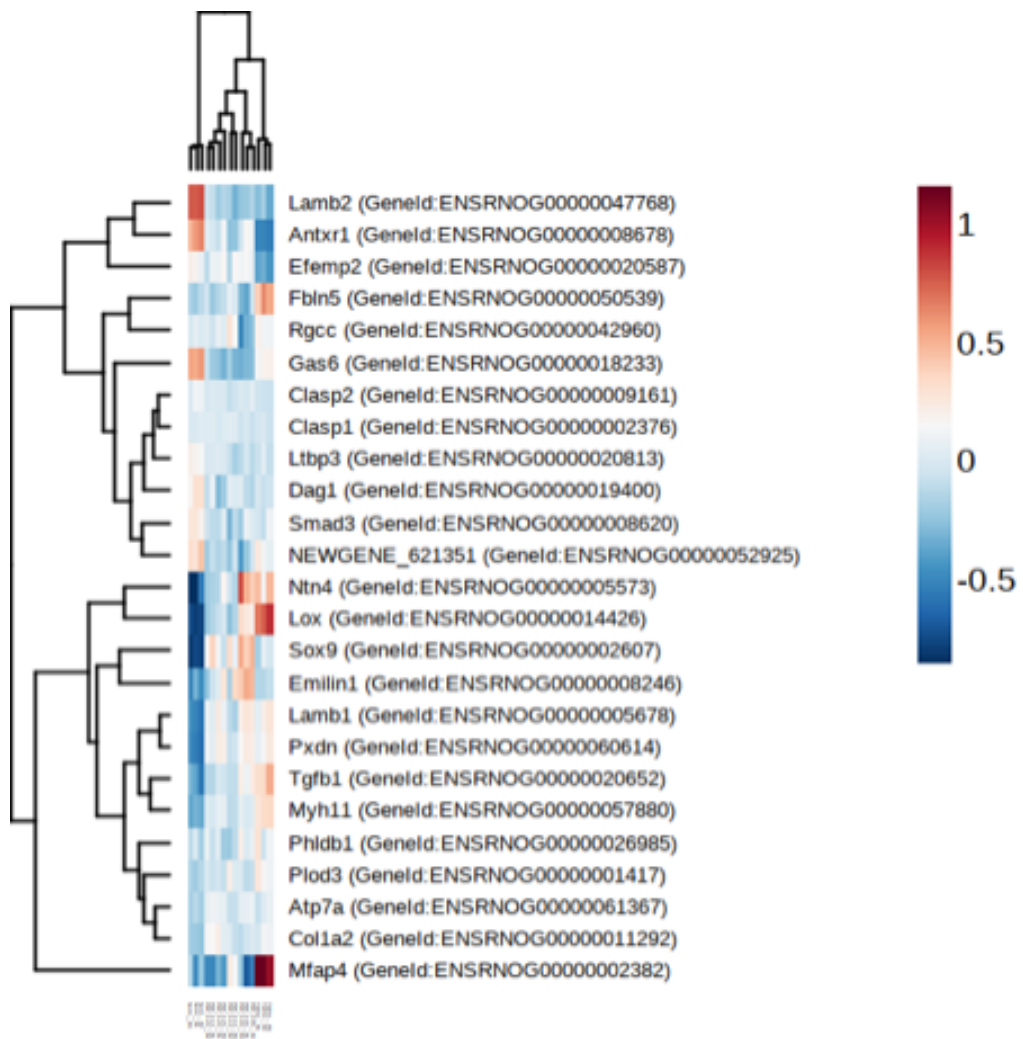
21C.



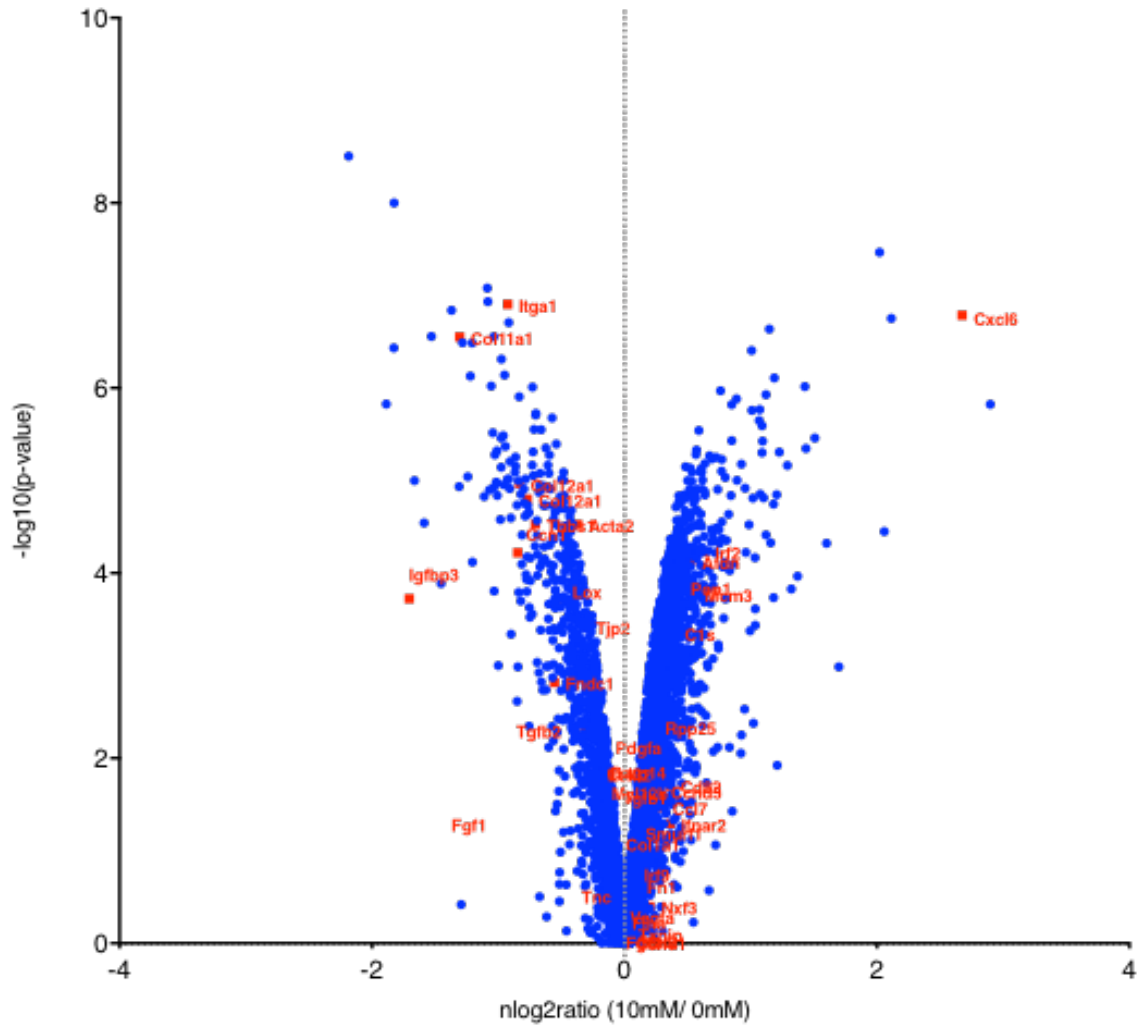
21D.



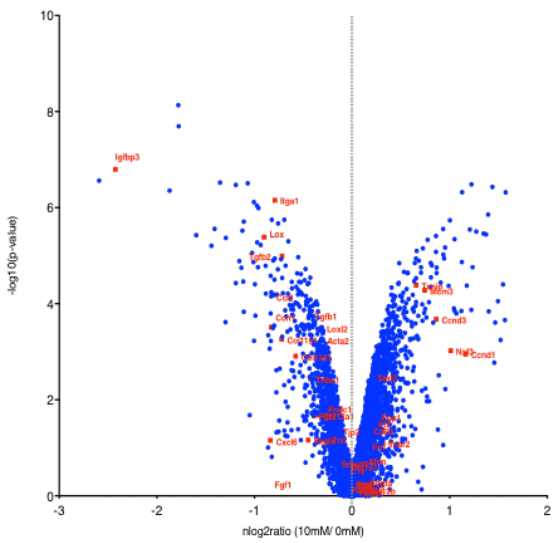
21E.



21G.



21H.



21I.

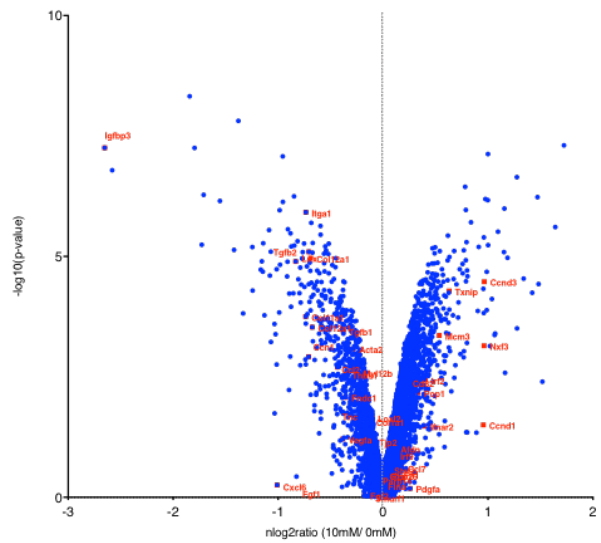


Figure 21: Proteomic analysis of TGF- β 1 induced fibrogenic phenotype in primary fibroblasts.

Primary Rat fibroblasts were activated with TGF- β 1 prior to treatment with PFD for 48h. Biological replicates including 3 independent peptide samples were analyzed for each condition – Normal Untreated Fibroblasts, TGF- β 1 activated fibroblasts, TGF- β 1 activated fibroblasts treated with 0.05 mg/ml PFD, TGF- β 1 activated fibroblasts treated with 0.1 mg/ml PFD and TGF- β 1 activated fibroblasts treated with 0.25 mg/ml PFD.

A. Principal component analysis of all proteomic data including the independent samples from every condition. **B.** Heatmap based on Total proteomics experiment from primary rat fibroblast subsets cultured under indicated conditions (visualized in the box and color-coded in the heatmap). Displayed is the euclidean distance between samples as calculated from regularized log transformed data. Darker color indicates higher expression of desired targets (n=3 donors, labeled as R1, R2 and R3). Information on the selection of the genes list can be found in the Results Section. Heatmap displaying TGF- β (**C**), Cell-Adhesion (**D**) and ECM (**E**) target genes colored according to deviation from gene average across shown samples for Normal, TGF- β 1 activated and TGF- β 1 activated and treated with PFD cells. **F-I.** Volcano plot visualization of Total Proteomics data from primary fibroblasts. All conditions including normal fibroblasts and PFD fibroblasts were compared to TGF- β 1 activated fibroblasts. Among downregulated peptides, ECM and pro-fibrotic targets are labeled in red, among downregulated transcripts, cell cycle regulator targets are labeled in red. Top differentially expressed genes are labelled. **F.** Volcano plot visualization of Total Proteomics data from normal primary fibroblasts vs TGF- β 1 activated fibroblasts. **G.** Volcano plot visualization of Total Proteomics data from TGF- β 1 activated fibroblasts treated with 0.05 mg/ml PFD vs TGF- β 1 activated fibroblasts. **H.** Volcano plot visualization of Total Proteomics data from TGF- β 1 activated fibroblasts treated with 0.1 mg/ml PFD vs TGF- β 1 activated fibroblasts. **I.** Volcano plot visualization of Total Proteomics data from TGF- β 1 activated fibroblasts treated with 0.25 mg/ml PFD vs TGF- β 1 activated fibroblasts.

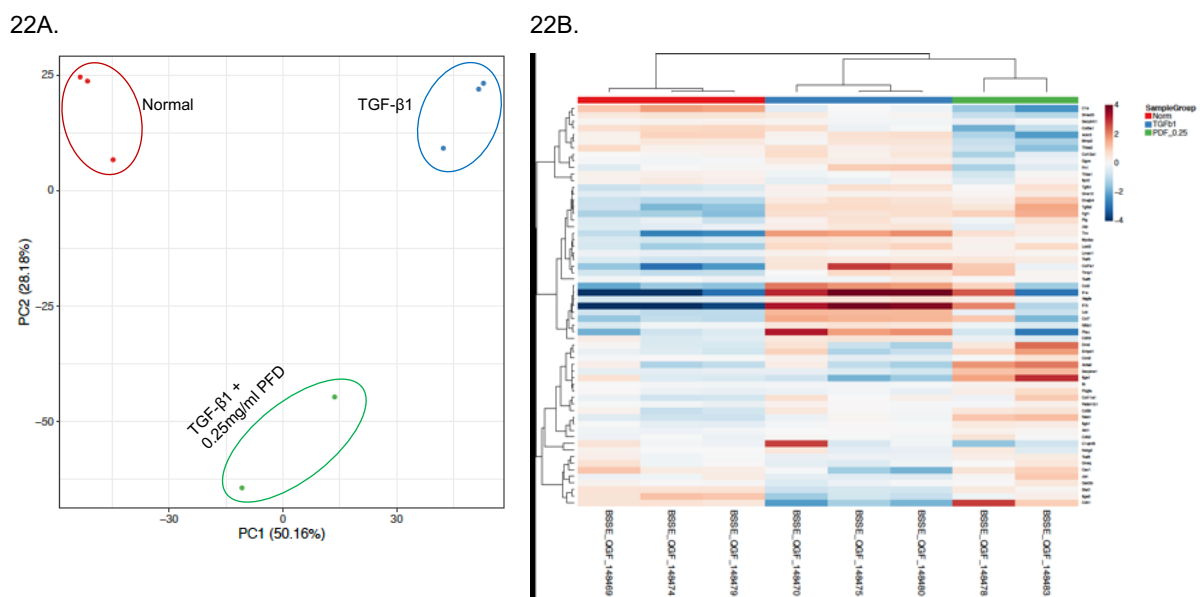
Abbreviations: ECM – Extracellular Matrix; PFD – Pirfenidone; TGF- β 1 - Transforming Growth Factor Beta 1

PFD arrests pro-fibrotic processes and targets TGF- β mediated gene upregulation

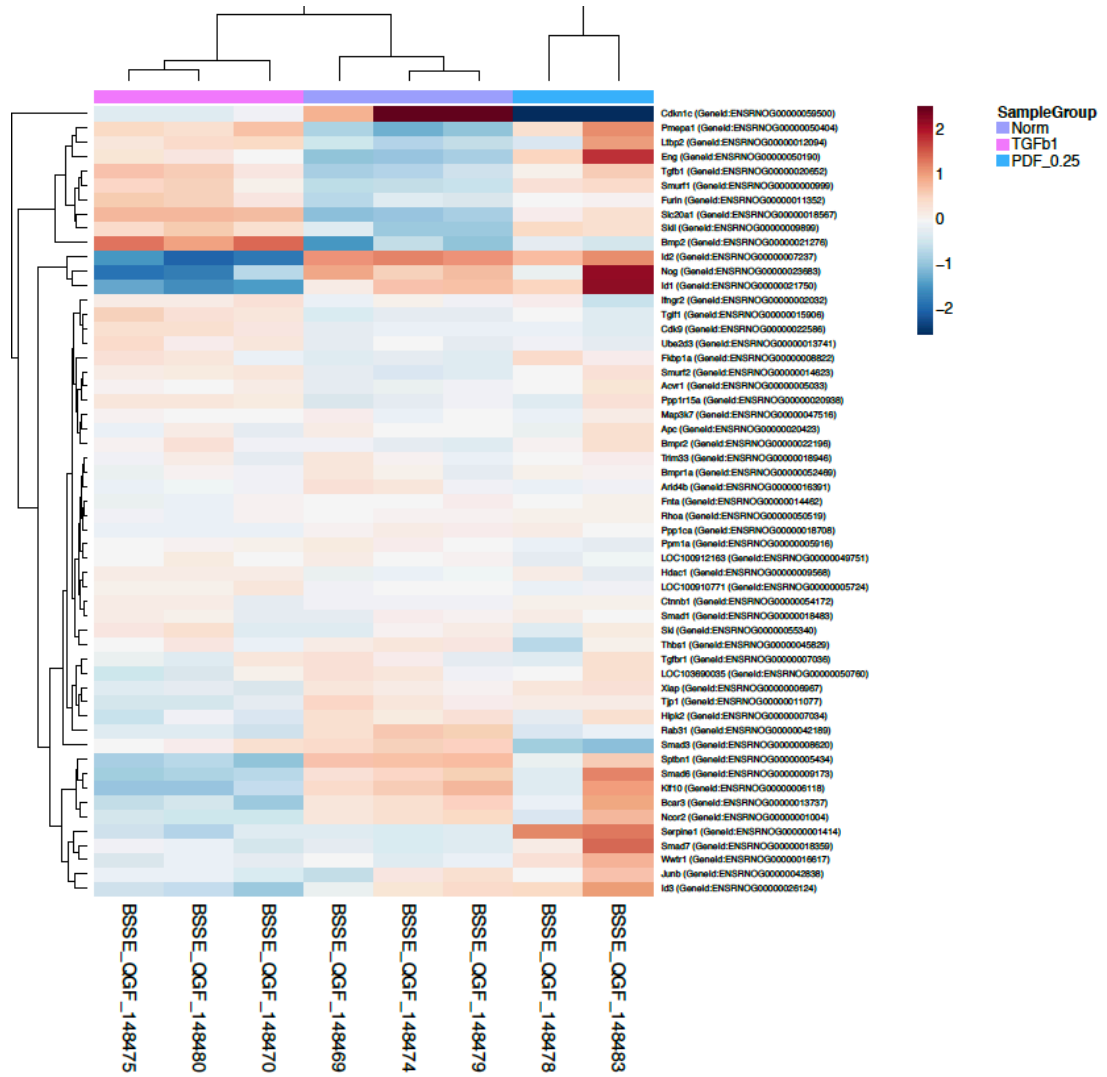
To further confirm our mechanistic understanding of disease regulation by PFD, we performed RNA sequencing, comparing untreated normal cells with TGF- β 1 stimulated fibroblasts with 0.25 mg/ml PFD treatment for 48 h on stimulated fibroblasts. After proteomic analysis, we also investigated if PFD acts dose-dependently at the genetic level. We did not observe any dose-dependent effect of PFD on stimulated population of fibroblasts (data not shown) and hence we concluded our analysis with 0.25mg/ml PFD only. Using unsupervised hierarchical clustering PCA analyses, we found that normal untreated fibroblasts (negative control), TGF- β 1 activated fibroblasts (positive control) and TGF- β 1 activated fibroblasts treated with 0.25 mg/ml PFD, each grouped together (Figure 22A). Expectedly, activation of primary fibroblasts with TGF- β 1 prior to PFD treatment did not affect the sub clusters, further indicating effective inhibition of TGF- β 1 by PFD. Additionally, absence of TGF- β 1 in untreated and inactivated fibroblasts did create a separate population.

The number of differentially expressed genes between these three conditions further revealed that significant inhibition of TGF- β 1 by PFD is in line with the PCA analysis. To further begin exploring the pathophysiological mechanisms regulated in these three groups, we performed a differential gene expression using the same gene list as was used for proteomic analysis. We found TGF- β 1 activated fibroblasts showed a 4-8fold difference in gene expression when compared to expression levels of individual genes in normal inactivated samples as well as to those treated with PFD (Figure 22B). From these analyses a hallmark signature analyses emerged with the most downregulated signatures corresponded to Tumor Necrosis Factor alpha (TNF α) signalling (adjusted p value – 2.633e-4), unfolded protein response (adjusted p value – 5.479e-49, inflammatory response (adjusted p value – 0.07305) amongst others in normal inactivated samples when compared with TGF- β 1 activated fibroblasts. Similarly, PFD treated fibroblasts when compared with TGF- β 1 activated fibroblasts, also showed downregulation of TNF α and inflammatory response signalling (data not shown). We therefore reasoned that PFD might induce anti-fibrotic phenotype through the transcriptional inhibition of key genes associated with TGF- β 1 signaling.

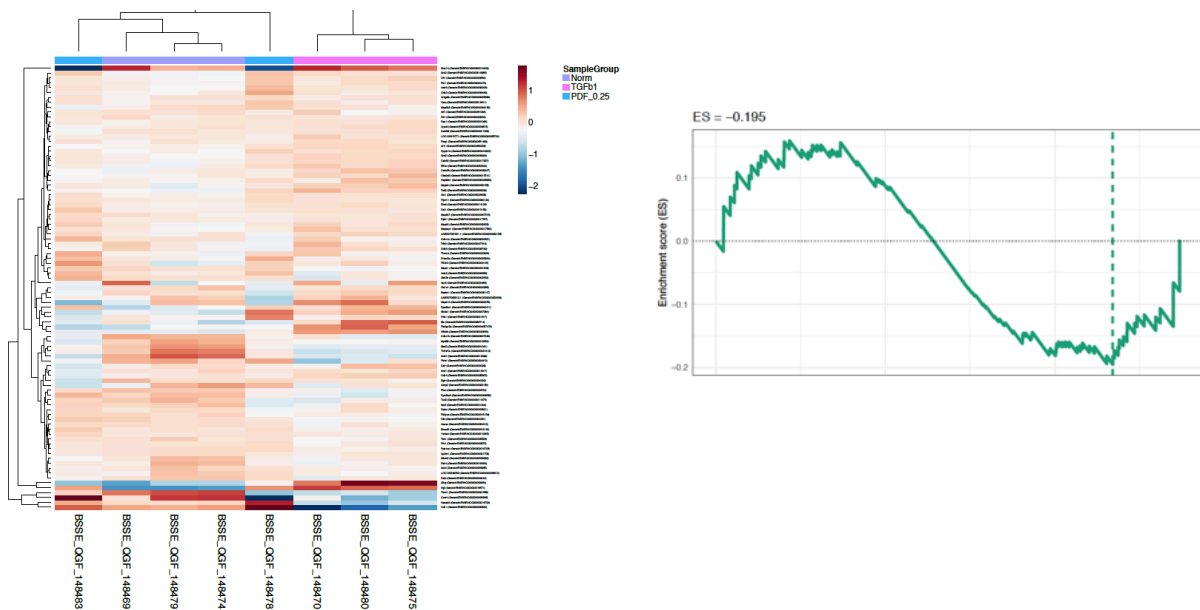
Indeed, our pathway analysis revealed the factors associated with TGF- β 1 signaling downregulated in response to PFD treatment (Figure 22C). In fact, classical TGF- β 1 signaling targets including, solute carrier family 20 member 1 (*Slc20a1*), spectrin, beta, non-erythrocytic 1 (*Sptbn1*), SMAD specific E3 ubiquitin protein ligase 1 (*Smurf1*), tight junction protein 1 (*Tjp1*), *Tgfb1*, bone morphogenetic protein 2 (*Bmp2*), amongst others were the most significantly downregulated in untreated fibroblasts and in PFD treated fibroblasts (data not shown). Our RNA sequencing analysis further revealed that PFD treatment significantly downregulation expression of genes associated with driving PI3K/ AKT/mTOR (Figure 22D), HIF-1 α (figure E) and ECM deposition pathways (Figure 22F). Interestingly, TGF- β 1 activated fibroblasts also significantly upregulated genes associated hepatic fibrosis (Figure 22G). Some of the genes known to drive hepatic fibrosis showed nearly a 6-fold differential regulation in TGF- β 1 activated fibroblasts. These included, transmembrane protein 231 (*Tmem231*), *Slc25a13*, macrophage stimulating 1 (*Mst1*), amongst others (Figure 22G). In order to further confirm our findings from RNA sequencing, we conducted qRT-PCR analysis of some of the influential ECM deposition targets. In line with our RNA sequencing data, we found PFD to negatively regulate key pro-fibrotic targets, inhibit TGF- β 1 and collagen biosynthesis (Supplementary Figure 5). Together, these data established a novel anti-fibrotic role of PFD in an *in vitro* neural fibrosis model.



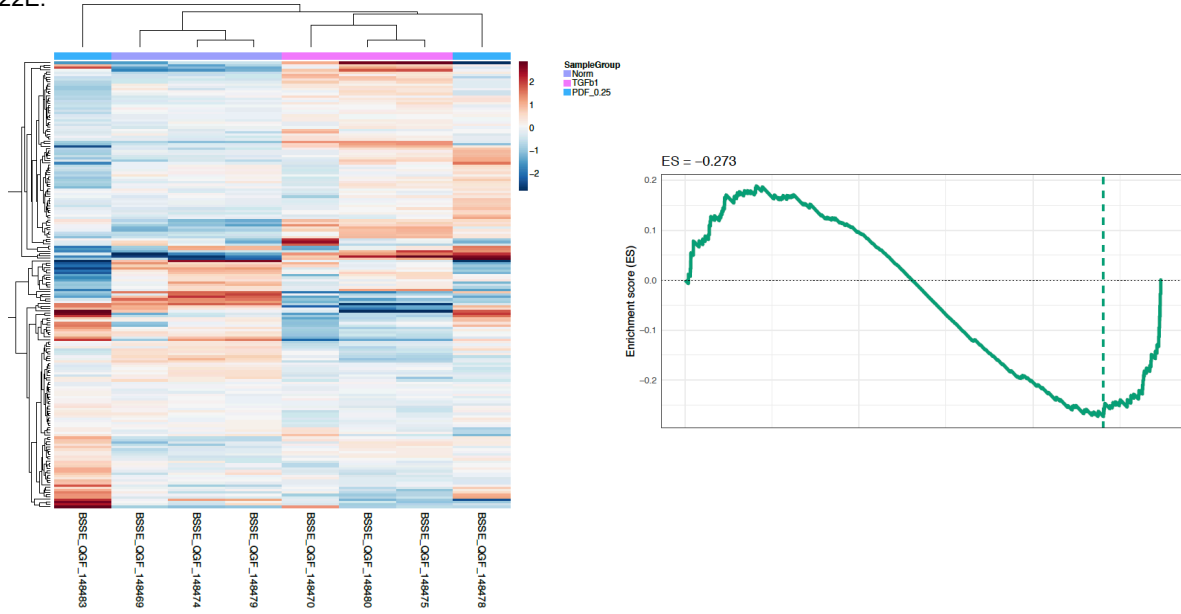
22C.



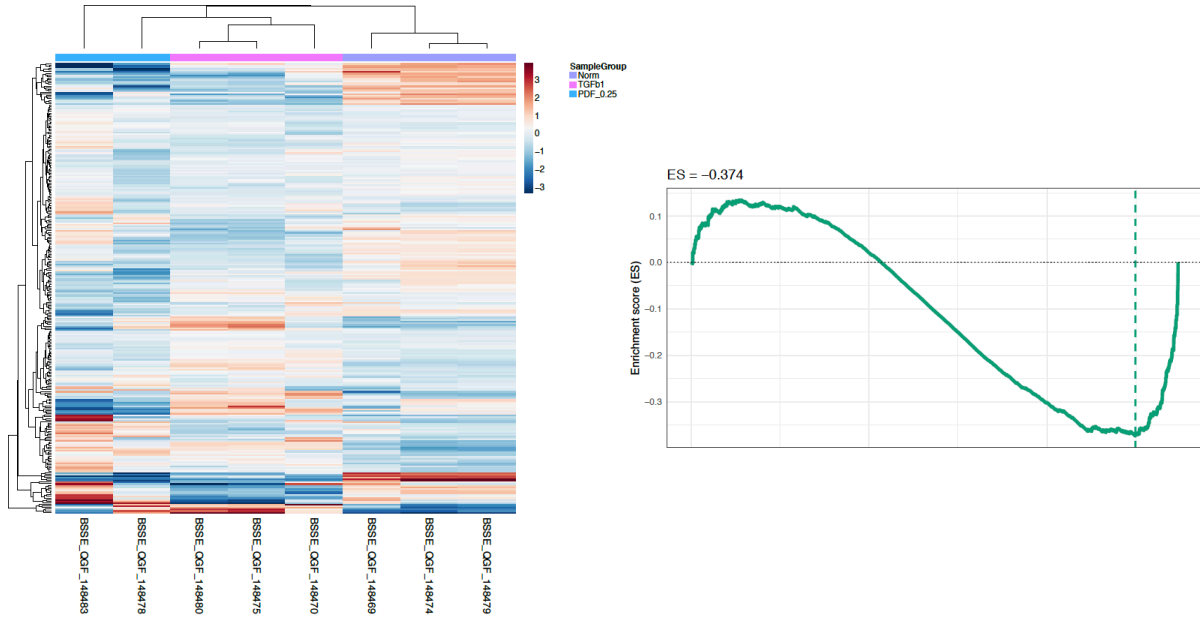
22D.



22E.



22F.



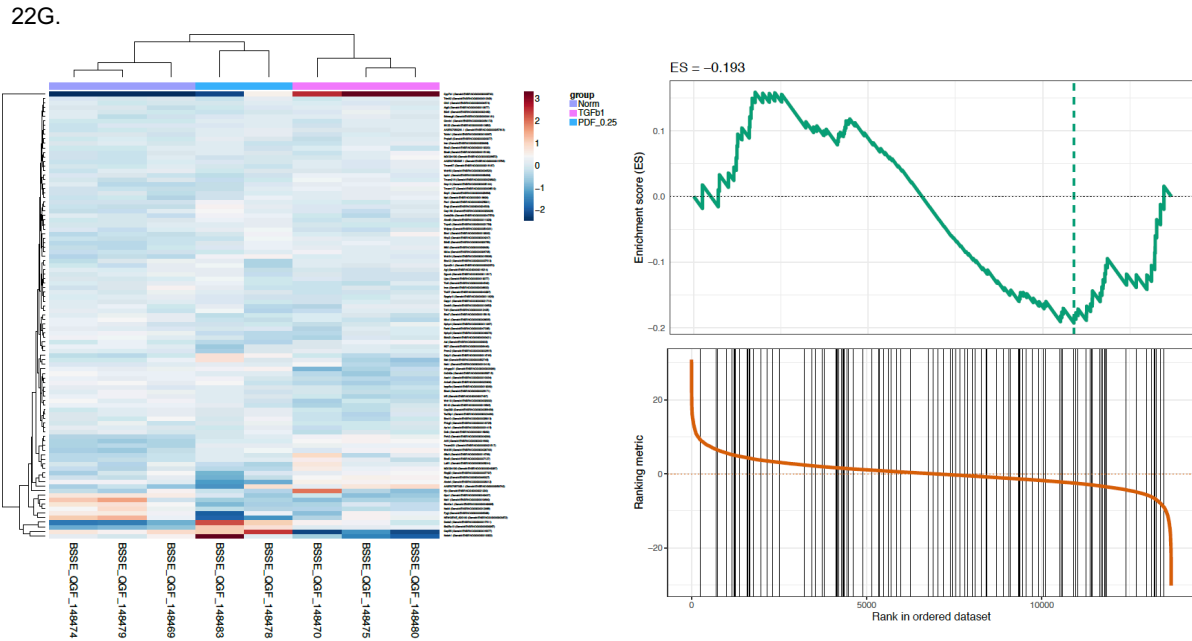


Figure 22: RNAseq analysis of TGF- β 1 induced fibrogenic phenotype in primary fibroblasts.

Primary Rat fibroblasts were activated with TGF- β 1 prior to treatment with PFD for 48h. Biological replicates including 3 independent peptide samples were analyzed for each condition – Normal Untreated Fibroblasts, TGF- β 1 activated fibroblasts, and TGF- β 1 activated fibroblasts treated with 0.25 mg/ml PFD.

A. Principal component analysis of all RNAseq data including the independent samples from every condition. **B.** Heatmap based on differential expression RNAseq experiment from primary rat fibroblast subsets cultured under indicated conditions (visualized in the box and color-coded in the heatmap). Displayed is the euclidean distance between samples as calculated from regularized log transformed data. Darker color indicates higher expression of desired targets (n=3 donors, labeled as Norm, TGF- β 1 and PFD_0.25). Information on the selection of the genes lists can be found in the Results Section. Heatmap displaying TGF- β (**C**), PI3K/ AKT/mTOR (**D**) and HIF-1 α (**E**) and ECM deposition (**F**) target genes colored according to deviation from gene average across shown samples for Normal, TGF- β 1 activated and TGF- β 1 activated and treated with PFD cells. **G.** Heatmap indicating genes associated with Hepatic Fibrosis. Data represents differential expression RNAseq experiment from primary rat fibroblast subsets cultured under indicated conditions (visualized in the box and color-coded in the heatmap).

Abbreviations: AKT - Protein kinase B (PKB); ECM – Extracellular Matrix; HIF-1 α - Hypoxia-inducible factor 1-alpha; mTOR - Mammalian target of rapamycin; PI3K - Phosphoinositide 3-kinase; PFD – Pirfenidone; TGF- β 1 - Transforming Growth Factor Beta 1; RNAseq – RNA sequencing

Discussion (Chapter: *L-Ala-L-Gln*)

Irrespective of the cause, chronic injury to any organ can lead to development of fibrosis. Fibrosis is characterized by excessive deposition of collagen, contraction of the ECM matrix, tissue damage and aberrant wound healing (107). Scarring and tissue fibrosis is driven by overactivation of effector cells including fibroblasts (108). Overactivation and differentiation of fibroblasts into myofibroblasts causes a differential abundance of collagen formation and formation of scar tissue. Excessive collagen deposition in peripheral nerves inhibits axonal regeneration at the injury site. Moreover, crosslinking of collagen induces tissue destruction which is resistant to protease degradation (62). Chronic injury to tissue fibrosis involves a series of biochemical signaling of several intra and extracellular factors. In addition to this, presence of hypoxic microenvironment can promote tissue damage and peripheral neuropathy (58).

HIF-1 acts on fibroblasts to regulate the ECM matrix under hypoxic conditions thereby making it a crucial regulator of the tissue architecture and functions (109). Together, compelling evidence suggests HIF-1 α modulates the complexity of fibrosis of various organs and signalling of HIF-1 α is of important clinical relevance. Its role on the pathological outcome of fibroblasts and macrophages makes it a suitable target for pharmacological and genetic inhibition in PNI as well. Furthermore, several components of the HIF-1 signalling cascade regulates biochemical signalling of various extracellular growth factors further indicating its varied role in tissue remodelling.

L-Alanyl-L-Glutamine is a dipeptide known for its ability to promote wound healing (94), immune modulation and regulation of ECM matrix and peritoneal fibrosis (95). In another recent study the potential therapeutic value for glutamine in the prevention of postoperative tissue fibrosis was studied using peritoneal fibroblasts (110). Considering the diverse effects of hypoxia on tissue modulation and fibrosis, we studied the therapeutic value of L-Alanyl-L-Glutamine on primary fibroblasts under continuous and episodic hypoxic conditions. For our study, we focused mainly on primary fibroblasts harvested from WT Wistar rats as this would enhance the relevance of the study keeping in mind its utility in future *in vivo* studies. The aim of our study was also to identify whether L-Alanyl-L-Glutamine is involved with anti-fibrotic phenotype in *in-vitro* controlled conditions using primary fibroblasts. In order to

increase the relevance of the project to understand fibrotic mechanisms, we used two different modes of hypoxic injury on our fibroblasts. We believe hypoxia in fibrotic tissues could be chronic and acute depending on the extent of injury and tissue damage. Chronic hypoxia is hypothesized to be present at the exact site of injury, which we have represented as consistent or continuous hypoxia. Whereas acute hypoxia could be present at the peripheral ends from the exact site of injury represented by irregular or episodic hypoxia.

Additionally, accumulation of ECM in fibrotic diseases is a resultant of transcriptional activation of fibrillar collagens. Since the production of functional collagens depends on a complex machinery of auxiliary proteins and specific phenotypic regulators (111), we analyzed the expression patterns of SMAD 2/3, HSP47, Collage-I and Collagen IV. In the present study, we found that HIF-1 α was dramatically downregulated in hypoxic primary rat fibroblasts treated with L-Ala-L-Gln. In addition, as HIF-1 α modulates other pro-fibrotic factors including SMAD signalling, we found that L-Ala-L-Gln was able to downregulate these factors as well. Our observations led us to conclude that L-Alanyl-L-Glutamine regulates both of modes of hypoxic injury in primary fibroblasts *in vitro*. As both of the modes of hypoxic injury is highly relevant in tissue fibrosis, we conclude that L-Ala-L-Gln might play an important role in reducing tissue damage and fibrotic phenotype.

As HSP47 and SMAD 2/3 are highly expressed in hypoxic primary fibroblasts, that contribute to collagen production, it is remarkable to see that L-Ala-L-Gln downregulates collagen biosynthesis and production without affecting the cell viability, motility and proliferative abilities. As myofibroblasts present in fibrotic tissues express additional cytokines/ growth factors, it would be interesting to see whether L-Ala-L-Gln is also associated with additional anti-inflammatory activities.

The results indicate that L-Ala-L-Gln induces a significant downregulation of major pro-fibrotic biomarkers in primary fibroblasts in both continuous and episodic hypoxic conditions. Our results also indicate that as low as 2h exposure of untreated samples to hypoxia (episodic hypoxia) is able to upregulate expression of key pro-fibrotic targets including fibronectin and collagen (Figure 8). Consequently, treatment of hypoxic fibroblasts with L-Ala-L-Gln was found to reduce the expression of these pro-fibrotic markers in a dose dependent manner.

Cellular responses towards anti-fibrotic compounds often elicit cytotoxic, inflammatory and redox reactions in patients and hence cellular cytotoxicity is an essential

component for studying the effect of anti-fibrotic compounds (112). We evaluated the cytotoxic and cell death effects of L-Ala-L-Gln on normoxic and hypoxic fibroblasts and found that the dipeptide does not induce any cell death/ damage to cell viability in normoxic as well as hypoxic primary fibroblasts. This is furthermore essential to understand that though L-Ala-L-Gln shows anti-fibrotic effects, it does not enhance any additional damage to the primary fibroblasts. This could be crucial while studying the anti-fibrotic effects of L-Ala-L-Gln on *in vivo* fibrotic models.

Enhanced metabolic stress causes a significant depletion of intramuscular glutamine due to accelerated outward transport in critically ill patients (113). Whole body rate of appearance of glutamine was recorded to be around 5.8 ± 1 micromol x kg⁻¹ body wt x min⁻¹. Keeping this in mind, we used several doses of L-Ala-L-Gln (1, 10 and 100 mM). Though 10 and 100mM doses are above the physiological concentrations, we wanted to check a dose-dependent effects of L-Ala-L-Gln on hypoxic fibroblasts. Our results indicate that it may be necessary to treat hypoxic fibroblasts with 10mM and 100mM of L-Ala-L-Gln to prevent and reduce PNF. Further studies should be performed to understand the metabolic regulation of L-Ala-L-Gln on hypoxic and stress induced fibroblasts and other effector cells responsible for fibrosis. Also, it is interesting to understand if L-Ala-L-Gln has any inflammatory role on these effector cells.

Understanding the molecular mechanisms involved with activation of fibroblasts up to development of scarring/ fibrosis is of paramount importance as this could help us to identify key biomarkers in disease progression. In a first of its kind, we evaluated protein expression profiles in perineurial derived *in-vitro* fibrosis model using a quantitative phosphor-proteomic approach and multivariate statistical analysis. The dipeptide L-Ala-L-Gln significantly cell adhesion and cellular response to hypoxia in association with reduced fibrogenic potential of hypoxic fibroblast. Our mass spectrometry-based phosphor-proteomic analysis demonstrated that L-Ala-L-Gln significantly inhibited the expression of a number of individual proteins associated with fibrosis disease progression. Our analysis identified key targets including Ak1s1, Ctnnd1, Irs1, Rragc, Plcg1, Itga11, Diaph1, Fcdc1, Fndc3b, Col1a1 and Pxn (Figure 11), amongst many others to be significantly downregulated upon treatment with L-Ala-L-Gln. Pathway analysis helped us to identify the correlation of these factors with Focal adhesion, PI3k, HIF-1 α , mTOR, ECM-interaction, ERBb, FOXO and TGF- β signaling pathways. Elevated levels of PI3k/mTOR and HIF signaling have long been

associated with progressive fibrosis in various organs (114-116). In addition to this ECM has long been identified as a key driver of fibrosis. Our analysis helped us to identify 2 key targets – *Camk2d* and *Plcg1* to be significantly downregulated in L-Ala-L-Gln treated samples. The proteins encoded by *Camk2d* and *Plcg1* are associated with increased oxygen delivery and VEGF signaling indicating a potential mechanism by which L-Ala-L-Gln inhibits HIF-1 α signaling. Furthermore, as ECM has long been found to be a key driver of organ fibrosis (117), we were particularly interested to investigate if our phosphor-proteomic analysis is in line with our initial findings. L-Ala-L-Gln treated fibroblasts reduced the expression of downstream targets associated with Collagen biosynthesis and major ECM-interacting partners (Figure 5 A-C).

Though our study didn't investigate the differentiation potential of hypoxic fibroblasts, our phosphor-proteomic analysis is consistent with previous findings in focal adhesion associated fibrosis progression (114). Among the focal adhesion signaling associated proteins, we found multiple factors including Cav1, Pxn, Itga11, amongst others (Table 3) to be significantly reduced, hence providing us with the mechanistic approach of L-Ala-L-Gln in inhibiting post-operative adhesions (NCT04250467), indicating its clinical relevance and significance.

Interestingly, along with its anti-fibrotic properties, we found some other targets associated with the glutaminergic and GnRH signalling pathways to be significantly upregulated in L-Ala-L-Gln treated fibroblasts. These findings are completely in contrast to usual anti-fibrotic pathway inhibitors and biological compounds. An emerging literature suggests that the GnRH signalling is associated with neuroprotective and neurodegeneration properties in the CNS. Though currently from our proteomic analysis we cannot unambiguously attribute these changes to neurogenerative abilities of L-Ala-L-Gln but these striking findings (Table 7) prompts us to propose that L-Ala-L-Gln might have additional biological functions in addition to exhibiting anti-fibrotic and anti-adhesion phenotypes. It will be important in future studies to dissect out the relative contributions of HIF-1 signalling in modulating regenerative capacities of injured neurons and if L-Ala-L-Gln indeed has any beneficial effects.

Our study clearly helps us to understand the mechanistic details of anti-fibrotic potential of L-Ala-L-Gln in an in-vitro model of neural fibrosis. Whether L-Alanyl-L-Glutamine plays a dual role (anti-inflammatory and anti-fibrotic) on hypoxic injury induced fibrosis needs to be investigated further. The ability to reduce tissue damage

and fibrosis by Glutamine in rats with colitis has been reported earlier (118). Our study further demonstrates a possible role of L-Alanyl-L-Glutamine in hypoxic injury induced fibrosis *in vitro*.

Discussion (Chapter: *Pirfenidone*)

Peripheral nerve fibrosis is a chronic, fibroproliferative disorder which causes grave debilitating effects despite surgical interventions. The cellular and molecular heterogeneity underlying PNF remains undeciphered. Hypoxic injury and TGF- β signaling creates a microenvironment that sustains diseases progression in fibrosis. Our work has shown that hypoxic and TGF- β injury induced fibroblasts have significantly altered patterns of transcriptional and translational signatures compared to untreated normal fibroblasts derived from sciatic nerves of WT Sprague-Dawley rats. These fibroblasts along with the hypoxic microenvironment may therefore represent a residual manifestation of fibrosis after traumatic/ non-traumatic injuries and post-operative surgical complications. The microenvironment may further lead to generation of chronic inflammation and lead to disease recurrence. As myofibroblasts, the key effector cells are formed from the differentiation of fibroblasts, therapies counteracting this differentiation may prove to be beneficial for PNF.

The purpose of this study was to find non-toxic antifibrotic agents which can prevent hypoxic and TGF- β injury induced disease progression at an early stage and assist in regeneration mechanisms. The anti-fibrotic effects of PFD were investigated in terms of cell proliferation, cell death, regulation of collagen biosynthesis and ECM deposition of TGF- β 1 stimulated primary rat fibroblasts and hypoxic primary fibroblasts. Our results demonstrated a clear suppressive effect of PFD on sciatic nerve derived primary fibroblasts as well as on human fibroblasts. PFD treated primary fibroblasts were associated with reduced expression of pro-fibrotic and ECM deposition factors, similar to what has been previously reported in other tissues as well (96, 98, 100). Based on our findings and earlier research, we can clearly conclude that PFD exerts its anti-fibrotic functions by inhibiting TGF- β 1 and TGF- β signaling.

TGF- β 1 has been found to regulate a wide array of cellular processes, including cell proliferation, migration, differentiation as well as transcriptional regulation of key genes associated with ECM remodeling. Though various cytokines have been implicated in disease progression, TGF- β 1 is the key mediator of tissue fibrosis. Keeping this in mind and to possibly mimic the tissue fibrotic microenvironment, we established an *in vitro* 'fibrotic' culture through the stimulation of primary fibroblasts with TGF- β 1. In this study, we successfully demonstrated that TGF- β 1 activated fibroblasts induced ECM deposition, myofibroblast differentiation and increased protein and mRNA expression

of factors associated with collagen biosynthesis. Activated myofibroblasts also showed increased proliferation and inflammatory signaling. We further demonstrated that PFD treatment significantly affected mRNA and protein of collagen-I, collagen-IV, α -SMA and TGF- β 1. Collectively, our data proved that PFD inhibited TGF- β 1-regulated fibrotic processes *in vitro* and could be key towards reducing disease associated complications in patients with PNF.

Scarring induces activation of cytokines which further leads to accumulation of excessive fibroblast and myofibroblast population at the fibrotic tissue. This core tissue eventually leads to excessive ECM synthesis, collagen deposition and distorted tissue architecture. It is hypothesized that hypoxic microenvironment and TGF- β regulates the core microenvironment and drives disease progression. Apoptosis is a key biological process responsible for regulating the accumulation of excessive myofibroblasts and remains an indispensable mechanism in maintaining tissue homeostasis (119). Activated and differentiated fibroblasts and myofibroblasts are often to be resistant to apoptosis. Hence, inhibition of proliferation and induction of apoptosis could be helpful in controlling the profibrogenic effects. In this context, we examined effects of PFD on the regulation of cell viability, proliferation and cell death of TGF- β 1 activated fibroblasts. PFD inhibited the proliferative activity of hypoxic and TGF- β 1 activated fibroblasts as demonstrated by Alamar and Cell Titer Glo assays. Additionally, PFD induced a Caspase 3/7 mediated cell death of hypoxic and TGF- β 1 activated fibroblasts, which could form to be crucial towards regulating the accumulation of excessive myofibroblasts and ECM deposition. We further ruled out that the anti-proliferative effects of PFD were mediated by drug toxicity, as evidenced by the cell proliferation and viability data of normoxic/ hypoxic Schwann cells treated with PFD. Our data on Schwann cells is particularly important because Schwann cells are key to nerve regeneration strategies and hence is key towards repair after injury.

Great strides have been made in understanding the pathophysiology behind fibrosis. However, the signaling regulation and the relationship between TGF- β and downstream targets remained unknown. Research suggest that the basis of fibrosis treatment lies in regulating three major barriers: hypoxic regulation, inflammation and ECM deposition mediated fibrogenesis. We have tried to establish all these in our *in vitro* models. Increase in TGF- β 1 significantly upregulated TNF- α and PFD significantly downregulated several factors involved with TNF- α at the translational

and transcriptional levels. In addition, PFD was also found to negatively regulate inflammatory response activated by TGF- β 1 in differentiated fibroblasts. Key factors including, interferon regulatory factor 7 (*irf7*), LIF interleukin 6 family cytokine (*lif*), interleukin 1 beta (*il1 β*), to name a few were the most significantly downregulated targets. Gene set enrichment analyses on pro-fibrotic macrophages, highlighted the presence of these targets in fibrosis of the lungs, thereby indicating an immunomodulatory role of PFD in TGF- β 1 in differentiated fibroblasts. How and whether the immune modulatory genes regulate the tissue fibrosis in neural fibrosis needs further investigation. Taken together, our data indicates PFD possesses an anti-inflammatory function and could hold key to negatively regulate the chronic inflammatory state present in scarred tissues.

This study showed an overall hypoxic injury induced fibrotic state in neural fibroblasts exposed under hypoxic conditions for 48 h, including a significant rise in HIF-1 α and other downstream targets including SMAD 2 and HSP47. Whether hypoxia also induces enzymatic activities of HSP47 to promote collagen biosynthesis, needs further experimentation, but our Western data clearly confirmed upregulation of pro-fibrotic collagen and fibronectin levels. This was further confirmed by proteomic and RNA expression analyses. We observed increase in expression of hypoxia promoting genes and their corresponding protein targets in differentiated fibroblast population. Lysyl oxidase (*lox*), ephrin A3 (*efna3*), heme oxygenase 1 (*hmox1*), caveolae associated protein 3 (*cavin3*), vascular endothelial factor A (*vegfa*) were some of the genes amongst others found to be up regulated in response to low oxygen levels in differentiated fibroblasts only. Correspondingly, PFD treatment abolished the expression of these genes and expression of these targets in PFD treatment were comparable to near normoxic levels. These data are in line with the fact that chronic hypoxia induces vascular remodeling, resulting in progressive exacerbations of the hypoxic microenvironment. Increasing evidence also suggests that chronic hypoxia is actively involved in fibrogenic phenotype and along with TGF- β is also involved in stimulating production of ECM. Our proteomic and Western analyses further highlight these key aspects of hypoxic injury in primary fibroblasts. ECM factors including fibronectin, IGF-binding protein 3, collagens, collagen-modifying enzymes including lysyl oxidase were persistently activated in hypoxic and TGF- β 1 activated fibroblasts and provides a key mechanism that is involved in aggravating tissue fibrosis. These

evidences further highlight how PFD successfully targets HIF-1 α and hypoxic signaling and might provide a rational strategy to control pathogenesis of fibrotic disease.

TGF- β can signal via the canonical SMAD signaling pathways or through the activation of non-SMAD signaling pathways such as the MAP Kinase, PI3 Kinase/ Akt, mTOR, resulting in the activation of the Epithelial to Mesenchymal Transition. In order to explore the exact mechanisms through which TGF- β 1 actions are regulated in neural fibrosis by PFD, we examined the regulation of SMAD as well as other non-canonical pathways. Studies from fibrosis in other organs indicate that PFD counteracts TGF- β 1 through the downregulation of phosphorylation mediated activation of SMAD 2/3. Interestingly, in our primary rat fibroblasts derived neural fibrosis model, we found PFD inhibit phosphorylation of SMAD 3 but not SMAD 2. Basal phosphorylation of SMAD 3 was significantly upregulated in TGF- β 1 stimulated primary fibroblasts, but not SMAD 2. Importantly, our Western analysis is further confirmed on our proteomic data, indicating that PFD negatively regulated activated canonical signaling through suppression of SMAD 3. Our cell type signature analysis revealed that populations belonging to fibroblasts, such as neuroepithelium fibroblasts, cardiac and retinal fibroblasts were reduced in PFD treated samples. As all the cell types are involved with activated SMAD signaling in fibrosis, these findings raise the possibility that PFD may represent a new therapeutic agent for neural fibrosis.

Finally, we also looked if non-canonical pathways activated by TGF- β is regulated by PFD. The PI3K/ protein kinase B(Akt) pathway in cells serves as a crucial regulator of numerous biological processes including protein synthesis, proliferation, differentiation and glucose metabolism, through phosphoryl transfer. In normal cellular processes it is involved in promoting cell survival and cell cycle, whereas inactivation of the PI3K/ Akt pathway causes apoptosis (120). The TGF- β -PI3K axis has been investigated in fibrosis previously and serves as a potential fibrogenic target. However, the mechanistic targets remain unknown. Here, we are the first to show that TGF- β increases the phosphorylation of Akt by activating PI3K in an *in vitro* model of neural fibrosis. Similarly, inhibition of Akt by PFD significantly attenuated fibrotic processes induced by TGF- β 1.

Our proteomic analyses further helped us to identify the key downstream targets of PI3k signaling in TGF- β stimulated fibroblasts. Genes up-regulated by the activation

of PI3K/AKT/mTOR pathway, including signal transducer and activator of transcription 2 (*stat2*), cyclin-dependent kinase 1 (*cdk1*), interleukin 2 receptor subunit gamma (*il2rg*), growth factor receptor bound protein 2 (*grb2*), phospholipase A2, group XIA (*pla2g12a*), mitogen activated protein kinase 1 (*mapk1*) and others were significantly downregulated after PFD treatment. Given, its central role in various diseases, intense efforts to identify PI3K/Akt inhibitors have been conducted. A lot of studies involving these inhibitors have been discontinued due to adverse effects. Our results suggest that PFD directly modulates PI3K/Akt/mTOR pathway of perineurial fibroblasts. PFD directly or indirectly modulates various downstream targets of the PI3K/Akt/mTOR pathway which further explains its protective role in neural fibrosis. Further research needs to be done to ascertain the actions of PFD in PNF and to establish its efficacy in *in vivo* fibrosis models.

Conclusions

In conclusion we demonstrate that L-Ala-L-Gln and PFD exhibit anti-fibrotic effects on an *in vitro* model of neural fibrosis. Our findings indicate that L-Ala-L-Gln induces anti-fibrotic effect through the regulation of HIF-1- α , SMAD2/3 and PI3k-AKT pathways. Evitar (L-Alanyl-L-Glutamine), which was initially brought in order to reduce post-operative fibrosis, is thought to work by redirecting metabolomic balance to restore cytokine balance at the cellular level and hence provides a new pre-emptive approach. The dipeptide is an exceptionally stable compound that actively intervenes in the molecular pathway of adhesion formation. Interestingly, this dipeptide blocks the inflammatory cascade known to trigger fibrosis thereby preserving tissue homeostasis and leading normal tissue healing. In a double blinded randomized controlled study (NCT04250467) in laparoscopic myomectomies, 93.3% of Evitar treated patients showed absence of tissue fibrosis at any of the 23 anatomical sites within the abdominal cavity, as compared to 58.8% in the control group. This indicates that Evitar could provide an eminent viable solution to post-operative tissue fibrosis/ scarring.

The second drug tested, Pirfenidone (PFD) exerts its anti-fibrotic effects through the regulation of TGF- β 1/SMAD 3/HIF-1 α and the PI3K/Akt/mTOR pathways. Most importantly, PFD is effective against actively differentiated primary fibroblasts but not Schwann cells, and hence can be expected to show similar efficacy *in vivo*, potentially

mitigating neural fibrosis and scarring and might assist in regeneration as well. In addition, our study provided novel mechanistic insights into the bioactivity of PFD. We successfully showed that the anti-fibrotic effects of PFD might be due to its ability to rescue TGF- β 1 activated fibroblasts from hypoxic and inflammatory stress and inhibition of EMT and ECM deposition regulated by canonical and non-canonical TGF- β signaling. Whether this anti-fibrotic action of PFD further assists in nerve regeneration after injury, remains unknown and further research needs to be performed.

Our analysis indicates that these findings are not only highly relevant for peripheral nerve fibrosis, but are of relevance to fibrosis of other organs as well. We were able to decipher critical pathways necessary for fibrotic regulation. Our work is the first to also identify how these compounds work in favour of reducing neural scarring as well as rescuing the effector cells from hypoxic tissue microenvironment. Though **TGF- β 1**, is the major player contributing to fibrosis, it also forms an indispensable network for the regulation of the immune system, cell proliferation and tissue repair. Inhibiting TGF- β 1 hence poses catastrophic adverse effects including modest cellular toxicities, including aberrant inflammation, damage to metabolic regulation of cells, aberrant expression of reactive oxygen species impaired wound healing carcinogenesis and autoimmunity. Furthermore, many inhibitors that target TGF- β pathway have incomplete inhibition of TGF- β 1, thereby damaging metabolic regulation. Here lies the potential limitation of both these drugs.

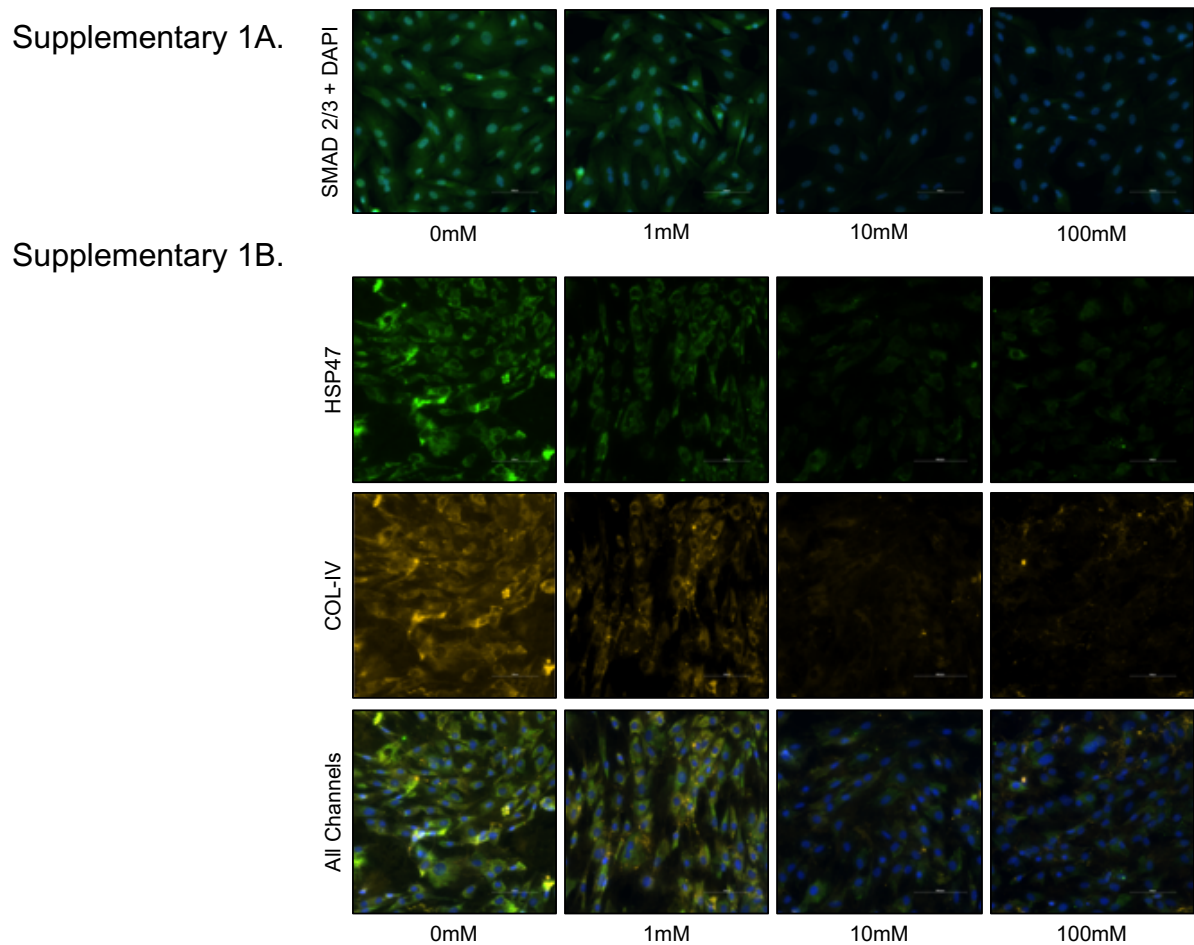
Fibroblast differentiation plays a key role in scarring and fibrosis. Though, L-Ala-L-Gln and PFD was found to effectively reduce collagen synthesis, both L-Ala-L-Gln and PFD fails to regulate fibroblast differentiation. On one hand, L-Ala-L-Gln acts on collagen synthesis, we did not find its role in differentiation. On the other hand, though PFD reduces differentiation, it induces cell death of naïve fibroblasts and hence can pose adverse reactions to patients. Additionally, L-Ala-L-Gln and PFD might have off-target glycolysis suppression and metabolic dysregulation, resulting in serious adverse events. Also, it remains to be determined how best to deliver L-Ala-L-Gln and PFD to specifically target diseased cellular populations in PNI. These need to be tested in vivo to better define the optimal route of delivery. Furthermore, elucidation of the suppressive mechanisms by which L-Ala-L-Gln and PFD exert their effects on

neural fibrosis *in vivo* may lead to the development of more effective drugs for the treatment of PNS injury and associated fibrosis.

As a next step, we hypothesize identification of an effective compound/ small molecule inhibitor that acts on the main target involved in the differentiation of fibroblasts, inhibit that target thereby regulating disease progression, otherwise left unchecked by the activated TGF- β pathway in neural fibrotic tissues. Our approach of reversing differentiation of myofibroblasts to fibroblasts will inhibit enhanced ECM synthesis and tissue contracture thereby enabling vascularization, reduce chronic inflammation and improve regenerative ability of underlying tissue. This could be a fine-tuned approach of pharmacological inhibition that will ensure maximized therapeutic benefit while avoiding damage to tissue integrity.

To test this hypothesis, we are now developing an efficient, reproducible and Go-to-Market therapeutic strategy in close collaboration with Novartis and we are hopeful of identifying breakthrough solutions for neural scarring and fibrosis in the near future.

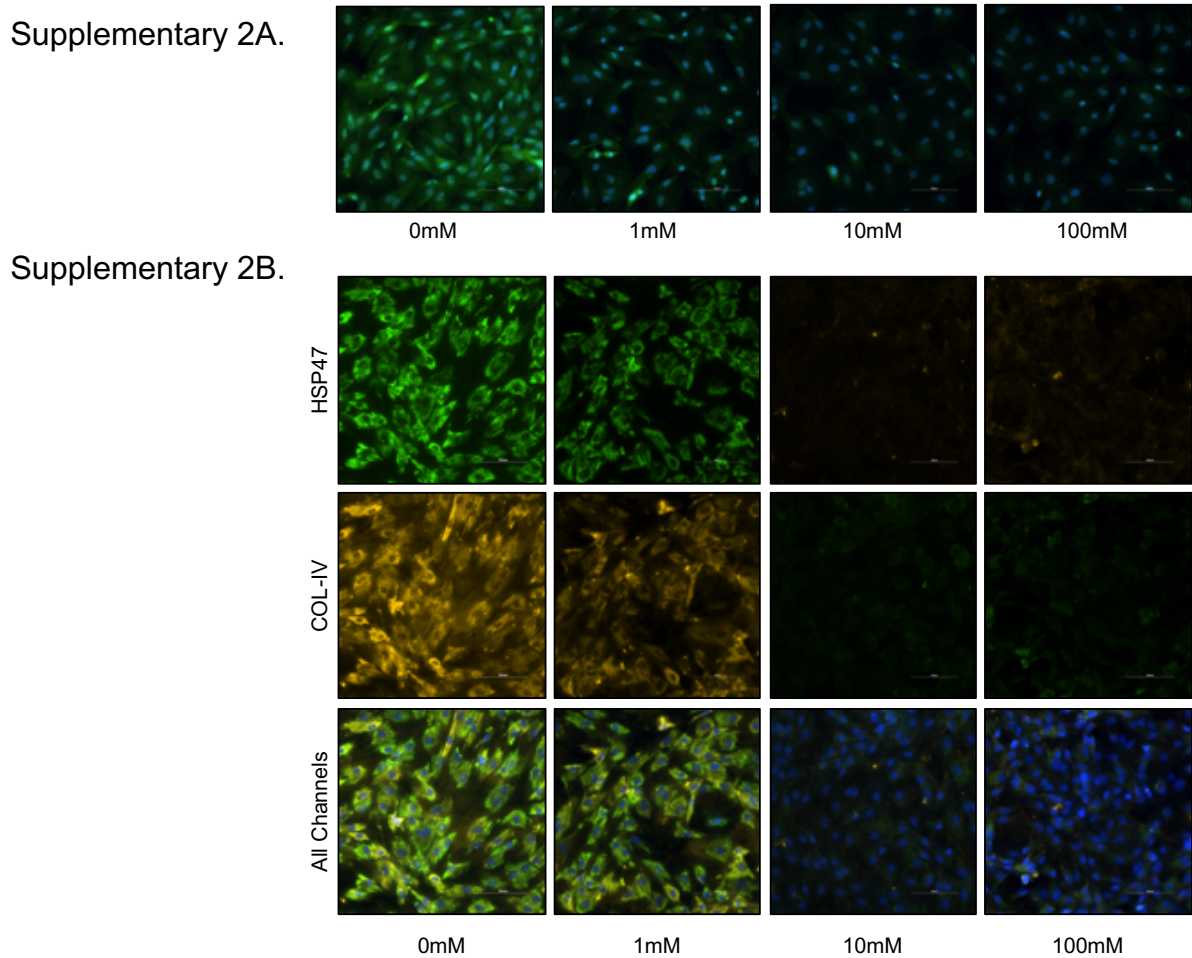
Supplementary Data:



Supplementary Figure 1: L-Ala-L-Gln reduces expression of pro-fibrotic markers in an *in-vitro* chronic hypoxic PNF model.

Hypoxic Primary Rat fibroblasts treated with different concentrations of L-Ala-L-Gln for 48h. Expression of SMAD 2/3 was characterized by immunofluorescence imaging. **A.** Representative immunofluorescence images of SMAD 2/3 staining. Nuclei were stained with DAPI. Original magnification, X40. Scale bar, 100 μ m. Data are representative of 2 independent experiments.

Abbreviations: DAPI - 4',6-diamidino-2-phenylindole; L-Ala-L-Gln - L-Alanyl-L-glutamine; PNF – Peripheral nerve fibrosis; SMAD 2/3 - Mothers against decapentaplegic homolog 2/3; PNF – Peripheral nerve fibrosis

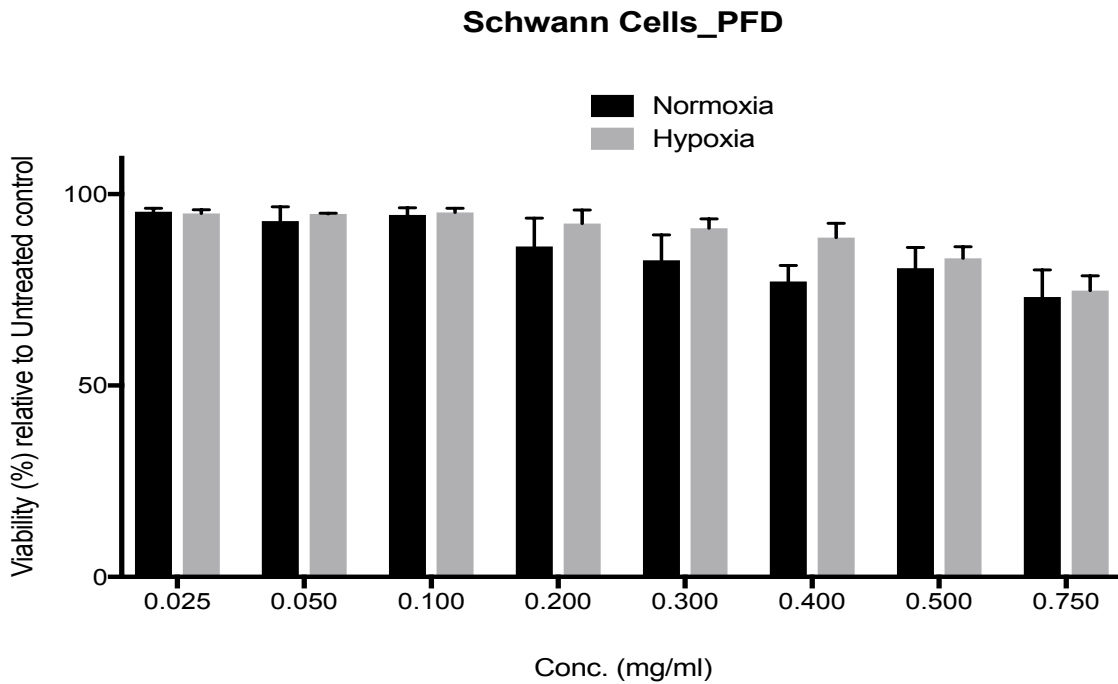


Supplementary Figure 2: L-Ala-L-Gln reduces expression of pro-fibrotic markers in an *in-vitro* acute hypoxic PNF model.

Primary Rat fibroblasts were exposed to episodic hypoxia (2% O₂ for 2h) followed by treatment with different concentrations of L-Ala-L-Gln for 48h. Expression of SMAD 2/3 was characterized by immunofluorescence imaging. **A.** Representative immunofluorescence images of SMAD 2/3 staining. Nuclei were stained with DAPI. Original magnification, X40. Scale bar, 100 μm. Data are representative of 2 independent experiments.

Abbreviations: DAPI - 4',6-diamidino-2-phenylindole; L-Ala-L-Gln - L-Alanyl-L-glutamine; PNF – Peripheral nerve fibrosis; SMAD 2/3 - Mothers against decapentaplegic homolog 2/3; PNF – Peripheral nerve fibrosis

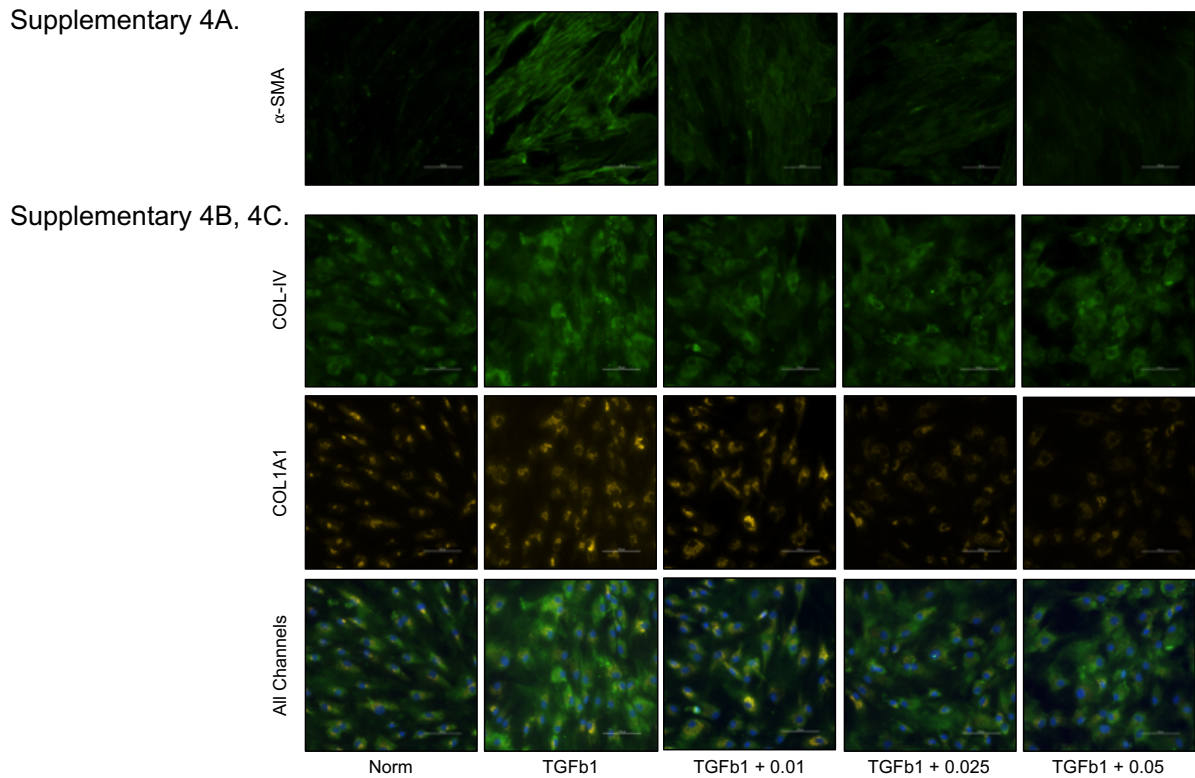
Supplementary 3.



Supplementary Figure 3: PFD does not reduce viability of Schwann cells in an *in-vitro* hypoxic PNF model.

Schwann cells were exposed to normoxic or hypoxic conditions (2% O₂ for 48h) followed by treatment with different concentrations of PFD for 48h. Viability was characterized by Alamar blue assay. Data are representative of 3 independent experiments.

Abbreviations: PFD - Pirfenidone; PNF – Peripheral nerve fibrosis

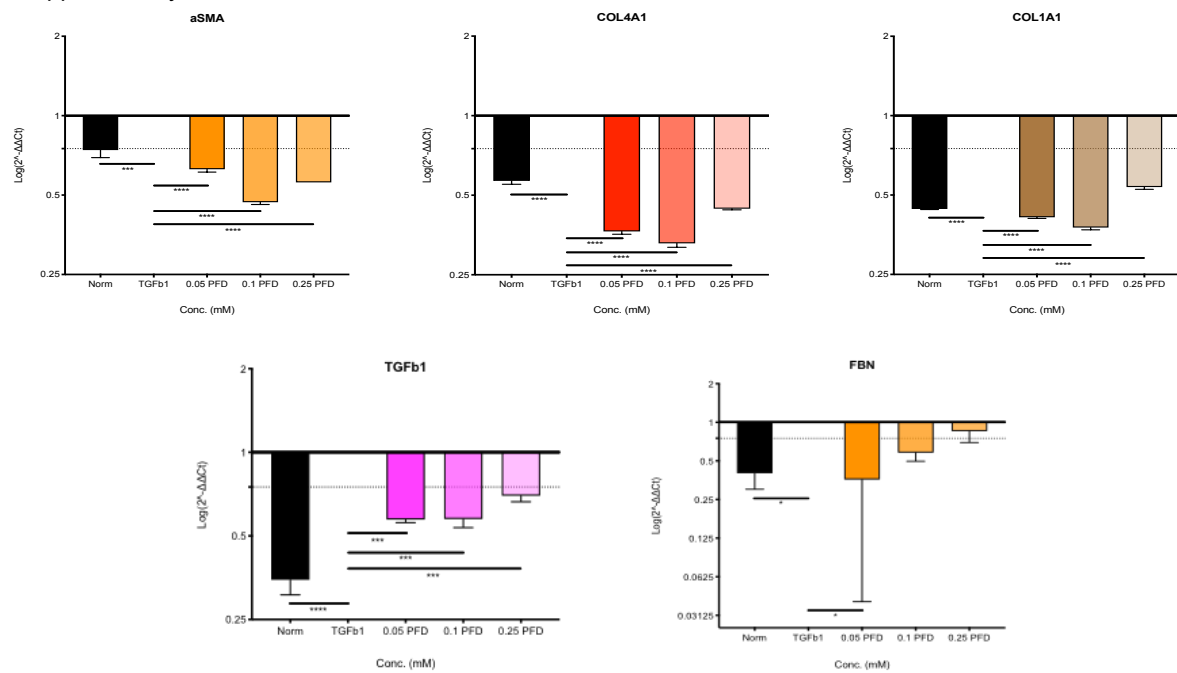


Supplementary Figure 4: PFD reduces expression of pro-fibrotic markers in an *in-vitro* human fibroblast derived PNF model.

Human fibroblasts were activated with TGF- β 1 followed by treatment with different concentrations of PFD for 48h. Expression of α -SMA, COL-IV and COL1A1 was characterized by immunofluorescence imaging. Representative immunofluorescence images of **A.** α -SMA; **B.** COL-IV and **C.** COL1A1 staining. Nuclei were stained with DAPI. Original magnification, X40. Scale bar, 100 μ m. Data are representative of 3 independent experiments.

Abbreviations: α -SMA – alpha Smooth Muscle Actin; COL1A1 – Collagen I A1 ; COL-IV – Collagen IV; DAPI - 4',6-diamidino-2-phenylindole; PNF – Peripheral nerve fibrosis; PFD – Pirfenidone; TGF- β 1 - Transforming Growth Factor Beta 1

Supplementary 5.



Supplementary Figure 5: PFD reduces gene expression of pro-fibrotic markers in an *in-vitro* primary rat fibroblast derived PNF model.

Cultured Primary Rat fibroblasts maintain fibrotic gene signature using quantitative RT-PCR analysis of α -SMA, Col1A1, Col4A1, TGF- β 1, and FBN in cells isolated from sciatic nerve derived fibroblasts activated with TGF- β 1. Results are normalized to GAPDH, mean \pm SE, n=3* denotes significance at P<0.05.

Reference:

1. D. Loring, *INS Dictionary of Neuropsychology and Clinical Neurosciences*. (Oxford University Press., ed. Second 1999).
2. M. V. S. Eric A. Zillmer, William C. Culbertson, *PRINCIPLES OF NEUROPSYCHOLOGY*. (Thomson Wadsworth, ed. Second 2001).
3. M. SE, *Nerve Surgery*. (Thieme Medical, New York, ed. First 2015).
4. J. D. Stewart, Peripheral nerve fascicles: anatomy and clinical relevance. *Muscle Nerve* **28**, 525-541 (2003).
5. J. L. Salzer, B. Zalc, Myelination. *Curr Biol* **26**, R971-R975 (2016).
6. K. A. Nave, H. B. Werner, Myelination of the nervous system: mechanisms and functions. *Annu Rev Cell Dev Biol* **30**, 503-533 (2014).
7. C. J. Cornbrooks, D. J. Carey, J. A. McDonald, R. Timpl, R. P. Bunge, In vivo and in vitro observations on laminin production by Schwann cells. *Proc Natl Acad Sci U S A* **80**, 3850-3854 (1983).
8. C. F. Eldridge, J. R. Sanes, A. Y. Chiu, R. P. Bunge, C. J. Cornbrooks, Basal lamina-associated heparan sulphate proteoglycan in the rat PNS: characterization and localization using monoclonal antibodies. *J Neurocytol* **15**, 37-51 (1986).
9. H. Grehl, J. M. Schroder, Significance of degenerating endoneurial cells in peripheral neuropathy. *Acta Neuropathol* **81**, 680-685 (1991).
10. D. Kaemmer *et al.*, Evaluation of tissue components in the peripheral nervous system using Sirius red staining and immunohistochemistry: a comparative study (human, pig, rat). *J Neurosci Methods* **190**, 112-116 (2010).
11. V. J. Obremski, P. M. Wood, M. B. Bunge, Fibroblasts promote Schwann cell basal lamina deposition and elongation in the absence of neurons in culture. *Dev Biol* **160**, 119-134 (1993).
12. S. Ohara, H. Takahashi, F. Ikuta, Specialised contacts of endoneurial fibroblasts with macrophages in wallerian degeneration. *J Anat* **148**, 77-85 (1986).
13. J. M. Vallat, M. J. Leboutet, A. Loubet, J. Hugon, J. J. Moreau, Effects of glycerol injection into rat sciatic nerve. *Muscle Nerve* **11**, 540-545 (1988).
14. R. S. Sauer *et al.*, Safety, efficacy, and molecular mechanism of claudin-1-specific peptides to enhance blood-nerve-barrier permeability. *J Control Release* **185**, 88-98 (2014).

15. A. P. Mizisin, A. Weerasuriya, Homeostatic regulation of the endoneurial microenvironment during development, aging and in response to trauma, disease and toxic insult. *Acta Neuropathol* **121**, 291-312 (2011).
16. M. A. Bell, A. G. Weddell, A descriptive study of the blood vessels of the sciatic nerve in the rat, man and other mammals. *Brain* **107 (Pt 3)**, 871-898 (1984).
17. T. K. Y. Lim *et al.*, Blood-nerve barrier dysfunction contributes to the generation of neuropathic pain and allows targeting of injured nerves for pain relief. *Pain* **155**, 954-967 (2014).
18. L. R. Robinson, Traumatic injury to peripheral nerves. *Muscle Nerve* **23**, 863-873 (2000).
19. F. Eser, L. A. Aktekin, H. Bodur, C. Atan, Etiological factors of traumatic peripheral nerve injuries. *Neurol India* **57**, 434-437 (2009).
20. G. Lundborg, Richard P. Bunge memorial lecture. Nerve injury and repair--a challenge to the plastic brain. *J Peripher Nerv Syst* **8**, 209-226 (2003).
21. N. Y. Li, G. I. Onor, N. J. Lemme, J. A. Gil, Epidemiology of Peripheral Nerve Injuries in Sports, Exercise, and Recreation in the United States, 2009 - 2018. *Phys Sportsmed* **49**, 355-362 (2021).
22. C. Schaefer *et al.*, Pain severity and the economic burden of neuropathic pain in the United States: BEAT Neuropathic Pain Observational Study. *Clinicoecon Outcomes Res* **6**, 483-496 (2014).
23. A. DeFrancesco-Lisowitz, J. A. Lindborg, J. P. Niemi, R. E. Zigmond, The neuroimmunology of degeneration and regeneration in the peripheral nervous system. *Neuroscience* **302**, 174-203 (2015).
24. D. Grinsell, C. P. Keating, Peripheral nerve reconstruction after injury: a review of clinical and experimental therapies. *Biomed Res Int* **2014**, 698256 (2014).
25. S. Y. Fu, T. Gordon, The cellular and molecular basis of peripheral nerve regeneration. *Mol Neurobiol* **14**, 67-116 (1997).
26. W. Tetzlaff, M. A. Bisby, G. W. Kreutzberg, Changes in cytoskeletal proteins in the rat facial nucleus following axotomy. *J Neurosci* **8**, 3181-3189 (1988).
27. E. Broude, M. McAtee, M. S. Kelley, B. S. Bregman, c-Jun expression in adult rat dorsal root ganglion neurons: differential response after central or peripheral axotomy. *Exp Neurol* **148**, 367-377 (1997).

28. H. Tsujino *et al.*, Activating transcription factor 3 (ATF3) induction by axotomy in sensory and motoneurons: A novel neuronal marker of nerve injury. *Mol Cell Neurosci* **15**, 170-182 (2000).
29. A. D. Gaudet, P. G. Popovich, M. S. Ramer, Wallerian degeneration: gaining perspective on inflammatory events after peripheral nerve injury. *J Neuroinflammation* **8**, 110 (2011).
30. L. Conforti, J. Gilley, M. P. Coleman, Wallerian degeneration: an emerging axon death pathway linking injury and disease. *Nat Rev Neurosci* **15**, 394-409 (2014).
31. J. A. Gomez-Sanchez *et al.*, After Nerve Injury, Lineage Tracing Shows That Myelin and Remak Schwann Cells Elongate Extensively and Branch to Form Repair Schwann Cells, Which Shorten Radically on Remyelination. *J Neurosci* **37**, 9086-9099 (2017).
32. S. Y. Jang *et al.*, Autophagic myelin destruction by Schwann cells during Wallerian degeneration and segmental demyelination. *Glia* **64**, 730-742 (2016).
33. R. Ozay *et al.*, Citicoline improves functional recovery, promotes nerve regeneration, and reduces postoperative scarring after peripheral nerve surgery in rats. *Surg Neurol* **68**, 615-622 (2007).
34. Q. P. Pham, U. Sharma, A. G. Mikos, Electrospun poly(epsilon-caprolactone) microfiber and multilayer nanofiber/microfiber scaffolds: characterization of scaffolds and measurement of cellular infiltration. *Biomacromolecules* **7**, 2796-2805 (2006).
35. A. Birbrair *et al.*, Type-1 pericytes accumulate after tissue injury and produce collagen in an organ-dependent manner. *Stem Cell Res Ther* **5**, 122 (2014).
36. A. Bellini, S. Mattoli, The role of the fibrocyte, a bone marrow-derived mesenchymal progenitor, in reactive and reparative fibroses. *Lab Invest* **87**, 858-870 (2007).
37. B. Hinz, The myofibroblast: paradigm for a mechanically active cell. *J Biomech* **43**, 146-155 (2010).
38. K. J. Hamill, K. Kligys, S. B. Hopkinson, J. C. Jones, Laminin deposition in the extracellular matrix: a complex picture emerges. *J Cell Sci* **122**, 4409-4417 (2009).
39. S. Atkins *et al.*, Scarring impedes regeneration at sites of peripheral nerve repair. *Neuroreport* **17**, 1245-1249 (2006).

40. S. L. Antunes *et al.*, Histopathological examination of nerve samples from pure neural leprosy patients: obtaining maximum information to improve diagnostic efficiency. *Mem Inst Oswaldo Cruz* **107**, 246-253 (2012).
41. L. Dreesmann, U. Mittnacht, M. Lietz, B. Schlosshauer, Nerve fibroblast impact on Schwann cell behavior. *Eur J Cell Biol* **88**, 285-300 (2009).
42. R. J. Starkweather, R. J. Neviasser, J. P. Adams, D. B. Parsons, The effect of devascularization on the regeneration of lacerated peripheral nerves: an experimental study. *J Hand Surg Am* **3**, 163-167 (1978).
43. D. A. Morgenstern *et al.*, Expression and glycanation of the NG2 proteoglycan in developing, adult, and damaged peripheral nerve. *Mol Cell Neurosci* **24**, 787-802 (2003).
44. J. Ara, P. Bannerman, A. Hahn, S. Ramirez, D. Pleasure, Modulation of sciatic nerve expression of class 3 semaphorins by nerve injury. *Neurochem Res* **29**, 1153-1159 (2004).
45. W. Tetzlaff, C. Leonard, C. A. Krekoski, I. M. Parhad, M. A. Bisby, Reductions in motoneuronal neurofilament synthesis by successive axotomies: a possible explanation for the conditioning lesion effect on axon regeneration. *Exp Neurol* **139**, 95-106 (1996).
46. S. S. *Nerve Injuries and Their Repair: A Critical Appraisal*. (London: Churchill Livingstone, London, ed. Third 1991).
47. D. Elliot, Surgical management of painful peripheral nerves. *Clin Plast Surg* **41**, 589-613 (2014).
48. I. Carroll, C. M. Curtin, Management of chronic pain following nerve injuries/CRPS type II. *Hand Clin* **29**, 401-408 (2013).
49. H. Millesi, T. Rath, R. Reihnsner, G. Zoch, Microsurgical neurolysis: its anatomical and physiological basis and its classification. *Microsurgery* **14**, 430-439 (1993).
50. L. Dvali, S. Mackinnon, The role of microsurgery in nerve repair and nerve grafting. *Hand Clin* **23**, 73-81 (2007).
51. H. Millesi, Bridging defects: autologous nerve grafts. *Acta Neurochir Suppl* **100**, 37-38 (2007).
52. S. Kehoe, X. F. Zhang, D. Boyd, FDA approved guidance conduits and wraps for peripheral nerve injury: a review of materials and efficacy. *Injury* **43**, 553-572 (2012).

53. H. C. Powell, R. R. Myers, Pathology of experimental nerve compression. *Lab Invest* **55**, 91-100 (1986).
54. R. R. Myers, H. M. Heckman, J. A. Galbraith, H. C. Powell, Subperineurial demyelination associated with reduced nerve blood flow and oxygen tension after epineurial vascular stripping. *Lab Invest* **65**, 41-50 (1991).
55. K. R. Ylitalo, M. Sowers, S. Heeringa, Peripheral vascular disease and peripheral neuropathy in individuals with cardiometabolic clustering and obesity: National Health and Nutrition Examination Survey 2001-2004. *Diabetes Care* **34**, 1642-1647 (2011).
56. J. X. Hao *et al.*, Development of a mouse model of neuropathic pain following photochemically induced ischemia in the sciatic nerve. *Exp Neurol* **163**, 231-238 (2000).
57. L. J. Ruger *et al.*, Characteristics of chronic ischemic pain in patients with peripheral arterial disease. *Pain* **139**, 201-208 (2008).
58. O. Kayacan, S. Beder, G. Deda, D. Karnak, Neurophysiological changes in COPD patients with chronic respiratory insufficiency. *Acta Neurol Belg* **101**, 160-165 (2001).
59. T. K. Lim *et al.*, Peripheral nerve injury induces persistent vascular dysfunction and endoneurial hypoxia, contributing to the genesis of neuropathic pain. *J Neurosci* **35**, 3346-3359 (2015).
60. H. Z. Imtiyaz, M. C. Simon, Hypoxia-inducible factors as essential regulators of inflammation. *Curr Top Microbiol Immunol* **345**, 105-120 (2010).
61. G. L. Semenza, Regulation of vascularization by hypoxia-inducible factor 1. *Ann N Y Acad Sci* **1177**, 2-8 (2009).
62. D. M. Gilkes, S. Bajpai, P. Chaturvedi, D. Wirtz, G. L. Semenza, Hypoxia-inducible factor 1 (HIF-1) promotes extracellular matrix remodeling under hypoxic conditions by inducing P4HA1, P4HA2, and PLOD2 expression in fibroblasts. *J Biol Chem* **288**, 10819-10829 (2013).
63. B. K. Nayak *et al.*, HIF-1 Mediates Renal Fibrosis in OVE26 Type 1 Diabetic Mice. *Diabetes* **65**, 1387-1397 (2016).
64. J. H. Distler *et al.*, Hypoxia-induced increase in the production of extracellular matrix proteins in systemic sclerosis. *Arthritis Rheum* **56**, 4203-4215 (2007).

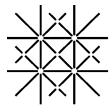
65. Q. Zhang *et al.*, Crosstalk of hypoxia-mediated signaling pathways in upregulating plasminogen activator inhibitor-1 expression in keloid fibroblasts. *J Cell Physiol* **199**, 89-97 (2004).
66. O. A. Mesarwi *et al.*, Hepatocyte Hypoxia Inducible Factor-1 Mediates the Development of Liver Fibrosis in a Mouse Model of Nonalcoholic Fatty Liver Disease. *PLoS One* **11**, e0168572 (2016).
67. J. Goodwin *et al.*, Targeting Hypoxia-Inducible Factor-1alpha/Pyruvate Dehydrogenase Kinase 1 Axis by Dichloroacetate Suppresses Bleomycin-induced Pulmonary Fibrosis. *Am J Respir Cell Mol Biol* **58**, 216-231 (2018).
68. J. Massague, TGFbeta signalling in context. *Nat Rev Mol Cell Biol* **13**, 616-630 (2012).
69. X. M. Meng, D. J. Nikolic-Paterson, H. Y. Lan, TGF-beta: the master regulator of fibrosis. *Nat Rev Nephrol* **12**, 325-338 (2016).
70. R. W. D. Gilbert, M. K. Vickaryous, A. M. Vilorio-Petit, Signalling by Transforming Growth Factor Beta Isoforms in Wound Healing and Tissue Regeneration. *J Dev Biol* **4**, (2016).
71. J. W. Penn, A. O. Grobbelaar, K. J. Rolfe, The role of the TGF-beta family in wound healing, burns and scarring: a review. *Int J Burns Trauma* **2**, 18-28 (2012).
72. A. B. Roberts *et al.*, Transforming growth factor type beta: rapid induction of fibrosis and angiogenesis in vivo and stimulation of collagen formation in vitro. *Proc Natl Acad Sci U S A* **83**, 4167-4171 (1986).
73. F. Verrecchia, A. Mauviel, Transforming growth factor-beta signaling through the Smad pathway: role in extracellular matrix gene expression and regulation. *J Invest Dermatol* **118**, 211-215 (2002).
74. A. Gingery *et al.*, TGF-beta signaling regulates fibrotic expression and activity in carpal tunnel syndrome. *J Orthop Res* **32**, 1444-1450 (2014).
75. M. La Fleur, J. L. Underwood, D. A. Rappolee, Z. Werb, Basement membrane and repair of injury to peripheral nerve: defining a potential role for macrophages, matrix metalloproteinases, and tissue inhibitor of metalloproteinases-1. *J Exp Med* **184**, 2311-2326 (1996).
76. M. Li *et al.*, Protein expression profiling during wallerian degeneration after rat sciatic nerve injury. *Muscle Nerve* **50**, 73-78 (2014).

77. A. Desmouliere, A. Geinoz, F. Gabbiani, G. Gabbiani, Transforming growth factor-beta 1 induces alpha-smooth muscle actin expression in granulation tissue myofibroblasts and in quiescent and growing cultured fibroblasts. *J Cell Biol* **122**, 103-111 (1993).
78. M. Li *et al.*, TGF-beta1 is critical for Wallerian degeneration after rat sciatic nerve injury. *Neuroscience* **284**, 759-767 (2015).
79. C. Schachtrup *et al.*, Fibrinogen triggers astrocyte scar formation by promoting the availability of active TGF-beta after vascular damage. *J Neurosci* **30**, 5843-5854 (2010).
80. R. K. Nath *et al.*, Antibody to transforming growth factor beta reduces collagen production in injured peripheral nerve. *Plast Reconstr Surg* **102**, 1100-1106; discussion 1107-1108 (1998).
81. M. P. Clements *et al.*, The Wound Microenvironment Reprograms Schwann Cells to Invasive Mesenchymal-like Cells to Drive Peripheral Nerve Regeneration. *Neuron* **96**, 98-114 e117 (2017).
82. P. Shephard *et al.*, Myofibroblast differentiation is induced in keratinocyte-fibroblast co-cultures and is antagonistically regulated by endogenous transforming growth factor-beta and interleukin-1. *Am J Pathol* **164**, 2055-2066 (2004).
83. N. Ghosh, D. Kalbermatten, S. Madduri, R. Guzman, Fibrosis and Regulation of Nerve Regeneration in the Peripheral and Central Nervous Systems. *CNS Neurol Disord Drug Targets* **19**, 560-571 (2020).
84. D. W. Wilmore, J. K. Shabert, Role of glutamine in immunologic responses. *Nutrition* **14**, 618-626 (1998).
85. M. Parry-Billings, J. Evans, P. C. Calder, E. A. Newsholme, Does glutamine contribute to immunosuppression after major burns? *Lancet* **336**, 523-525 (1990).
86. R. Stangl *et al.*, Reduction of liver ischemia-reperfusion injury via glutamine pretreatment. *J Surg Res* **166**, 95-103 (2011).
87. Y. Inoue, J. P. Grant, P. J. Snyder, Effect of glutamine-supplemented intravenous nutrition on survival after Escherichia coli-induced peritonitis. *JPEN J Parenter Enteral Nutr* **17**, 41-46 (1993).
88. P. Furst, S. Albers, P. Stehle, Glutamine-containing dipeptides in parenteral nutrition. *JPEN J Parenter Enteral Nutr* **14**, 118S-124S (1990).

89. K. Kratochwill *et al.*, Alanyl-glutamine dipeptide restores the cytoprotective stress proteome of mesothelial cells exposed to peritoneal dialysis fluids. *Nephrol Dial Transplant* **27**, 937-946 (2012).
90. T. E. Haynes *et al.*, L-Glutamine or L-alanyl-L-glutamine prevents oxidant- or endotoxin-induced death of neonatal enterocytes. *Amino Acids* **37**, 131-142 (2009).
91. J. R. Hoffman *et al.*, Examination of the efficacy of acute L-alanyl-L-glutamine ingestion during hydration stress in endurance exercise. *J Int Soc Sports Nutr* **7**, 8 (2010).
92. P. Dechelotte *et al.*, L-alanyl-L-glutamine dipeptide-supplemented total parenteral nutrition reduces infectious complications and glucose intolerance in critically ill patients: the French controlled, randomized, double-blind, multicenter study. *Crit Care Med* **34**, 598-604 (2006).
93. C. Fuentes-Orozco *et al.*, L-alanyl-L-glutamine-supplemented parenteral nutrition decreases infectious morbidity rate in patients with severe acute pancreatitis. *JPEN J Parenter Enteral Nutr* **32**, 403-411 (2008).
94. V. Cruzat, M. Macedo Rogero, K. Noel Keane, R. Curi, P. Newsholme, Glutamine: Metabolism and Immune Function, Supplementation and Clinical Translation. *Nutrients* **10**, (2018).
95. E. Ferrantelli *et al.*, The dipeptide alanyl-glutamine ameliorates peritoneal fibrosis and attenuates IL-17 dependent pathways during peritoneal dialysis. *Kidney Int* **89**, 625-635 (2016).
96. J. Macias-Barragan, A. Sandoval-Rodriguez, J. Navarro-Partida, J. Armendariz-Borunda, The multifaceted role of pirfenidone and its novel targets. *Fibrogenesis Tissue Repair* **3**, 16 (2010).
97. J. Rosenbloom, F. A. Mendoza, S. A. Jimenez, Strategies for anti-fibrotic therapies. *Biochim Biophys Acta* **1832**, 1088-1103 (2013).
98. H. Oku *et al.*, Antifibrotic action of pirfenidone and prednisolone: different effects on pulmonary cytokines and growth factors in bleomycin-induced murine pulmonary fibrosis. *Eur J Pharmacol* **590**, 400-408 (2008).
99. E. S. Kim, G. M. Keating, Pirfenidone: a review of its use in idiopathic pulmonary fibrosis. *Drugs* **75**, 219-230 (2015).
100. C. L. Hall, A. R. Wells, K. P. Leung, Pirfenidone reduces profibrotic responses in human dermal myofibroblasts, in vitro. *Lab Invest* **98**, 640-655 (2018).

101. P. B. Poble *et al.*, Therapeutic effect of pirfenidone in the sugen/hypoxia rat model of severe pulmonary hypertension. *FASEB J* **33**, 3670-3679 (2019).
102. B. Khanum *et al.*, Pirfenidone inhibits post-traumatic proliferative vitreoretinopathy. *Eye (Lond)* **31**, 1317-1328 (2017).
103. E. Ahrne *et al.*, Evaluation and Improvement of Quantification Accuracy in Isobaric Mass Tag-Based Protein Quantification Experiments. *J Proteome Res* **15**, 2537-2547 (2016).
104. Y. Wang *et al.*, Reversed-phase chromatography with multiple fraction concatenation strategy for proteome profiling of human MCF10A cells. *Proteomics* **11**, 2019-2026 (2011).
105. T. M. Maher *et al.*, Diminished prostaglandin E2 contributes to the apoptosis paradox in idiopathic pulmonary fibrosis. *Am J Respir Crit Care Med* **182**, 73-82 (2010).
106. C. Gu *et al.*, Identification of Common Genes and Pathways in Eight Fibrosis Diseases. *Front Genet* **11**, 627396 (2020).
107. T. Moore-Morris *et al.*, Resident fibroblast lineages mediate pressure overload-induced cardiac fibrosis. *J Clin Invest* **124**, 2921-2934 (2014).
108. A. J. van der Slot *et al.*, Increased formation of pyridinoline cross-links due to higher telopeptide lysyl hydroxylase levels is a general fibrotic phenomenon. *Matrix Biol* **23**, 251-257 (2004).
109. L. M. Robertson, N. M. Fletcher, M. P. Diamond, G. M. Saed, Evitar (l-Alanyl-l-Glutamine) Regulates Key Signaling Molecules in the Pathogenesis of Postoperative Tissue Fibrosis. *Reprod Sci* **26**, 724-733 (2019).
110. B. Mittendorfer, D. C. Gore, D. N. Herndon, R. R. Wolfe, Accelerated glutamine synthesis in critically ill patients cannot maintain normal intramuscular free glutamine concentration. *JPEN J Parenter Enteral Nutr* **23**, 243-250; discussion 250-242 (1999).
111. D. Lagares *et al.*, Inhibition of focal adhesion kinase prevents experimental lung fibrosis and myofibroblast formation. *Arthritis Rheum* **64**, 1653-1664 (2012).
112. C. V. Agnes W. Boots, Michael Kreuter, Marc Schneider, Michael Meister, Frederik-Jan Van Schooten, Nicolas Kahn, paper presented at the ERS International Congress, 2019.
113. B. San-Miguel *et al.*, Glutamine prevents fibrosis development in rats with colitis induced by 2,4,6-trinitrobenzene sulfonic acid. *J Nutr* **140**, 1065-1071 (2010).

114. H. Y. Li, Q. G. Zhang, J. W. Chen, S. Q. Chen, S. Y. Chen, The fibrotic role of phosphatidylinositol-3-kinase/Akt pathway in injured skeletal muscle after acute contusion. *Int J Sports Med* **34**, 789-794 (2013).
115. A. Aquino-Galvez *et al.*, Dysregulated expression of hypoxia-inducible factors augments myofibroblasts differentiation in idiopathic pulmonary fibrosis. *Respir Res* **20**, 130 (2019).
116. J. Herrera, C. A. Henke, P. B. Bitterman, Extracellular matrix as a driver of progressive fibrosis. *J Clin Invest* **128**, 45-53 (2018).
117. C. G. Martinez-Moreno, D. Calderon-Vallejo, S. Harvey, C. Aramburo, J. L. Quintanar, Growth Hormone (GH) and Gonadotropin-Releasing Hormone (GnRH) in the Central Nervous System: A Potential Neurological Combinatory Therapy? *Int J Mol Sci* **19**, (2018).
118. M. Dobaczewski *et al.*, Smad3 signaling critically regulates fibroblast phenotype and function in healing myocardial infarction. *Circ Res* **107**, 418-428 (2010).
119. J. Luna, M. C. Masamunt, I. C. Lawrance, M. Sans, Mesenchymal cell proliferation and programmed cell death: key players in fibrogenesis and new targets for therapeutic intervention. *Am J Physiol Gastrointest Liver Physiol* **300**, G703-708 (2011).
120. J. A. Engelman, J. Luo, L. C. Cantley, The evolution of phosphatidylinositol 3-kinases as regulators of growth and metabolism. *Nat Rev Genet* **7**, 606-619 (2006).



Universität Basel, Student Services, Postfach, 4001 Basel

Nilabh Ghosh
Zeughausstrasse 31
4052 Basel

Datenabschrift – Gesamtauszug per 31.03.2022

Name Ghosh, Nilabh
Matrikelnummer 16-067-084
Geburtsdatum 08.01.1993

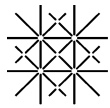
Total erworbene Kreditpunkte: 21

	Semester	Note	KP	bewertet am
Dissertation: "Repair and Regeneration of Peripheral Nerve Fibrosis"	HS 2021	6.00		06.01.2022
Doktoratsexamen	HS 2021	6.0		06.01.2022
54877 Vorlesung: Regulatory Affairs and its Applications	FS 2019	5.0	2	25.09.2020
20458 Vorlesung mit Übungen: Essentials in Drug Development & Clinical Trials	FS 2019	PASS	2	06.06.2019
45395 Vorlesung: Good Clinical Practice	HS 2018	PASS	1	21.02.2019
12420 Vorlesung: Translational Cancer Research	FS 2018	PASS	2	26.06.2018
Erweiterte Kompetenzen: LTK Module-1	FS 2017	PASS	2	17.05.2018
15629 Seminar: Experimental Hematology I	HS 2017	PASS	6	18.01.2018
15576 Seminar: New Literature in Cell Adhesion, Extracellular Matrix, Cancer and Metastasis I	HS 2017	PASS	2	09.01.2018
18367 Vorlesung: Translational Control and Post-Translational Protein Modification	HS 2017	FAIL	0	22.12.2017
34604 Vorlesung mit Praktikum: Introduction to Protein Interaction Analysis by Affinity Purification - Mass Spectrometry	FS 2017	PASS	1	24.08.2017
34605 Vorlesung mit Praktikum: Introduction into Fluorescence and Live	FS 2017	PASS	1	11.08.2017
12424 Vorlesung: Molecular Medicine II	FS 2017	PASS	2	03.08.2017
*** Ende der Datenabschrift ***				

Studierende können eine Leistungsbewertung nach deren Bekanntgabe in den Online Services innerhalb von 30 Tagen beanstanden. Der vorliegende Gesamtauszug kann Leistungen aufführen, für die diese Kontrollfrist noch nicht verstrichen ist.

Gesamtauszüge der Universität Basel werden als PDF-Dateien zur Verfügung gestellt. Deren Authentizität kann unter verify.unibas.ch überprüft werden. Gegen eine Gebühr sind sie auch auf Papier mit Sicherheitsmerkmalen gedruckt erhältlich (siehe unibas.ch/datenabschrift).

Dokument ohne Unterschrift



Universität Basel, Student Services, Postfach, 4001 Basel

Nilabh Ghosh
Zeughausstrasse 31
4052 Basel

Academic record as of 31.03.2022

Translation from German original

Name	Ghosh, Nilabh
Matriculation no.	16-067-084
Date of birth	08.01.1993

Total number of credit points earned: 21

		Semester	Grade	CP	Assessed on
	PhD examination	fs 2021	6.0		06.01.2022
	PhD thesis: "Repair and Regeneration of Peripheral Nerve Fibrosis"	fs 2021	6.00		06.01.2022
54877	Lecture: Regulatory Affairs and its Applications	ss 2019	5.0	2	25.09.2020
20458	Lecture with practical courses: Essentials in Drug Development & Clinical Trials	ss 2019	PASS	2	06.06.2019
45395	Lecture: Good Clinical Practice	fs 2018	PASS	1	21.02.2019
12420	Lecture: Translational Cancer Research	ss 2018	PASS	2	26.06.2018
	Advanced skills: LTK Module-1	ss 2017	PASS	2	17.05.2018
15629	Seminar: Experimental Hematology I	fs 2017	PASS	6	18.01.2018
15576	Seminar: New Literature in Cell Adhesion, Extracellular Matrix, Cancer and Metastasis I	fs 2017	PASS	2	09.01.2018
18367	Lecture: Translational Control and Post-Translational Protein Modification	fs 2017	FAIL	0	22.12.2017
34604	Lecture with internship: Introduction to Protein Interaction Analysis by Affinity Purification - Mass Spectrometry	ss 2017	PASS	1	24.08.2017
34605	Lecture with internship: Introduction into Fluorescence and Live	ss 2017	PASS	1	11.08.2017
12424	Lecture: Molecular Medicine II	ss 2017	PASS	2	03.08.2017
***	End of academic record	***			

Students have 30 days from the publication of a student assessment via Online Services in which to query any results. This academic record may include assessments for which this verification period has not yet expired.

Academic records issued by the University of Basel are made available in PDF form. The authenticity of these documents can be verified at verify.unibas.ch. Printed paper versions with security features are also available for a fee (see unibas.ch/transcriptofrecords).

This document may contain untranslated academic achievements. Please contact the relevant department or faculty if you require further information.

For the purposes of student administration, the University of Basel uses the date format DD.MM.YYYY in all documents and communication.

Document bearing no signature